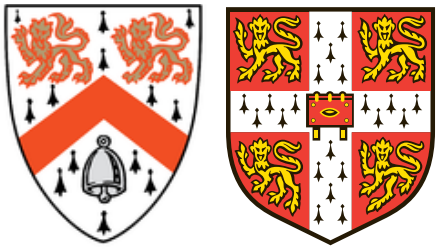

Molecular tuning of a neural circuit that drives aggregation behaviour in *C. elegans*

This dissertation is submitted for the degree of
Doctor of Philosophy

by

Sean Flynn

MRC Laboratory of Molecular Biology

Wolfson College
University of Cambridge

April 2017

Abstract

Modulation of network state is a ubiquitous feature of nervous systems. A major challenge in understanding the physiological flexibility of neural circuits is linking molecules that regulate behaviour to changes in the properties of individual neurons. Here, we use a defined neural circuit in *C. elegans* to frame this universal problem. By genetic dissection of the behavioural state that sustains escape of 21% O_2, we identify novel neuronal functions for several highly conserved genes, including a paracaspase similar to human MALT1, a calmodulin-binding transcription activator (CAMTA), and two accessory subunits of the eIF3 complex. These molecules have been implicated in diverse forms of human disease, but their role in the nervous system is either unexplored or poorly understood. Using *in vivo* Ca^{2+} imaging techniques to investigate neuron physiology in immobilized and behaving animals, we demonstrate their effect on the properties of individual neurons.

The activity of RMG hub neurons is associated with the switch in behavioural state induced by 21% O_2. Recently it has been shown that the input-output relationship of RMG is controlled by cytokine signaling, an increasingly appreciated form of neuromodulation. We now present biochemical and genetic evidence that MALT-1 functions downstream of IL-17 receptors to mediate cytokine signaling in RMG. Our data suggest that, reminiscent of its role in the immune system, MALT1 performs both scaffolding and enzymatic functions in neurons. Additionally, we show that RMG responsiveness is controlled by the widely expressed, putative regulators of gene expression CAMT-1 and EIF-3.K/L. Our analyses of these proteins elucidate their function within the URX-RMG circuit, but also raise hypotheses that can be tested more generally in the nervous system. We propose that CAMT-1 regulates adaptation to ambient O_2 conditions, which may reflect a widespread requirement for controlling homeostatic plasticity. EIF-3.K and EIF-3.L have been shown to be dispensable for general translation, but important for regulation of the response to stress. Our study raises the possibility that their role in promoting the activity of all, or some

subset of, neurons might underlie this contextual requirement. Together, our findings provide mechanistic insight into the regulation of a behavioural state associated with a specific environmental context.

Preface

This dissertation is the result of my own work and includes nothing that is the outcome of work done in collaboration except as specified in the text.

It is not substantially the same as any that I have submitted, or, is being concurrently submitted for a degree or diploma or other qualification at the University of Cambridge or any other University or similar institution. I further state that no substantial part of my dissertation has already been submitted, or, is being concurrently submitted for any such degree, diploma or other qualification at the University of Cambridge or any other University or similar institution.

It does not exceed 60,000 words in length.

Acknowledgements

All work described in this thesis was carried out in the de Bono lab. Mario has been a patient and always-supportive advisor. I hope that I have learned from his way of finding questions that are interesting, and pursuing them with care. Most of all, it has been inspiring to experience his enthusiasm for science. Changchun Chen shared with me his collection of mutants, on which this thesis is based, and provided help, reagents, techniques, and advice on countless occasions. It has been nice too, that he has let me win at ping pong every once in a while (or maybe just once).

I have greatly enjoyed the light-hearted breaks, and helpful ideas provided over coffee by Geoff Nelson, Isabel Beets, Giulio Valperga and Patrick Laurent. Geoff performed WGS-based analysis of mutants in this study. It was a pleasure too to collaborate with Alastair Crisp, who analyzed RNA-seq data. My thanks to Mark Skehel and the LMB Mass Spec team for proteomic analyses, to Marta Grzelak and the CRUK Genomics Core who performed Illumina sequencing, and to Mark, Heather and Martyn in the LMB media kitchen.

I am grateful to Jonathan Hodgkin and Greg Jefferis for constructive and thought-provoking discussions. I would also like to thank my second supevisors Berthold Hedwig and Madan Babu for helpful advice.

Thanks to Alison Turnock and Amie Blake, who were a constant source of invaluable support, to Robin Burns for helpful comments, and to Tom Williams, Susan Shao, Jack Monahan and Callum Hayes for fond memories of my time here. I am indebted to Mani Ramaswami and Stephen Goodwin for inspiring me to follow this path, to Mum who taught me that no goal is unachievable, and to Dad, from whom I learned that anything worth doing is worth doing right. Finally, to Abi, who has shared everything with me, and without whom this wouldn’t have been half as fun.

Contents **Page**

Figures **Page**

Glossary

AMPA	α-amino-3-hydroxy-5-methyl-4-isoxazolepropionic acid
ANOVA	analysis of variance
C. elegans	*Caenorhabditis elegans*
cho-1	CHOline transporter
CNS	Central Nervous System
CRISPR	clustered regularly interspaced short palindromic repeats
Drosophila	*Drosophila melanogaster*
egl	EGg Laying defective
flp	FMRF-Like peptide
GABA	γ-Aminobutyric acid
Gcn	GCN (yeast General Control Nondepressible) homolog
gcy	Guanylyl CYclase
GFP	green fluorescent protein
HA	human influenza hemagglutinin
HEK	human embryonic Kidney
HSD	honest significant difference
ife	Initiation Factor 4E (eIF4E) Family
hsp	Heat Shock Protein
lon	LONg
KO	Knockout
NMDA	N-methyl-D-aspartate
npr	NeuroPeptide Receptor family
rab	RAB family
slo	SLOwpoke potassium channel family
tax	abnormal chemotaxis
unc	UNCoordinated
WGS	whole genome sequencing
WT	wild type

1

Immune signaling in neuromodulation

The healthy nervous system expresses many molecules that were once thought to be specific to the immune response (Kioussis and Pachnis, 2009; Kipnis, 2016). Rather than being markers of injury or infection, it is now clear that the presence of these proteins in the brain reflects their fundamental role in neuronal physiology (Boulanger et al., 2001). Conceptual parallels between the immune system and the brain were first drawn by Jerne, who likened the adaptability of immunity to the *"miracle that young children easily learn the language of any environment into which they were born"* (Jerne, 1984). In fact, we now know that the inherent plasticity of both systems is encoded in part by the same genes (Boulanger, 2009; Habibi et al., 2009; Pribiag and Stellwagen, 2014). Whether they have specialized from a common ancestral cell-type or co-opted the same mechanisms independently, an emerging picture is that the brain and immune system make use of the same molecular pathways to serve their own tissue-specific functions (Kioussis and Pachnis, 2009).

The classical complement cascade facilitates the recognition and removal of pathogens by opsonizing (tagging) harmful cells. In neural networks, it also functions to eliminate inappropriate synapses (Stephan et al., 2012); during a developmental window when activity-dependent synaptic pruning is critical for the formation of functional circuits, complement proteins are used to opsonize synapses (Stevens et al., 2007). Similarly, cell-surface proteins of the major histocompatibility complex class I (MHCI) family, which mediate the presentation of non-self antigens in the adaptive immune system, are required for activity-dependent changes at neuronal synapses (Boulanger and Shatz, 2004). As well as remodeling neuronal projections, MHCI proteins control changes in synapse strength by promoting long-term depression (LTD) and inhibiting long-term potentiation (LTP) (Huh et al., 2000).

The inflammatory response is controlled by secreted molecules, including cytokines that regulate the expression of pro-inflammatory genes, and chemokines (chemotactic chemokines) that attract leukocytes to inflamed areas

(Turner et al., 2014). In the brain, these chemical messengers function as neuromodulators (Rostene et al., 2007; Vezzani and Viviani, 2015). There is substantial evidence that by driving neuroinflammation, aberrant cytokine signaling can induce depression and neurodegeneration, making mechanistic delineation of the link between pathological immune signaling and brain dysfunction an area of immense therapeutic interest (Heppner et al., 2015; Wohleb et al., 2016; Yirmiya et al., 2015). In the non-inflamed brain however, basal cytokine levels are critical for a range of developmental and behavioural functions that are only beginning to be understood (Bauer et al., 2007; see below). Many of the intracellular signaling pathways that mediate cytokine function in immune cells are constitutively expressed in the nervous system, although an understanding of how they specifically alter neuronal properties has lagged behind functional studies of the cytokines themselves.

Neuromodulation by brain-borne cytokines

Neuromodulators confer behavioural adaptability by controlling the gain of sensory responses or altering the excitability of specific neural circuits dependent on context (Taghert and Nitabach, 2012). The list of molecules now considered neuromodulators is long and diverse, including hormones, neuropeptides, gases and amines that can be released in combination or in isolation (Kumar, 2011; Marder, 2012; Stein, 2009). Accumulating evidence indicates that cytokine signaling systems are yet another class of state-specific modulators.

Almost three decades ago Breder and colleagues identified interleukin-1 (IL-1) protein in neurons innervating the hypothalamus, and speculated that it may function there to modulate neuronal activity (Breder et al., 1988). Since then a range of other cytokines have been found to be expressed in neurons and/or glia (Rostene et al., 2007; Vezzani and Viviani, 2015). In most cases, their functions seem to be context-specific, exerting little or no effect on basal neuronal activity/transmission, but augmenting or limiting certain adaptive changes - such

as learning (Goshen et al., 2007; Rostene et al., 2007; Stellwagen and Malenka, 2006).

Memory is thought to be encoded by activity-dependent changes in synaptic strength (Martin et al., 2000). LTP and LTD represent a feed-forward relationship between post-synaptic response and sustained pre-synaptic activity that allow circuit properties to be modified over time. To prevent long-term destabilizing change however, homeostatic plasticity mechanisms function to keep average activity close to an optimal set point (Turrigiano, 2017). Interestingly, cytokinergic neuromodulation plays a role in regulating both of these two opposing forms of plasticity. The most important examples characterized to date are the pro-inflammatory cytokines IL-1β and tumour necrosis factor α (TNFα).

IL-1β regulates LTP

During LTP, IL-1β mRNA expression is induced in the CA1 region of the hippocampus (Schneider et al., 1998). Initially, it was thought that hippocampal IL-1β was an inhibitor of LTP (Murray and Lynch, 1998), but it was later shown that its effect is dose-dependent, following an inverted U-shape curve . At low levels, IL-1β facilitates LTP in culture and learning *in vivo* (Brennan et al., 2003; Schneider et al., 1998). Thus, physiological and pathological IL-1β signaling may have opposite effects in the hippocampus. Both IL-1 receptor (IL-1R) KO mice and animals treated with an IL-1R antagonist are defective in hippocampal-dependent memory tasks, confirming that physiological levels of IL-1β are required for learning (Avital et al., 2003; Goshen et al., 2007; Yirmiya, 2002)

NMDA receptors (NMDARs) are the primary source of LTP-driving Ca^{2+} influx at hippocampal CA1 synapses (Kumar, 2011). IL-1β can strengthen glutamatergic synapses through Src-kinase mediated phosphorylation of NMDARs, thereby facilitating long-lasting Ca^{2+} influx (Viviani et al., 2003). Blocking IL-1R has no effect under basal conditions, consistent with a specific role during LTP (Zhu et al., 2006).

Interestingly, a CNS-specific isoform of the IL-1R accessory protein (AcP), AcPb, has been identified that is able to transduce IL-1β signals in neurons but not in lymphocytes (Smith et al., 2009). AcPb forms a functional complex with an IL-1R isoform, IL-1R3, that is preferentially expressed in the nervous system (Qian et al., 2012). These findings suggest that some degree of divergence has occurred between tissues. Therefore, although extensive immunological studies of IL-1 signaling provide a valuable framework for exploring its role in the neurons, they are not necessarily predictive of the specific signaling pathways used. IL-1β commonly signals through multiple intracellular pathways including nuclear factor kappa B proteins (NF-κB), c-Jun N-terminal kinases (JNKs), extracellular signal-regulated kinases (ERK) 1/2 and p38 mitogen-activated protein kinases (MAPKs) (Fig. 1.1A) (Risbud and Shapiro, 2014). In hippocampal cells, IL-1β signaling is independent of NF-κB, JNK and ERK1/2 activation (Choi and Friedman, 2009; Srinivasan et al., 2004). Instead, by inducing the p38 MAPK pathway it activates cyclic AMP response element binding protein (CREB), a transcription factor (TF) important for the formation long-term memory (Silva et al., 1998), but not a target of IL-1 in immune cells (Srinivasan et al., 2004).

TNFα controls homeostatic plasticity

Synaptic scaling occurs widely in the nervous system in response to a long-term reduction or overload in synaptic input (Turrigiano and Nelson, 2004; Turrigiano et al., 1998). TNFα, mostly of glial origin, regulates homeostatic upregulation of synaptic strength during activity blockade in the hippocampus, cortex and striatum (Lewitus et al., 2014; 2016; Stellwagen and Malenka, 2006). Hippocampal slices from TNF receptor (TNFR) KO mice are WT in terms of basal activity, but show abnormal changes during activity perturbation (Albensi and Mattson, 2000; Stellwagen and Malenka, 2006). Specifically, TNF signaling is upregulated by pre-synaptic blockade in the hippocampus, and functions to increase post-synaptic AMPA receptor (AMPAR) levels (Beattie et al., 2002; Stellwagen and Malenka, 2006). Similarly *in vivo*, after monocular deprivation,

the increased sensitivity of visual cortex neurons to input from the open eye depends on TNFα signaling (Kaneko et al., 2008). Interestingly, in GABAergic medium spiny neurons (MSNs) of the striatum, TNFα is again upregulated by activity blockade, but functions to reduce AMPAR currents (Lewitus et al., 2014). Together, these findings suggest that (i) TNFα serves to simultaneously promote excitatory and reduce inhibitory output during periods of low circuit activity and (ii) that its modulation of AMPAR currents may be secondary to specific effects that vary with neuronal type (Konefal and Stellwagen, 2017). Importantly, temporal delineation of the role played by TNFα during synaptic homeostasis showed that it is not itself a signal that correlates with scaling, but rather its long-term levels determine whether a synapse has the ability to induce scaling (i.e. it is permissive not instructive) (Steinmetz and Turrigiano, 2010).

One mechanism by which TNFα is able to influence AMPAR levels is by controlling the activity of protein phosphatase 1 (PP1). In MSN neurons, TNFα signaling downregulates DARP-32 phosphorylation, thereby activating PP1 and increasing AMAPR endoctytosis (Lewitus et al., 2014). PP1 also mediates TNFα-induced endocytosis of $GABA_A$ receptors ($GABA_A$Rs) in hippocampal neurons (Pribiag and Stellwagen, 2013). Like IL-1β, TNFα function depends on p38 MAPKs (Pribiag and Stellwagen, 2013). Unlike IL-1β however, TNFα signaling has no effect on CREB activation, but is mediated specifically by NF-κB (Albensi and Mattson, 2000; Choi and Friedman, 2009; Segond von Banchet et al., 2016). One reason that TNFα but not IL-1β signals through NF-κB in neurons is that IL-1β requires TRAF6 to activate NF-κB, whereas TNFα does not (Fig. 1.1B) (Cao et al., 1996); TRAF6 is highly expressed in immune cells, but was not detected in hippocampal neurons (Srinivasan et al., 2004).

Towards a network view of cytokines in the CNS

Although IL-1β and TNFα are the best-characterized examples, it is likely that other cytokines play a role in the healthy brain. Stimulation of cortical neurons upregulates IL-6 expression (Sallman et al., 2000). Furthermore, chemokines

such as SDF1/CXCL12, MCP1/CCL2 and fractalkine/CX3CL1 are constitutively expressed in neurons, are released in response to neural activity, and have neuromodulatory effects (Rostene et al., 2007). For example, both fractalkine and its receptor CX3CR1 are expressed by hippocampal neurons (Harrison et al., 1998; Meucci et al., 2000) and fractalkine expression is induced by spatial learning (Sheridan and Murphy, 2014).

Transcriptional fingerprinting during retrieval and extinction of fear-conditioned memories show that a number of chemokines and pro-inflammatory cytokines (including IL-1 and IL-6) are specifically associated with memory retrieval, while a non-overlapping range (that includes TNF receptor family genes) are associated with extinction (Scholz et al., 2016). This suggests that most cytokine-type neuromodulators are yet to be characterized.

Ancient origins of cytokinergic neuromodulation

Recent work in invertebrate models show that neuromodulation by cytokine-like molecules is an evolutionary conserved feature of nervous systems. Additionally, the remarkable conservation of the signaling pathways identified raises the hypothesis that homologous molecular mechanisms function in invertebrate and mammalian neurons.

In mammals, the Janus kinase/signal transducers and activators of transcription (JAK/STAT) pathway is an important intracellular target of Type I cytokines such as IL-6 (Fig. 1.1C) (O'Shea et al., 2002). Homologs of this signaling pathway are present in *Drosophila*, including a ligand, Unpaired (Upd), with an α-helical structure typical of the IL-6 family (Copf et al., 2011). Upd is expressed in a subset of mushroom body (MB) neurons, where it specifically promotes associative long-term memory (LTM) via JAK/STAT signaling (Copf et al., 2011). A second Upd family member, Upd2, acts as a neuromodulator in a manner analogous to human leptin (Rajan and Perrimon, 2012). By engaging JAK/STAT signaling in GABAergic neurons in well-fed flies, it reduces inhibitory signaling

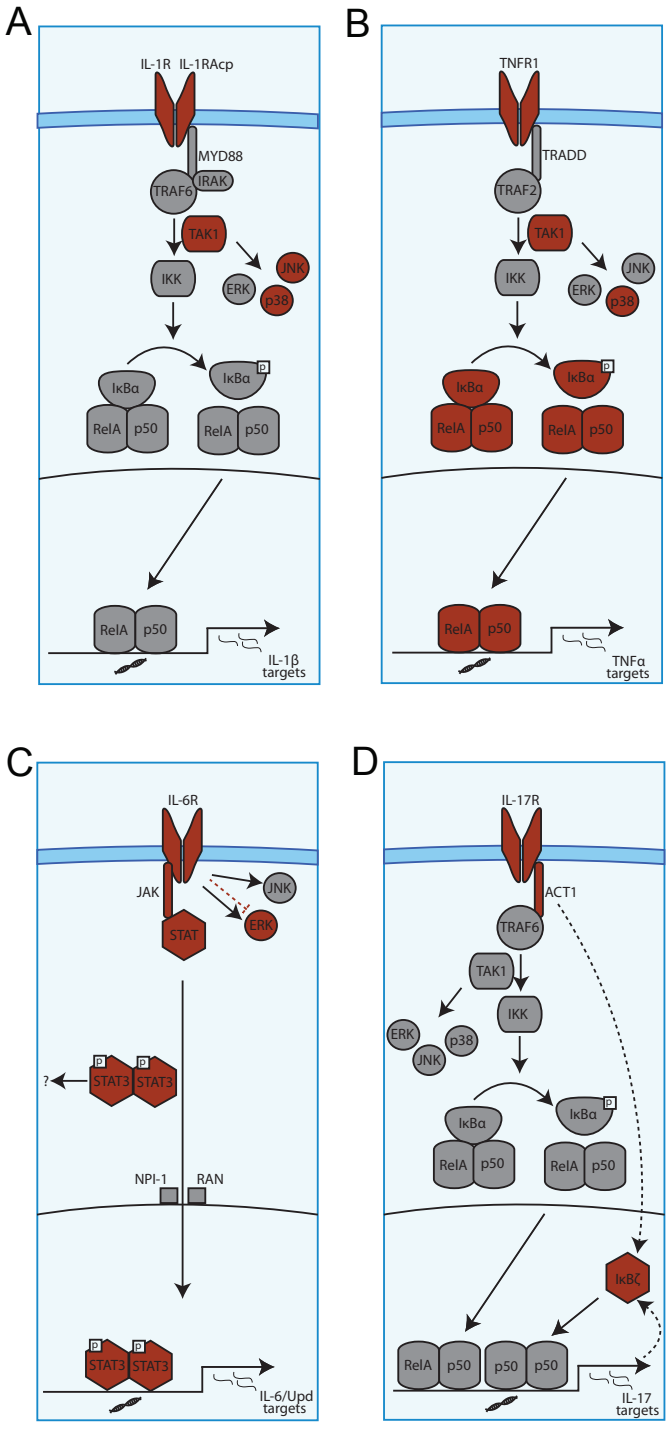

Figure 1.1 Inflammatory cytokine signaling pathways. Cytokine signaling components also implicated in neuromodulation are shown in red. (A) IL-1β stimulates the assembly of an IL-1R/Acp/MyD88/IRAK complex, which recruits TRAF6 to induce TAK1-mediated activation of IKK, JNK, ERK1/2, and p38 MAPK signaling. IKK phosphorylates IκB, triggering its ubiquitination and degradation, and allowing NF-κB complexes to translocate to the nucleus and activate transcription (O'Neill and Greene, 1998; Risbud and Shapiro, 2014). MAPK pathways have a large range of intracellular targets (Johnson and Lapadat, 2002). (B) TNFα drives IKK activation through the formation of a scaffolding complex containing TNFR-associated death domain (TRADD) and TRAF2 at TNFR1 (Aggarwal, 2003; Ting and Bertrand, 2016). (C) IL-6 type cytokines activate JAK tyrosine kinases, which phosphorylate latent cytoplasmic STAT TFs. Phosphorylated STATs dimerize and enter the nucleus, dependent on nucleoprotein-interactor 1 (NPI-1) and Ras-related nuclear protein (Ran), to drive transcription. STAT3 is able to directly interact with intracellular trafficking machinery, independent of its role in the nucleus (Gao and Bromberg, 2006; Rawlings, 2004). (D) In response to IL-17R activation, Act1 acts as a scaffolding hub for signaling molecules including TRAF6, culminating in the activation of NF-κB heterodimers. A non-canonical IκB, called IκBζ, boosts IL-17R/Act1 signaling by promoting the activity of NF-κB homodimers (Amatya et al., 2017; Johansen et al., 2015).

onto neurons that release insulin-like peptides (Rajan and Perrimon, 2012). Interestingly, JAK/STAT signaling mediates NMDAR-dependent LTD (NMDAR-LTD) in hippocampal neurons (Nicolas et al., 2012). Surprisingly however, this process does not depend on STAT TF activity – usually the culmination of JAK/STAT signaling (Sacktor, 2012); STAT3 is able to promote NMDAR-LTD without translocating to the nucleus (Nicolas et al., 2012). Together, these findings suggest that the role of JAK/STAT in neuromodulation of synaptic strength is conserved between diverged nervous systems. Additionally, they serve as motivation for exploring the function of IL-6 family cytokines in neuromodulation and learning. Indeed, there is already some evidence that IL-6 signals through STAT3 to modulate transmitter release and LTP (D'Arcangelo et al., 2000; Tancredi et al., 2000).

A recent study in *C. elegans* raises the possibility that IL-17 family cytokines may function as neuromodulators in the healthy brain. In worms, IL-17/ILC-17.1 and its receptors are constitutively expressed in hub neurons called RMG that integrate a variety of sensory responses (Chen et al., 2017). IL-17 signaling in RMG neurons specifically promotes these sensory responses and drives escape of unfavourable environments. The evidence so far suggests that signal transduction mechanisms engaged by mammalian IL-17 is at least partly conserved in worms. Like in mammals, *C. elegans* IL-17 receptors (IL-17Rs) contain an intracellular SEF/IL17R (SEFIR) domain, form a functional complex with an Act1-type adaptor, and signal through a non-canonical IκB (inhibitor of NF-κB) similar to IκBζ (Fig. 1.1D). Additionally, an IRAK (IL-1R-associated kinase)-like protein, usually associated with toll-like receptor or IL-1 signaling (Flannery and Bowie, 2010), is recruited to the IL-17Rs in RMG neurons. Interestingly, although IL-17 is thought to signal primarily through NF-κB (Amatya et al., 2017), no Rel homology transcription factors have been identified in *C. elegans* (Sullivan et al., 2009). Therefore, a different transcriptional regulator may be engaged by IL-17 signaling in neurons. In humans, IL-17 is known to induce neuroinflammation (Kang et al., 2013; Xiao et al., 2014), perhaps explaining its

link to anxiety and depression (Haroon et al., 2011; Liu et al., 2012), but its role under basal conditions in the CNS awaits investigation.

Specificity of signal transduction pathways

In general, molecular studies of the nervous system have been biased towards membrane proteins that sit at the interface of ion gradients and cell-cell communication (Kennedy, 2017). As a result, the intricate molecular signaling pathways that regulate or mediate the function of cell-surface receptors have been characterized in less detail in neurons than in other tissues. Yet, it is likely that they lie at the heart of a significant outstanding question in the study of cytokines in the nervous system: how do specific biological effects arise from common signals?

Several mechanisms have been proposed to explain the puzzling specificity of broadly expressed signaling proteins, including (i) qualitative or quantitative differences in their expression (ii) cell-specific proteomic context and (iii) the diversity of information encoded by Ca^{2+} signatures (Crabtree, 1999). The following examples suggest that all three contribute to the specificity of cytokine signaling.

1) As described above, neurons express a repertoire of IL-1β signal-transducers that is both qualitatively (AcPb) and quantitatively (IL-1R3) different from that of immune cells. By abolishing the ability of IL-1R complexes to recruit Myd88/ IRAK4, IL-1R3/AcPb complexes appear to direct signaling towards different downstream effectors (Qian et al., 2012; Smith et al., 2009). 2) Cytokines can engage different signaling pathways in different cell-types/conditions. The presence or absence of TRAF6 directs IL-1β signaling towards different fates in astrocytes and neurons (Choi and Friedman, 2009; Huang et al., 2011; Srinivasan et al., 2004). Additionally, for reasons that are not well understood, IL-1β specifically activates the p38 MAPK pathway in some contexts (Choi and Friedman, 2009; Srinivasan et al., 2004), but can also activate JNK signaling in

others (Curran et al., 2003; Vereker et al., 2000). Similarly, cellular context likely underlies the opposing effects of IL-6 signaling on ERK activity in neurons and other tissues; whereas in most cell-types IL-6 stimulates ERK activity, it deactivates ERK in the cerebral cortex to downregulate transmitter release (D'Arcangelo et al., 2000). 3) Both CREB and NF-κB are regulated by spatiotemporal Ca^{2+} codes (Berridge, 2010; Dolmetsch et al., 1998). The fact that, depending on cell-type, IL-1β can signal specifically through either of these Ca^{2+}-sensitive TFs (Srinivasan et al., 2004) suggests that Ca^{2+} profiles of a particular cell type influence the outcome of cytokine-receptor stimulation.

Regulation of gene expression

NF-κB and NFAT (nuclear factor of activated T cells) were initially thought to be lymphocyte-specific activators of inflammatory gene programmes (Sen and Baltimore, 1986; Shaw et al., 1988). Subsequent studies showed them to be constitutively expressed in neurons too (Ho et al., 1994; Kaltschmidt et al., 1994), where their translocation from the cytoplasm to the nucleus is driven by excitatory input and depolarization (Graef et al., 1999; Kaltschmidt et al., 1995). Interestingly, although both NF-κB and NFAT are activated by Ca^{2+}, their sensitivity to the frequency of Ca^{2+} oscillations differs – suggesting specific roles in linking Ca^{2+} signatures to transcriptional state (Dolmetsch et al., 1998). In the nervous system, synapse-to-nucleus signaling is fundamental to long-term, activity-dependent change (Tully, 1997; West et al., 2002). It is thought that Ca^{2+}-sensitive transcriptional regulators provide an important means of coupling synaptic use to gene expression during neuronal development and long-term plasticity (Berridge et al., 2000; West et al., 2002).

Recent work suggests that NF-κB and NFAT play opposing roles in regulating the persistence of associative memory (de la Fuente et al., 2011). Associative memories are thought to undergo two rounds of consolidation. Initially, training establishes changes in gene expression that stabilize the memory until it is first reactivated. Re-exposure to the training condition then disrupts this stabilization,

leaving memories open to either reconsolidation or extinction (Misanin et al., 1968). In mammals and crabs, NF-κB-mediated transcriptional changes are essential for reconsolidation, and inhibiting NF-κB is a mechanism used to promote extinction (Boccia et al., 2007; Merlo and Romano, 2008). Extinction itself is also an active process that depends on changes in gene expression mediated by NFAT (la Fuente et al., 2011). Inhibition of NFAT signaling promotes reconsolidation in a manner dependent on NF-κB, suggesting that altering the balance in activity of these two TFs is used as a transcriptional switch to determine the fate of re-activated memories in the hippocampus (la Fuente et al., 2011; 2014).

A range of extracellular and intracellular factors regulate the activity NF-κB and NFAT in lymphyocytes, making them important nodes for the integration of Ca^{2+} and other signaling cues (Macian, 2005; Zhang et al., 2017). In the nervous system, neuromodulators (Choi and Friedman, 2009; Kim et al., 2014) and ion-permeable cell-surface receptors (Kaltschmidt et al., 1995; Murphy et al., 2014; Sheridan et al., 2007) are important upstream regulators.

A number of intracellular Ca^{2+} sensors converge on NF-κB, including PKC, PI3K/Akt, and calmodulin (CaM) (Lilienbaum and Israel, 2003). The CaM-regulated phosphatase calcineurin maintains constitutive NF-κB activity, while Ca^{2+}/CaM-dependent protein kinase II (CAMKII) contributes to full NF-κB activation following Ca^{2+} influx (Lilienbaum and Israel, 2003). Interestingly, TNFα-induced NF-κB activation does not proceed via IκB degradation, indicating that an alternative pathway, such as MEKK-3-dependent IκB-dissociation (Yao et al., 2007), facilitates NF-κB activation in hippocampal neurons (Choi and Friedman, 2009). Furthermore, contrary to its role in immune cells, NF-κB ‘inducing’ kinase (NIK) was found to inhibit NF-κB in neurons, suggesting that regulatory mechanisms vary between tissues (Mao et al., 2016).

Dephosphorylation of NFAT by calcineurin drives its nuclear localization in response to Ca^{2+} signaling. The Ca^{2+} signatures sufficient to keep NFAT in the nucleus, however, differ between lymphocytes, where a prolonged Ca^{2+} increase is required, and neurons, where a short spike is sufficient (Graef et al., 1999). Phosphorylation by glycogen synthase kinase-3β (GSK-3β) is one means of driving nuclear export of NFAT in neurons (Graef et al., 1999), but otherwise mechanisms that regulate its localization in the CNS are not well understood.

An interesting question is how NF-κB and NFAT interact with other Ca^{2+}-dependent neuronal TFs. Cooperative function of different transcription and epigenetic factors is a common feature of transcriptional regulation (Reiter et al., 2017). Indeed, NF-κB is known to coordinate with multiple chromatin remodelers and TFs to activate transcription (Pradhan et al., 2011; Wienerroither et al., 2015). In the hippocampus, it promotes the function of histone acetyltransferase(s) to potentiate memory consolidation (Federman et al., 2013). Importantly, NF-κB-dependent histone acetylation at the *Camk2d* locus is required for the upregulation of CAMKIIδ during memory stabilization (Federman et al., 2013). Furthermore, the expression of hippocampal MHCI, required for use-dependent synaptic plasticity, is upregulated by the combined action of NF-κB, CREB, and IRF-1 (Lv et al., 2015).

One well-characterized target of NFAT in the hippocampus is IP_3R1 (1,4,5 inositol triphosphate receptor 1), which controls Ca^{2+} release from endoplasmic reticulum (ER) and is essential for LTD (Graef et al., 1999; Sugawara et al., 2013). Activator protein 1 (AP-1) is the most common transcriptional partner of NFAT (Jain et al., 2002; Macian, 2005), although others, such as Sox10 in Schwann cells, have been described (Kao et al., 2009). AP-1 was ruled out as a potential NFAT binding partner for hippocampal IP_3R1 regulation (Graef et al., 1999), so transcriptional complexes formed by NFAT in the nervous system remain uncharacterized. Intriguingly, the promoter of the brain-derived neurotrophic factor (BDNF) gene harbours binding sites for CREB, NFAT and

CaRF (Calcium Regulatory Factor) (Groth and Mermelstein, 2003). It will be interesting to discover whether Ca^{2+}-sensitive TFs commonly regulate the same genes, and if so how they function in combination.

The transcriptional targets of NF-κB and NFAT in neurons represent a significant gap in our understanding of long-term plasticity. CAMKIIδ, MHCI and IP_3R1 are strong candidates for the molecular link between proinflammatory transcription factors and synaptic plasticity, but it is as yet unknown whether they are functionally relevant targets. Attempts to gain a transcriptome-wide gene expression profiles during learning will also be valuable. Finally, uncovering the full repertoire of transcription factors and their targets regulated by neuromodulatory cyotokine signaling is an important long-term goal.

Modulation of the 21% O_2-escape circuit of *C. elegans*

Many general principles of neuromodulation have been gleaned from studies of simple nervous systems (Marder et al., 2014). With only 302 neurons, the nematode *C. elegans* offers an opportunity to dissect neural circuits coordinating behavioural responses at single-cell resolution. The small size of this nervous system does not, however, reflect a reduced repertoire of neuromodulatory systems. On the contrary, the fact that *C. elegans* expresses almost as many peptide neuromodulators as neurons suggests that the structural simplicity of its nervous system carries hidden complexity in terms of molecular modulation (Schafer, 2016). Neuromodulatory pathways, such as cytokine signaling, continue to be uncovered, so it is not yet known how rich this picture is in its entirety.

As a rapidly reproducing, hermaphroditic, genetically-tractable organism, *C. elegans* offers special opportunities to study neuromodulatory mechanisms. As a case in point, the unexpected role for IL-17 signaling in promoting specific sensory responses was identified by a forward genetic screen for mutants

defective in aggregation behaviour (Chen et al., 2017). Here, we further exploit this approach and describe novel molecular mechanisms that regulate behaviour.

Aggregation describes the accumulation of foraging nematode populations in the thickest regions of a bacteria food lawn (Fig. 1.2A) (de Bono and Bargmann, 1998). It is driven largely by the activity of sensory neurons that are stimulated when O_2 concentrations approach 21% (Cheung et al., 2004; Gray et al., 2004). Two neurons in the head, called URX, extend dendritic endings to the tip of the nose. Two additional O_2 sensors, AQR and PQR, have sensory endings exposed to the pseudocoelomic body fluid and thereby tuned to internal O_2 conditions. In mid-low O_2 concentrations (~7%), preferred by *C. elegans*, these neurons show low activity. When O_2 levels rise to 21%, URX, AQR and PQR sensory receptors signal to downstream neurons to initiate first a transient bout of re-orientation as animals seek to avoid the 21% O_2, and then, if this fails, a switch to rapid locomotion that is sustained until the animal has escaped the stimulus (Busch et al., 2012). The responses that enable *C. elegans* to avoid and escape 21% O_2 also enable them to aggregate, since groups of animals generate local low O_2 environments. Animals kept in 7% O_2 do not aggregate.

The ecological relevance of 21% O_2-avoidance for *C. elegans* is not clear, but it is known that O_2-deprived environments such as decomposing fruits and plants make the primary natural habitat for this animal (Frézal and Félix, 2015). Environmental O_2 might be a proxy for the availability of food, or dangers associated with surface exposure. Although almost all known wild isolates aggregate and avoid 21% O_2, these behaviours were lost in the N2 laboratory reference strain that accumulated a gain of function mutation in the neuropeptide receptor NPR-1 during domestication (Rockman and Kruglyak, 2009; Weber et al., 2010). Circuit-level dissection of NPR-1 function showed that it acts primarily to inhibit the activity of RMG hub interneurons (Macosko et al., 2009; Laurent et al., 2015). RMG neurons are connected by gap junctions to (i) URX O_2 sensors (ii) ASH and ADL nociceptors and (iii) ASK pheromone receptors, and therefore

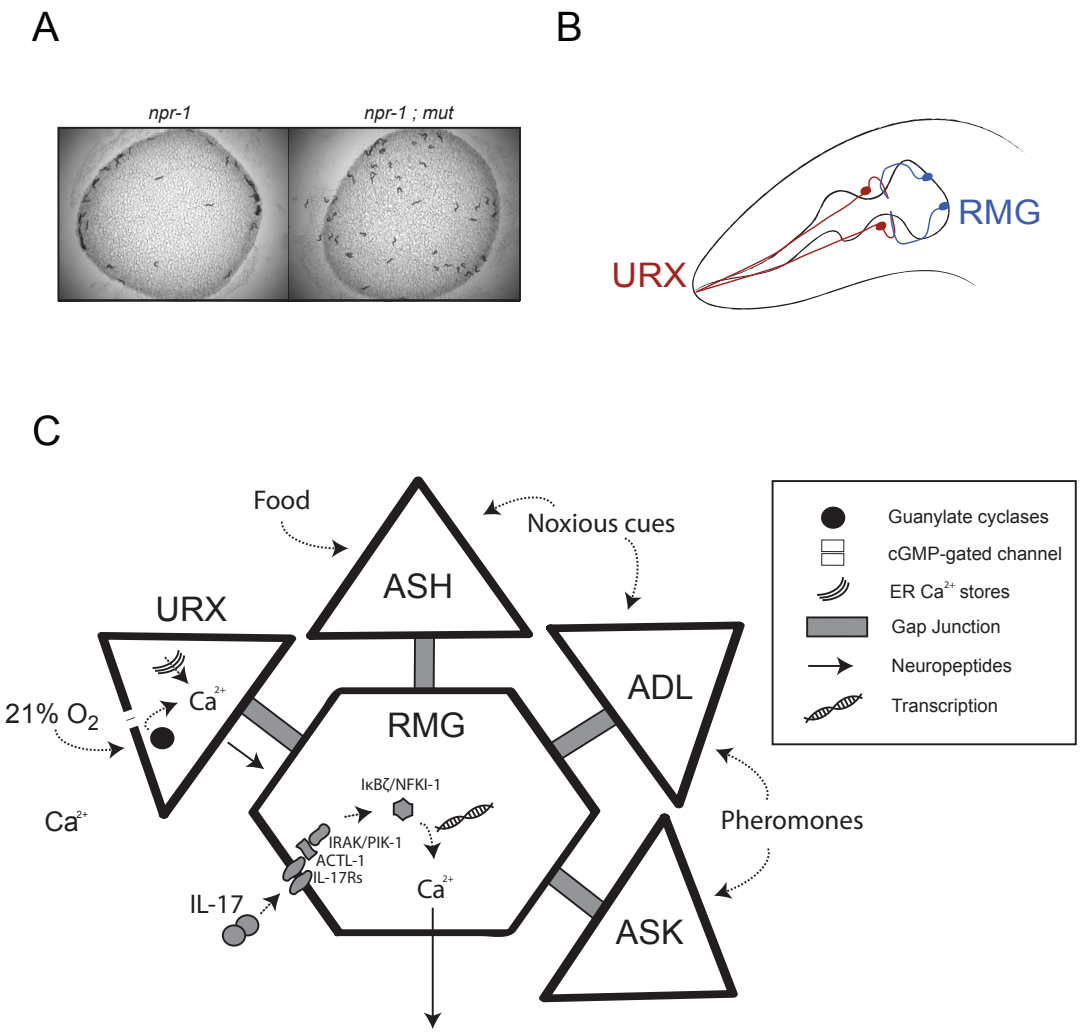

Figure 1.2 Signaling from URX and RMG drives aggregation behaviour. (A) *npr-1* animals aggregate on the borders of an *E. coli* food lawn (left). Mutants isolated in an EMS-based genetic screen do not (right). (B) Cartoon showing the location of URX and RMG neuron pairs in the anterior of the worm. (C) RMG hub-and-spoke circuit. URX and other sensory neurons (spokes) are connected by electrical synapses to RMG (hub). High activity in RMG drives fast forward speed through peptidergic communication with downstream command interneurons (Jang et al., 2017; Laurent et al., 2015; Macosko et al., 2009). In 21% O_2, URX tonically activates RMG via gap junctions and neuropeptide transmission. O_2-sensation in URX is mediated by soluble guanylate cylcases (GCY-35/GCY-36) that synthesize cGMP and stimulate opening of cGMP-gated ion channels (TAX-2/TAX-4). Ca^{2+} release from intracellular stores is necessary to sustain tonic URX activity (Busch et al., 2012). IL-17 signaling enhances the input-output ratio of RMG, promoting Ca^{2+} signaling and neuropeptide secretion in response to 21% O_2. An IL-17R/Actl-1/IRAK complex signals to IκBζ to mediate neuromodulation by IL-17 (Chen et al., 2017).

serve as a site of integration for sensory information (Fig. 1.2C). In 21% O_2, chronically high activity in RMG drives fast locomotion through the secretion of

neuropeptides (Laurent et al., 2015). IL-17 enhances O_2-evoked Ca^{2+} responses in RMG and sustains this behavioural state (Chen et al., 2017). Consequently, blocking IL-17 signaling attenuates behavioural responses to pheromones and 21% O_2, without any noticeable effect on other sensory modalities.

The goal of this project was to characterize additional molecular mechanisms that regulate the URX-RMG circuit. A collection of *npr-1* animals that fail to aggregate had already been generated by EMS-mutagenesis, providing a resource for gene discovery. Using a combination of linkage analysis, reverse genetics and transgenic rescue experiments, I identified the causal genetic loci in several of these mutants. Then, using Ca^{2+} imaging to explore their function *in vivo* I focused on novel genes that modulate the responsiveness of the URX-RMG circuit.

In Chapter 2 I explore the signal transduction mechanisms that mediate neuromodulation by IL-17, and show that the paracaspase MALT1 is critical for promoting RMG responsiveness. In chapter 3 I explore the role of a putative Ca^{2+}-regulated TF, CAMTA. I propose that CAMTA has pan-neuronal function in regulating Ca^{2+} homeostasis and adaptation. In chapter 4 I demonstrate that accessory subunits of the eIF3 complex, a universal component of the translation initiation machinery, play a specific regulatory role in neurons. In chapter 5 I present additional, as yet uncharacterized, genes linked to aggregation and consider approaches for probing the natural genetic basis and evolution of this behaviour. Finally in chapter 6 I discuss major questions raised by this work and hypotheses that can now be tested more directly.

References

Aggarwal, B.B. (2003). Signalling pathways of the TNF superfamily: a double-edged sword. Nat Rev Immunol *3*, 745–756.

Albensi, B., and Mattson, M.P. (2000). Evidence for the Involvement of TNF and NF-κB in Hippocampal Synaptic Plasticity. Synapse *35*, 151–159.

Amatya, N., Garg, A.V., and Gaffen, S.L. (2017). IL-17 Signaling: The Yin and the Yang. Trends in Immunology. doi: 10.1016–j.it.2017.01.006.[Epub ahead of print].

Avital, A., Goshen, I., Kamsler, A., Segal, M., Iverfeldt, K., Richter-Levin, G., and Yirmiya, R. (2003). Impaired interleukin-1 signaling is associated with deficits in hippocampal memory processes and neural plasticity. Hippocampus *13*, 826–834.

Bauer, S., Kerr, B.J., and Patterson, P.H. (2007). The neuropoietic cytokine family in development, plasticity, disease and injury. Nat Rev Neurosci *8*, 221–232.

Beattie, E.C., Stellwagen, D., Morishita, W., Bresnahan, J.C., Keun Ha, B., Zastrow, Von, M., Beattie, M.S., and Malenka, R.C. (2002). Control of Synaptic Strength by Glial TNFα. Science *295*, 2282–2285.

Berridge, M.J. (2010). Calcium Signalling and Alzheimer's Disease. Neurochem Res *36*, 1149–1156.

Berridge, M.J., Lipp, P., and Bootman, M.D. (2000). THE VERSATILITY AND UNIVERSALITY OF CALCIUM SIGNALLING. Nat Rev Mol Cell Biol *1*, 11–21.

Boccia, M., Freudenthal, R., Blake, M., la Fuente, de, V., Acosta, G., Baratti, C., and Romano, A. (2007). Activation of hippocampal nuclear factor-kappa B by retrieval is required for memory reconsolidation. J Neurosci *27*, 13436–13445.

Boulanger, L.M. (2009). Immune Proteins in Brain Development and Synaptic Plasticity. Neuron *64*, 93–109.

Boulanger, L.M., and Shatz, C.J. (2004). Immune signalling in neural development, synaptic plasticity and disease. Nat Rev Neurosci *5*, 521–531.

Boulanger, L.M., Huh, G.S., and Shatz, C.J. (2001). Neuronal plasticity and cellular immunity: shared molecular mechanisms Lisa M Boulanger. Curr Opin Neurobiol *11*, 568–578.

Breder, C.D., Dinarello, C.A., and Saper, C.B. (1988). Interleukin-1 immunoreactive innervation of the human hypothalamus. Science *240*, 321–324.

Brennan, F.X., Beck, K.D., and Servatius, R.J. (2003). Low doses of interleukin-1β improve the leverpress avoidance performance of Sprague–Dawley rats. Neurobiol Learn Mem *80*, 168–171.

Busch, K.E., Laurent, P., Soltesz, Z., Murphy, R.J., Faivre, O., Hedwig, B., Thomas, M., Smith, H.L., and de Bono, M. (2012). Tonic signaling from O2 sensors sets neural circuit activity and behavioral state. Nat Neurosci *15*, 581–591.

Cao, Z., Xiong, J., Takeuchi, M., Kurama, T., and Goeddel, D.V. (1996). TRAF-6 is a signal transducer for interleukin-1. Nature *383*, 443–446.

Chen, C., Itakura, E., Nelson, G.M., Sheng, M., Laurent, P., Fenk, L.A., Butcher, R.A., Hegde, R.S., and de Bono, M. (2017). IL-17 is a neuromodulator of Caenorhabditis elegans sensory responses. Nature *542*, 43–48.

Cheung, B.H.H., Arellano-Carbajal, F., Rybicki, I., and de Bono, M. (2004). Soluble Guanylate Cyclases Act in Neurons Exposed to the Body Fluid to Promote C. elegans Aggregation Behavior. Curr Biol *14*, 1105–1111.

Choi, S., and Friedman, W.J. (2009). Inflammatory Cytokines IL-1 βand TNF-αRegulate p75 NTRExpression in CNS Neurons and Astrocytes by Distinct Cell-Type-Specific Signalling Mechanisms. ASN Neuro *1*, AN20090009–AN20090011.

Copf, T., Goguel, V., Lampin-Saint-Amaux, A., Scaplehorn, N., and Preat, T. (2011). Cytokine signaling through the JAK/STAT pathway is required for long-term memory in Drosophila. Proc Natl Acad Sci USA *108*, 8059–8064.

Crabtree, G.R. (1999). Generic Signals and Specific Minireview: Signaling through Ca^{2+}, Calcineurin, and NF-AT. Cell *96*, 611–614.

Curran, B.P., Murray, H.J., and O'Connor, J.J. (2003). A role for c-jun n-terminal kinase in the inhibition of long-term potentiation by interleukin-1β and long-term depression in the rat dentate gyrus in vitro. Neuroscience *118*, 347–357.

D'Arcangelo, G., Tancredi, V., Onofri, F., DAntuono, M., Giovedi, S., and Benfenati, F. (2000). Interleukin-6 inhibits neurotransmitter release and the spread of excitation in the rat cerebral cortex. Eur J Neurosci *12*, 1241–1252.

de Bono, M., and Bargmann, C.I. (1998). Natural Variation in a Neuropeptide Y Receptor Homolog Modifies Social Behavior and Food Response in. Cell *94*, 679–689.

Dolmetsch, R.E., Xu, K., and Lewis, R.S. (1998). Calcium oscillations increase the efficiency and specificity of gene expression. Nature *392*, 933–936.

Federman, N., la Fuente, de, V., Zalcman, G., Corbi, N., Onori, A., Passananti, C., and Romano, A. (2013). Nuclear Factor κB-Dependent Histone Acetylation is Specifically Involved in Persistent Forms of Memory. Journal of Neuroscience *33*, 7603–7614.

Flannery, S., and Bowie, A.G. (2010). The interleukin-1 receptor-associated kinases: Critical regulators of innate immune signalling. Biochemical Pharmacology *80*, 1981–1991.

Frézal, L., and Félix, M.-A. (2015). C. elegans outside the Petri dish. eLife

4:e05849.

Gao, S.P., and Bromberg, J.F. (2006). Touched and Moved by STAT3. Science Signaling *343*, pe30.

Sheridan, G.K., and Murphy, K.J. (2014). CX3CL1 is up-regulated in the rat hippocampus during memory-associated synaptic plasticity. Front Cell Neurosci *8*, Article233.

Goshen, I., Kreisel, T., Ounallah-Saad, H., Renbaum, P., Zalzstein, Y., Ben Hur, T., Levy-Lahad, E., and Yirmiya, R. (2007). A dual role for interleukin-1 in hippocampal-dependent memory processes. Psychoneuroendocrinology *32*, 1106–1115.

Graef, I.A., Mermelstein, P.G., Stankunas, K., Neilson, J.R., Deisseroth, K., Tsien, R.W., and Crabtree, G.R. (1999). L-type calcium channels and GSK-3 regulate the activity of NF-ATc4 in hippocampal neurons. Nature *401*, 703–708.

Gray, J.M., Karow, D.S., Lu, H., Chang, A.J., Chang, J.S., Ellis, R.E., Marletta, M.A., and Bargmann, C.I. (2004). Oxygen sensation and social feeding mediated by a C. elegans guanylate cyclase homologue. Nature *430*, 317–322.

Groth, R.D., and Mermelstein, P.G. (2003). Brain-Derived Neurotrophic Factor Activation of NFAT (Nuclear Factor of Activated T-Cells)-Dependent Transcription: A Role for the Transcription Factor NFATc4 in Neurotrophin-Mediated Gene Expression. J Neurosci *23*, 8125–8134.

Habibi, L., Ebtekar, M., and Jameie, S.B. (2009). Immune and Nervous Systems Share Molecular and Functional Similarities: Memory Storage Mechanism. Scandinavian J Immunol *69*, 291–301.

Haroon, E., Raison, C.L., and Miller, A.H. (2011). Psychoneuroimmunology Meets Neuropsychopharmacology: Translational Implications of the Impact of Inflammation on Behavior. Neuropsychopharmacology *37*, 137–162.

Harrison, J.K., Jiang, Y., Chen, S., Xia, Y., Maciejewski, D., McNamara, R.K., Streit, W.J., Salafranca, M.N., Adhikari, S., Thompson, D.A., et al. (1998). Role for neuronally derived fractalkine in mediating interactions between neurons and CX3CR1-expressing microglia. Proc Natl Acad Sci USA *95*, 10896–10901.

Heppner, F.L., Ransohoff, R.M., and Becher, B. (2015). Immune attack: the role of inflammation in Alzheimer disease. Nat Rev Neurosci *16*, 358–372.

Ho, A.M., Jain, J., Rao, A., and Hogan, P.G. (1994). Expression of the Transcription Factor NFATp in a Neuronal Cell Line andin the Murine Nervous System. J Biol Chem *269*, 28181–28186.

Huang, Y., Smith, D.E., Ibanez-Sandoval, O., Sims, J.E., and Friedman, W.J.

(2011). Neuron-Specific Effects of Interleukin-1 Are Mediated by a Novel Isoform of the IL-1 Receptor Accessory Protein. J Neurosci *31*, 18048–18059.

Huh, G.S., Boulanger, L.M., Du, H.D., Riquelme, P.A., Brotz, T.M., and Shatz, C.J. (2000). Functional Requirement for Class I MHC in CNS Development and Plasticity. Science *290*, 2155–2159.

Jain, J., McCaffrey, P.G., Valge-Archer, V.E., and Rao, A. (2002). Nuclear factor of activated T cells contains Fos and Jun. Nature *356*, 801–804.

Jang, H., Levy, S., Flavell, S.W., Mende, F., Latham, R., Zimmer, M., and Bargmann, C.I. (2017). Dissection of neuronal gap junction circuits that regulate social behavior in Caenorhabditis elegans. Proc. Natl. Acad. Sci. U.S.a. *114*, E1263–E1272.

Jerne, N.K. (1984). THE GENERATIVE GRAMMAR OF. Nobel Lecture.

Johansen, C., Mose, M., Ommen, P., Bertelsen, T., Vinter, H., Hailfinger, S., Lorscheid, S., Schulze-Osthoff, K., and Iversen, L. (2015). IκBζ is a key driver in the development of psoriasis. Proc Natl Acad Sci USA *112*, E5825–E5833.

Johnson, G.L., and Lapadat, R. (2002). Mitogen-Activated Protein Kinase Pathways Mediated by ERK, JNK, and p38 Protein Kinases. Science *298*, 1911–1912.

Kaltschmidt, C., Kaltschmidt, B., and Baeuerle, P.A. (1995). Stimulation of ionotropic glutamate receptors activates transcription factor NF-κB in primary neurons. Proc Natl Acad Sci USA *92*, 9618–9622.

Kaltschmidt, C., Kaltschmidt, B., Neumann, H., Wekerle, H., and Baeuerle, P.A. (1994). Constitutive NF-KB Activity in Neurons. Molecular and Cellular Biology *14*, 3981–3992.

Kaneko, M., Stellwagen, D., Malenka, R.C., and Stryker, M.P. (2008). Tumor Necrosis Factor-α Mediates One Component of Competitive, Experience-Dependent Plasticity in Developing Visual Cortex. Neuron *58*, 673–680.

Kang, Z., Wang, C., Zepp, J., Wu, L., Sun, K., Zhao, J., Chandrasekharan, U., DiCorleto, P.E., Trapp, B.D., Ransohoff, R.M., et al. (2013). Act1 mediates IL-17–induced EAE pathogenesis selectively in NG2+ glial cells. Nat Neurosci *16*, 1401–1408.

Kao, S.-C., Wu, H., Xie, J., Chang, C.-P., Ranish, J.A., Graef, I.A., and Crabtree, G.R. (2009). Calcineurin/NFAT Signaling Is Required for Neuregulin-Regulated Schwann Cell Differentiation. Science *323*, 651–654.

Kennedy, M.B. (2017). ScienceDirect Biochemistry and neuroscience: the twain need to meet. Current Opinion in Neurobiology *43*, 79–86.

Kim, M.S., Shutov, L.P., Gnanasekaran, A., Lin, Z., Rysted, J.E., Ulrich, J.D., and Usachev, Y.M. (2014). Nerve growth factor (NGF) regulates activity of nuclear factor of activated T-cells (NFAT) in neurons via the phosphatidylinositol 3-kinase (PI3K)-Akt-glycogen synthase kinase 3β (GSK3β) pathway. J. Biol. Chem. *289*, 31349–31360.

Kioussis, D., and Pachnis, V. (2009). Immune and Nervous Systems: More Than Just a Superficial Similarity? Immunity *31*, 705–710.

Kipnis, J. (2016). Multifaceted interactions between adaptive immunity and the central nervous system. Science 766–771.

Konefal, S.C., and Stellwagen, D. (2017). Tumour necrosis factor-mediated homeostatic synaptic plasticity in behavioural models: testing a role in maternal immune activation. Phil. Trans. R. Soc. B *372*, 20160160–12.

Kumar, A. (2011). Long-term potentiation at CA3–CA1 hippocampal synapses with special emphasis on aging, disease, and stress. Front Aging Neurosci *3*, 7.

de la Fuente, V., Freudenthal, R., and Romano, A. (2011). Reconsolidation or Extinction: Transcription Factor Switch in the Determination of Memory Course after Retrieval. J Neurosci *31*, 5562–5573.

de la Fuente, V., Federman, N., Fustiñana, M.S., Zalcman, G., and Romano, A. (2014). Calcineurin phosphatase as a negative regulator of fear memory in hippocampus: Control on nuclear factor- κB signaling in consolidation and reconsolidation. Hippocampus *24*, 1549–1561.

Laurent, P., Soltesz, Z., Nelson, G.M., Chen, C., Arellano-Carbajal, F., Levy, E., and de Bono, M. (2015). Decoding a neural circuit controlling global animal state in C. elegans. eLife *4*, e04241.

Lewitus, G.M., Pribiag, H., Duseja, R., St-Hilaire, M., and Stellwagen, D. (2014). An Adaptive Role of TNF in the Regulation of Striatal Synapses. J Neurosci *34*, 6146–6155.

Lewitus, G.M., Konefal, S.C., Greenhalgh, A.D., Pribiag, H., Augereau, K., and Stellwagen, D. (2016). Microglial TNF-α Suppresses Cocaine-Induced Plasticity and Behavioral Sensitization. Neuron *90*, 483–491.

Lilienbaum, A., and Israel, A. (2003). From Calcium to NF-κB Signaling Pathways in Neurons. Mol Cell Biol *23*, 2680–2698.

Liu, Y., Ho, R.C.-M., and Mak, A. (2012). The role of interleukin (IL)-17 in anxiety and depression of patients with rheumatoid arthritis. International Journal of Rheumatic Diseases *15*, 183–187.

Lv, D., Shen, Y., Peng, Y., Liu, J., Miao, F., and Zhang, J. (2015). Neuronal MHC

Class I Expression Is Regulated by Activity Driven Calcium Signaling. PLoS ONE *10*, e0135223–16.

Macian, F. (2005). NFAT proteins: key regulators of T-cell development and function. Nat Rev Immunol *5*, 472–484.

Macosko, E.Z., Pokala, N., Feinberg, E.H., Chalasani, S.H., Butcher, R.A., Clardy, J., and Bargmann, C.I. (2009). A hub-and-spoke circuit drives pheromone attraction and social behaviour in C. elegans. Nature *458*, 1171–1175.

Mao, X., Phanavanh, B., Hamdan, H., Moerman-Herzog, A.M., and Barger, S.W. (2016). NFκB-inducing kinase inhibits NFκB activity specifically in neurons of the CNS. J Neurochem *137*, 154–163.

Marder, E. (2012). Neuromodulation of Neuronal Circuits: Back to the Future. Neuron *76*, 1–11.

Marder, E., O'Leary, T., and Shruti, S. (2014). Neuromodulation of Circuits with Variable Parameters: Single Neurons and Small Circuits Reveal Principles of State-Dependent and Robust Neuromodulation. Annu Rev Neurosci. *37*, 329–346.

Martin, S.J., Grimwood, P.D., and Morris, R. (2000). SYNAPTIC PLASTICITY AND MEMORY: An Evaluation of the Hypothesis. Annu Rev Neurosci. *23*, 649–711.

Merlo, E., and Romano, A. (2008). Memory Extinction Entails the Inhibition of the Transcription Factor NF-κB. PLoS ONE *3(11)*, e3687.

Meucci, O., Fatatis, A., Simen, A.A., and Miller, R.J. (2000). Expression of CX3CR1 chemokine receptors on neurons and their role in neuronal survival. Proc Natl Acad Sci USA *97*, 8075–8080.

Misanin, J.R., Miller, R.R., and Lewis, D.J. (1968). Retrograde Amnesia Produced by Electroconvulsive Shock after Reactivation of a Consolidated Memory Trace. Science *160*, 554–555.

Murphy, J.G., Sanderson, J.L., Gorski, J.A., Scott, J.D., Catterall, W.A., Sather, W.A., and Dell'Acqua, M.L. (2014). AKAP-Anchored PKA Maintains Neuronal L-type Calcium Channel Activity and NFAT Transcriptional Signaling. Cell Rep *7*, 1577–1588.

Murray, C.A., and Lynch, M.A. (1998). Evidence That Increased Hippocampal Expression of the Cytokine Interleukin-1. J Neurosci *15*, 2974–2981.

Nicolas, C.S., Peineau, S., Amici, M., Csaba, Z., Fafouri, A., Javalet, C., Collett, V.J., Hildebrandt, L., Seaton, G., Choi, S.-L., et al. (2012). The JAK/STAT Pathway Is Involved in Synaptic Plasticity. Neuron *73*, 374–390.

O'Neill, L., and Greene, C. (1998). Signal transduction pathways activated by the IL-1 receptor family: ancient signaling machinery in mammals, insects, and plants. J Leukoc Biol *63*, 650–657.

O'Shea, J.J., Gadina, M., and Schreiber, R.D. (2002). Cytokine Signaling in 2002: Review New Surprises in the Jak/Stat Pathway. Cell *109*, S121–S131.

Pradhan, M., Baumgarten, S.C., Bembinster, L.A., and Frasor, J. (2011). CBP Mediates NF-κB-Dependent Histone Acetylation and Estrogen Receptor Recruitment to an Estrogen Response Element in the BIRC3 Promoter. Mol Cell Biol *32*, 569–575.

Pribiag, H., and Stellwagen, D. (2013). TNF-α Downregulates Inhibitory Neurotransmission through Protein Phosphatase 1-Dependent Trafficking of GABAA Receptors. J Neurosci *33*, 15879–15893.

Pribiag, H., and Stellwagen, D. (2014). Neuroimmune regulation of homeostatic synaptic plasticity. Neuropharmacology *78*, 13–22.

Qian, J., Zhu, L., Li, Q., Belevych, N., Chen, Q., Zhao, F., Herness, S., and Quan, N. (2012). Interleukin-1R3 mediates interleukin-1–induced potassium current increase through fast activation of Akt kinase. Proc Natl Acad Sci USA *109*, 12189–12194.

Rajan, A., and Perrimon, N. (2012). Drosophila Cytokine Unpaired 2 Regulates Physiological Homeostasis by Remotely Controlling Insulin Secretion. Cell *151*, 123–137.

Rawlings, J.S. (2004). The JAK/STAT signaling pathway. J Cell Sci *117*, 1281–1283.

Reiter, F., Wienerroither, S., and Stark, A. (2017). Combinatorial function of transcription factors and cofactors. Curr Opin Genet Dev *43*, 73–81.

Risbud, M.V., and Shapiro, I.M. (2014). Role of cytokines in intervertebral disc degeneration: pain and disc content. Nat Rev Rheumatol *10*, 44–56.

Rockman, M.V., and Kruglyak, L. (2009). Recombinational Landscape and Population Genomics of Caenorhabditis elegans. PLoS Genet *5*, e1000419–16.

Rostene, W., Kitabgi, P., and Parsadaniantz, S.M. (2007). Chemokines: a new class of neuromodulator? Nat Rev Neurosci *8*, 895–904.

Sacktor, T.C. (2012). JAK/STAT: The Enigma within the Mystery of NMDAR-LTD. Neuron *73*, 211–213.

Sallman, S., Jüttler, E., Pinz, S., Petersen, N., Knopf, U., Weiser, T., and Schwaninger, M. (2000). Induction of Interleukin-6 by Depolarization of Neurons.

J Neurosci *20*, 8637–8642.

Schafer, W. (2016). Nematode nervous systems. Curr Biol *26*, R955–R959.

Schneider, H., Pitossi, F., Balschun, D., Wagner, A., Del Rey, A., and Besedovsky, H.O. (1998). A neuromodulatory role of interleukin-1. Proc Natl Acad Sci USA *95*, 7778–7783.

Scholz, B., Doidge, A.N., Barnes, P., Hall, J., Wilkinson, L.S., and Thomas, K.L. (2016). The Regulation of Cytokine Networks in Hippocampal CA1 Differentiates Extinction from Those Required for the Maintenance of Contextual Fear Memory after Recall. PLoS ONE *11*, e0153102–e0153129.

Segond von Banchet, G., König, C., Patzer, J., Eitner, A., Leuchtweis, J., Ebbinghaus, M., Boettger, M.K., and Schaible, H.-G. (2016). Long-Lasting Activation of the Transcription Factor CREB in Sensory Neurons by Interleukin-1β During Antigen-Induced Arthritis in Rats: A Mechanism of Persistent Arthritis Pain? Arthritis Rheumatol *68*, 532–541.

Sen, R., and Baltimore, D. (1986). Inducibility of κ Immunoglobin Enhancer-Binding Protein NF-κB by a Posttranslational Mechanism. Cell *47*, 921–928.

Shaw, J.-P., Utz, P.J., Durand, D.B., Toole, J.J., Emmel, E.A., and Crabtree, G.R. (1988). Identification of a Putative Regulator of Early T Cell Activation Genes. Science *241*, 202–205.

Sheridan, G.K., Pickering, M., Twomey, C., Moynagh, P.N., O'Connor, J.J., and Murphy, K.J. (2007). NF-κB activity in distinct neural subtypes of the rat hippocampus: Influence of time and GABA antagonism in acute slice preparations. Learn Mem *14*, 525–532.

Silva, A.J., Kogan, J.H., Frankland, P.W., and Kida, S. (1998). CREB AND MEMORY. Annu Rev Neurosci *21*, 127–148.

Smith, D.E., Lipsky, B.P., Russell, C., Ketchem, R.R., Kirchner, J., Hensley, K., Huang, Y., Friedman, W.J., Boissonneault, V., Plante, M.-M., et al. (2009). A Central Nervous System-Restricted Isoform of the Interleukin-1 Receptor Accessory Protein Modulates Neuronal Responses to Interleukin-1. Immunity *30*, 817–831.

Srinivasan, D., Yen, J.-H., Joseph, D.J., and Friedman, W. (2004). Cell type-specific interleukin-1beta signaling in the CNS. J Neurosci *24*, 6482–6488.

Stein, W. (2009). Modulation of stomatogastric rhythms. J Comp Physiol A *195*, 989–1009.

Steinmetz, C.C., and Turrigiano, G.G. (2010). Tumor Necrosis Factor- Signaling Maintains the Ability of Cortical Synapses to Express Synaptic Scaling. J

Neurosci *30*, 14685–14690.

Stellwagen, D., and Malenka, R.C. (2006). Synaptic scaling mediated by glial TNF-α. Nature *440*, 1054–1059.

Stephan, A.H., Barres, B.A., and Stevens, B. (2012). The Complement System: An Unexpected Role in Synaptic Pruning During Development and Disease. Annu Rev Neurosci *35*, 369–389.

Stevens, B., Allen, N.J., Vazquez, L.E., Howell, G.R., Christopherson, K.S., Nouri, N., Micheva, K.D., Mehalow, A.K., Huberman, A.D., Stafford, B., et al. (2007). The Classical Complement Cascade Mediates CNS Synapse Elimination. Cell *131*, 1164–1178.

Sugawara, T., Hisatsune, C., Le, T.D., Hashikawa, T., Hirono, M., Hattori, M., Nagao, S., and Mikoshiba, K. (2013). Type 1 Inositol Trisphosphate Receptor Regulates Cerebellar Circuits by Maintaining the Spine Morphology of Purkinje Cells in Adult Mice. Journal of Neuroscience *33*, 12186–12196.

Sullivan, J.C., Wolenski, F.S., Reitzel, A.M., French, C.E., Traylor-Knowles, N., Gilmore, T.D., and Finnerty, J.R. (2009). Two Alleles of NF-κB in the Sea Anemone Nematostella vectensis Are Widely Dispersed in Nature and Encode Proteins with Distinct Activities. PLoS ONE *4*, e7311–e7312.

Taghert, P.H., and Nitabach, M.N. (2012). Peptide Neuromodulation in Invertebrate Model Systems. Neuron *76*, 82–97.

Tancredi, V., M, D., Cafe, C., Giovedi, S., Bue, M.C., D'Arcangelo, G., Onofri, F., and Benfenati, F. (2000). The Inhibitory Effects of Interleukin-6 on Synaptic Plasticity in the Rat Hippocampus Are Associated with an Inhibition of Mitogen-Activated Protein Kinase ERK. J Neurochem *75*, 634–643.

Ting, A.T., and Bertrand, M.J.M. (2016). More to Life than NF-κB in TNFR1 Signaling. Trends Immunol *37*, 535–545.

Tully, T. (1997). Regulation of gene expression and its role in long-term memory and synaptic plasticity. Proc Natl Acad Sci USA *94*, 4239–4241.

Turner, M.D., Nedjai, B., Hurst, T., and Pennington, D.J. (2014). Cytokines and chemokines: At the crossroads of cell signalling and inflammatory disease. Biochim Biophys Acta *1843*, 2563–2582.

Turrigiano, G.G. (2017). The dialectic of Hebb and homeostasis. Phil Trans R Soc B *372*, 20160258–7.

Turrigiano, G.G., and Nelson, S.B. (2004). Homeostatic plasticity in the developing nervous system. Nat Rev Neurosci *5*, 97–107.

Turrigiano, G.G., Leslie, K.R., Desai, N.S., Rutherford, L.C., and Nelson, S.B. (1998). Activity-dependent scaling of quantal amplitude in neocortical neurons. Nature *391*, 892–896.

Vereker, E., ODonnell, E., and Lynch, M.A. (2000). The Inhibitory Effect of Interleukin-1. J Neurosci *20*, 6811–6819.

Vezzani, A., and Viviani, B. (2015). Neuromodulatory properties of inflammatory cytokines and their impact on neuronal excitability. Neuropharmacology *96*, 70–82.

Viviani, B., Bartesaghi, S., Gardoni, F., Vezzani, A., Behrens, M.M., Bartfai, T., Binaglia, M., Corsini, E., Di Luca, M., Galli, C.L., et al. (2003). Interleukin-1β

Enhances NMDA Receptor-Mediated Intracellular Calcium Increase through Activation of the Src Family of Kinases. J Neurosci *24*, 8692–8700.

Weber, K.P., De, S., Kozarewa, I., Turner, D.J., Babu, M.M., and de Bono, M. (2010). Whole Genome Sequencing Highlights Genetic Changes Associated with Laboratory Domestication of C. elegans. PLoS ONE *5*, e13922–10.

West, A.E., Griffith, E.C., and Greenberg, M.E. (2002). Regulation of transcription factors by neuronal activity. Nat Rev Neurosci *3*, 921–931.

Wienerroither, S., Shukla, P., Farlik, M., Majoros, A., Stych, B., Vogl, C., Cheon, H., Stark, G.R., Strobl, B., Müller, M., et al. (2015). Cooperative Transcriptional Activation of Antimicrobial Genes by STAT and NF-κB Pathways by Concerted Recruitment of the Mediator Complex. Cell Rep *12*, 300–312.

Wohleb, E.S., Franklin, T., Iwata, M., and Duman, R.S. (2016). Integrating neuroimmune systems in the neurobiology of depression. Nat Rev Neurosci *17*, 497–511.

Xiao, Y., Jin, J., Chang, M., Nakaya, M., Hu, H., Zou, Q., Zhou, X., Brittain, G.C., Cheng, X., and Sun, S.-C. (2014). TPL2 mediates autoimmune inflammation through activation of the TAK1 axis of IL-17 signaling. J Exp Med *211*, 1689–1702.

Yao, J., Kim, T.W., Qin, J., Jiang, Z., Qian, Y., Xiao, H., Lu, Y., Qian, W., Gulen, M.F., Sizemore, N., et al. (2007). Interleukin-1 (IL-1)-induced TAK1-dependent Versus MEKK3-dependent NFB Activation Pathways Bifurcate at IL-1 Receptor-associated Kinase Modification. J Biol Chem *282*, 6075–6089.

Yirmiya, R. (2002). Brain Interleukin-1 Is Involved in Spatial Memory and Passive Avoidance Conditioning. Neurobiology of Learning and Memory *78*, 379–389.

Yirmiya, R., Rimmerman, N., and Reshef, R. (2015). Depression as a Microglial Disease. Trends Neurosci *38*, 637–658.

Zhang, Q., Lenardo, M.J., and Baltimore, D. (2017). 30 Years of NF-κB: A Blossoming of Relevance to Human Pathobiology. Cell *168*, 37–57.

Zhu, G., Okada, M., Yoshida, S., Mori, F., Ueno, S., Wakabayashi, K., and Kaneko, S. (2006). Effects of interleukin-1β on hippocampal glutamate and GABA releases associated with Ca2+-induced Ca2+ releasing systems. Epilepsy Res *71*, 107–116.

2

MALT1 mediates IL-17 signaling in *C. elegans* neurons

Introduction

Neuromodulators tune the nervous systems to an ever-changing environment by locally and/or globally reconfiguring circuit activity (Katz and Lillvis, 2014; Taghert and Nitabach, 2012). As their contribution to brain state is typically contextual, assigning their functional roles in circuits and behaviour remains a significant challenge (Marder, 2012; Wester and McBain, 2014).

Cytokines are intercellular messengers that regulate the immune response. Accumulating evidence suggests these messengers can also play neuromodulatory roles in the CNS (Marin and Kipnis, 2013; Chapter 1). For example, during hippocampal-dependent memory formation, tight control of IL-1β levels is critical for LTP (Goshen et al., 2007; Schneider et al., 1998), while glutamatergic synaptic strength in the nucleus accumbens is homeostatically regulated by TNF-α (Beattie et al., 2002; Lewitus et al., 2016). Several studies over the last two decades suggest the neuromodulatory roles of cytokines are widespread (Vezzani and Viviani, 2015). However, the intracellular signaling pathways by which they alter neuronal properties are poorly understood.

Named after their sequence and structural similarity to caspases, paracaspases are a family of cysteine proteases with specificity for arginine residues (Hachmann et al., 2012; Uren et al., 2000). Their caspase-like protease domain is highly conserved, most notably containing an invariant histidine-cysteine pair. Their domain organization has also been retained across much of the animal kingdom (Hulpiau et al., 2015) and consists of an N-terminal death domain (DD) followed by 2-3 Ig (immunoglobulin)-like motifs that flank the paracaspase domain. Paracaspases have been studied almost exclusively in the mammalian immune system.

Human paracaspase, better known as MALT1 (mucosa-associated lymphoid tissue translocation protein 1), is a key signaling molecule in mammalian innate and adaptive immunity. Reduced *MALT1* expression is linked to combined

immunodeficiency (Jabara et al., 2013; McKinnon et al., 2014; Punwani et al., 2015), a phenotype recapitulated in *Malt1*$^{-/-}$ mice (Ruefli-Brasse et al., 2003; Ruland et al., 2003). Conversely, MALT1 hyper-activation drives the lymphocyte proliferation found in two forms of lymphoma: mucosa-associated lymphoid tissue (MALT) lymphoma (Dierlamm et al., 2008) and activated B-cell subtype of diffuse large B-cell lymphoma (ABC-DLBCL) (Dierlamm et al., 2008; Ngo et al., 2006). *MALT1* has also been identified as a susceptibility locus for multiple sclerosis (Sawcer et al., 2011).

MALT1 promotes NF-κB signaling downstream of ITAM-containing receptors by two mechanisms (Jaworski and Thome, 2015). First, MALT1 forms a complex, called the CBM signalosome, by interacting with BCL10 and CARD-containing proteins. This assembly serves a scaffolding function during activation of the IKK complex (Qiao et al., 2013; Sun et al., 2004). In addition, MALT1's protease activity contributes to the immune response by cleaving factors that inhibit NF-κB (Coornaert et al., 2008) or destabilize its target mRNAs (Jeltsch et al., 2014; Uehata et al., 2013).

NF-κB-dependent (McAllister-Lucas, 2001) and -independent (Klei et al., 2016) effects have also been reported for MALT1 downstream of specific GPCRs, suggesting it has diverse functions across different tissues. In the brain, in situ hybridization data indicate widespread MALT1 expression (Allen Mouse Brain Atlas, 2004), however no physiological role in neurons has been reported yet.

It was recently discovered that IL-17 acts like a neuromodulator in *C. elegans* (Chen et al., 2017). By acting directly on RMG hub interneurons, IL-17 increases neuronal output and sustains escape from an aversive cue, 21% O_2. Here, I show that *C.elegans* paracaspase (MALT-1) contributes to IL-17-mediated neuromodulation. Biochemical and genetic data suggest MALT-1 forms a complex with ACT1 and IRAK homologs, consistent with a scaffolding role. Additionally, using a paracaspase-dead mutant I identify a functional role for

MALT-1 protease activity in regulating neural function and behavioural state. These results represent the first described role for MALT1 signaling in the nervous system in any animal.

Results

MALT-1 promotes *C. elegans* aggregation and escape from 21% O_2

We studied mutants isolated after EMS-induced mutagenesis of *npr-1* animals that had lost the ability to aggregate on the border of bacterial food lawns. The phenotypes of two mutants, *db699* and *db867*, mapped to mutations in *F22D3.6* (Fig. 2.1A and B). Reciprocal BLAST showed that this gene encodes the *C. elegans* ortholog of human MALT1, with a conserved protease, death- and Ig-like domains (Fig. 2.1C and D). We therefore named *F22D3.6 malt-1*.

In the wild, *C. elegans* thrives in decomposing substrates, which are typically O_2-depleted, but rich in CO_2 (Frézal and Félix, 2015). Aggregation is driven largely by a preference for such conditions (Cheung et al., 2004; 2005; Gray et al., 2004). Feeding *npr-1* animals, like natural *C. elegans* isolates, dramatically increase their locomotory activity when subjected to 21% O_2, but exhibit little or no increased activity in response to elevated CO_2 (Bretscher et al., 2008; Rogers et al., 2006). The *db699; npr-1* and *db867; npr-1* mutants showed defects in escape from 21% O_2 and increased escape from elevated CO_2. To confirm that these phenotypes reflected loss of MALT-1, we generated three independent deletions in the *malt-1* locus using CRISPR-Cas9 (Fig. 2.1E). Among these, *db1194* encodes a premature stop codon resulting in the loss of all but the first 101 amino acids. These mutants recapitulated the aggregation, O_2-response and CO_2-response defects we observed in our original mutants. The *db1194* phenotypes were rescued by pan-neuronal expression of *malt-1* cDNA (Fig. 2.1G and H), suggesting MALT-1 functions in the nervous system.

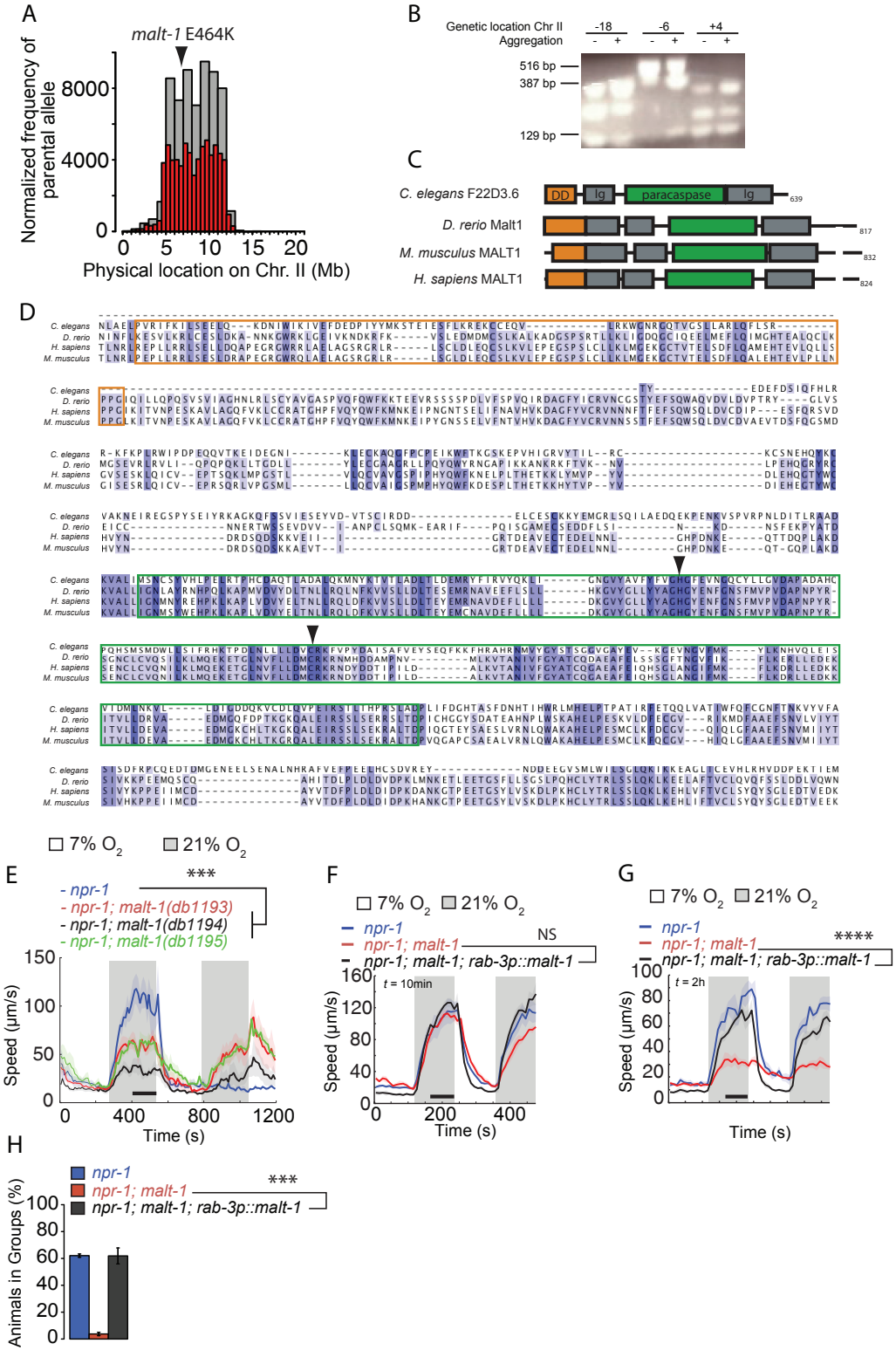

Figure 2.1 *C. elegans* paracaspase mediates O_2-related behaviours. (A) WGS-based CloudMap Hawaiian Variant Mapping of *db867*. An enrichment of parental SNPs on chromosome II is shown in aggregation-defective recombinant F_2 harboring a missense mutation in *malt-1* (physical location 6.9 Mb).

Strikingly, the O_2-evoked locomotory responses of *malt-1* mutants were normal when assayed immediately after animals were transferred to assay plates (Fig. 2.1F), but became defective by 2h after transfer (Fig. 2.1G). This phenotype is highly reminiscent of that of IL-17 signaling, (Chen et al., 2017), and suggested that *malt-1* mutants have reduced IL-17 signaling.

To determine whether *malt-1* is required developmentally we limited its expression to adults using a heat-shock-inducible promoter. Without heat-shock, a *hsp-16::malt-1* cDNA transgene did not rescue the O_2-response phenotype of

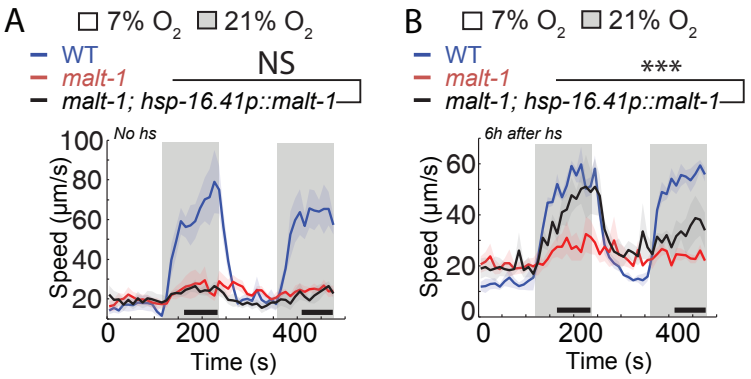

Figure 2.2 Temporal dynamics of MALT-1 requirement. (A) A transgene expressing *malt-1* cDNA from the *hsp-16.41* promoter does not rescue *malt-1* phenotypes in the absence of heat-shock. (B) Heat-shock-induced cDNA expression in adults restores O_2–evoked responses to *malt-1* mutants. Average speed (line) and SEM (shaded regions) are plotted (n ≥ 35 animals, N = 4 assays). **** = P < 0.0001, Mann-Whitney *U* test

(B) *DraI* digest-based Hawaiian variant mapping of *db699.* An enrichment of parental SNPs is visible at -6 (516bp band) and +4 (224 band) surrounding a nonsense mutation in *malt-1* (W495*, genetic location 0). (C) Paracaspase domain organization. DD=death domain, Ig=Immunoglobulin-like fold. (D) Sequence alignment of paracaspases, highlighting the conserved Death Domain (orange) and Paracaspase Domain (green). Arrowheads point to active site histidine and cysteine residues. Residue colouring indicates % identity. (E) Lesions generated by sgRNA-directed Cas9 cleavage at the *malt-1* locus reduce locomotory responses to 21% O_2, and increase responses to 3% CO_2 (n ≥ 48 animals, N = 4 assays). O_2 responses immediately after transfer to assay plate are not *malt-1* dependent (F), but are not sustained over a 2h period in *malt-1* mutants (G), n ≥ 43 animals, N = 4 assays. Average speed (line) and SEM (shaded regions) are plotted. Time of assay, after transfer, is shown at top left. **** = P < 0.0001, Mann-Whitney *U* test. (H) *malt-1* is required for aggregation (N ≥ 4 assays). *** = P < 0.001, ANOVA with Tukey's post hoc HSD.

malt-1 mutants (Fig. 2.2A). Delivering a heat-shock during the 4th larval stage was sufficient to restore behavioural responses (Fig. 2.2B). MALT-1 expression is therefore able to regulate 21% O_2 responsiveness acutely.

MALT-1 modulates RMG activity

To identify cells in which MALT-1 is expressed, we tagged MALT-1 at its C-terminus with RFP. This construct was expressed broadly in the nervous system, including the RMG neuron pair, ASG, URX, and AQR (Fig. 2.3A and C). As it appears that most neurons express MALT-1 we have not characterized this pattern fully.

Previous work has shown that escape from 21% O_2 is driven by the RMG interneurons, which are tonically stimulated by the URX O_2 sensors when O_2 levels approach 21% (Busch et al., 2012; Laurent et al., 2015). To test whether MALT-1 acts in RMG to promote responsiveness to 21% O_2, we imaged O_2-evoked Ca^{2+} responses in this neuron using Yellow Cameleon, a genetically encoded FRET-based reporter (Kerr et al., 2000). RMG responses were significantly reduced in *malt-1* mutants in both freely moving (Fig. 2.3D) and immobilized animals (Fig. 2.3F). This defect was rescued by expressing *malt-1* cDNA from the *npr-1* promoter (Fig. 2.3F), which drives expression in a broad subset of neurons including RMG (de Bono and Bargmann, 1998; Macosko, 2009).

We next asked whether *malt-1* influences Ca^{2+} transients specifically at the interneuron level, or whether upstream sensory responses are also altered. Ca^{2+} responses in the URX sensory neurons were normal in freely moving (Fig. 2.3B) and immobilized (Fig. 2.3E) *malt-1* mutants. We also tested the dependency of Ca^{2+} transients in BAG sensory neurons exposed to 3% CO_2 on *malt-1*. *malt-1* mutants responded at least as well as WT animals (Fig. 2.3G), indicating that MALT-1 does not universally promote neuronal responsiveness but does so dependant on context/signal.

We directly addressed the question of where MALT-1 functions by testing its sufficiency in different subsets of neurons to promote O_2-escape. Consistent with its role not being confined to RMG, we observed most complete rescue when MALT-1 was expressed broadly by the *rab-3* promoter (Fig. 2.1G and H) or in both O_2-sensing neurons and RMG simultaneously (Fig. 2.4A and B).

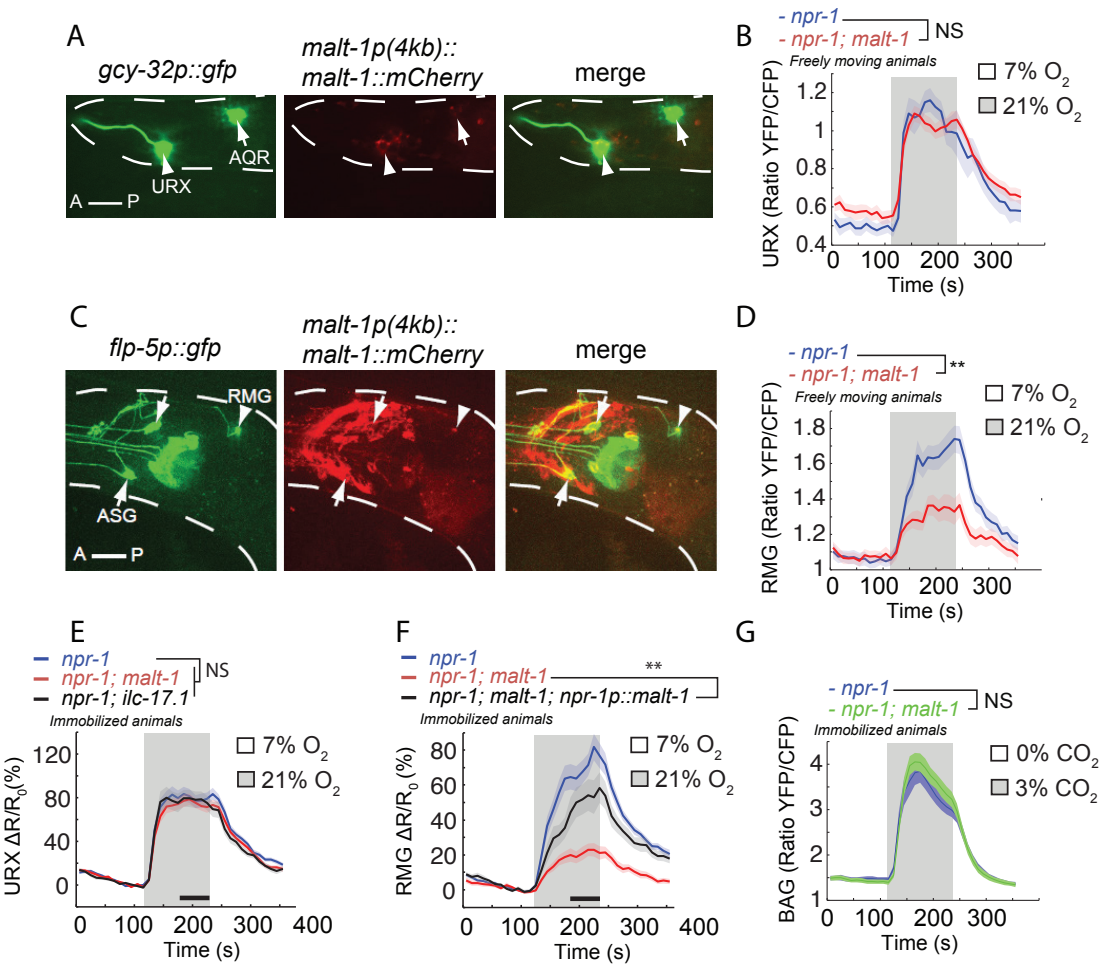

Figure 2.3 MALT-1 modulates RMG physiology. (A,C) A MALT-1::mCherry translational fusion, driven by 4kb of upstream sequence, colocalizes with a *gcy-32* reporter that stains URX, AQR and PQR neurons (A), and a *flp-5* reporter that is expressed in RMG, ASG and several other neurons (C, Kim and Li, 2004). The effect of *malt-1* LOF on Ca^{2+} transients in RMG (D and F), URX (B and E) and BAG (G), as reported by YC2.60 (B, D, E and F) or YC3.60 (G) are shown. RMG responses are attenuated in *malt-1* mutants (D and F), whereas URX neurons are WT in freely moving and immobilized animals (B and E). n ≥ 13 (B), n ≥ 32 (D), n ≥ 32 (E), n ≥ 25 (F), n ≥ 19 (G). ** = P < 0.01, Mann-Whitney *U* test.

Limiting expression to O_2-sensing neurons, or a small subset of neurons including RMG conferred significant but only partial rescue (Fig. 2.4A and B). This supports a scenario in which MALT-1 functions in multiple neurons to promote aggregation and responsiveness to 21% O_2.

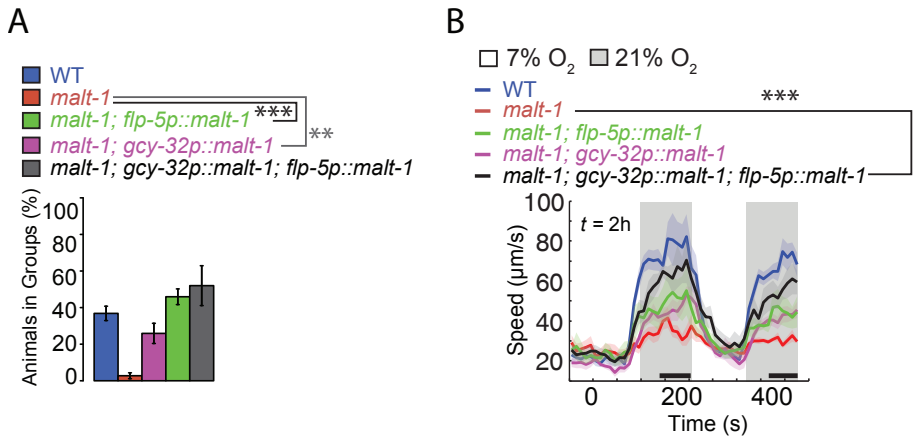

Figure 2.4 Expression of *malt-1* in RMG and O_2-sensing neurons rescues behavioural defects. (A) The aggregation phenotype of *malt-1* mutants is rescued by expressing *malt-1* cDNA from the *flp-5* promoter (RMG, ASG, PVT, I4, M4 and pharyngeal muscle), or the *gcy-32* promoter (URX, AQR and PQR). N = 4 assays. ** = P < 0.01, *** = P < 0.001, ANOVA with Tukey's post hoc HSD. (B) The O_2-response phenotype of *malt-1* mutants is rescued by expressing *malt-1* cDNA from the *gcy-32* promoter (URX, AQR and PQR) and *flp-5* promoter simultaneously. Lines indicate average and shaded regions indicate SEM. n ≥ 46 animals, N = 4 assays. *** = P < 0.001, Mann-Whitney *U* test.

MALT-1 functions downstream of IL-17 receptors

To identify partners that interact with MALT-1 we expressed C-terminally GFP-tagged MALT-1 throughout the nervous system in *malt-1* mutants, and performed immunoprecipitation from whole worm extracts using anti-GFP antibody. MALT-1-GFP rescued the *malt-1* phenotype (Fig. 2.1G) and localized to the cytoplasm of neurons (Fig. 2.5A). As a control we also performed immunoprecipitation from a strain that expressed GFP pan-neuronally. By mass spectrometry, we identified peptides corresponding to ACTL-1 and PIK-1 bound specifically to MALT-1 (Fig. 2.5B). In *C. elegans* ACTL-1 and PIK-1 encode an adaptor similar to Act1 and an IRAK-like kinase respectively, and mediate signaling downstream of the IL-17 receptor (Chen et al., 2017).

To confirm their physical interaction, we co-immunoprecipitated MALT-1-GFP and PIK-1-HA heterologously expressed in 293T cells. Preliminary experiments suggest pull-down of PIK-1-HA specifically captured MALT-1-GFP, while we observed an enrichment for PIK-1-HA after MALT-1-GFP pulldown (Fig. 2.5C and D). These results suggest MALT-1 forms a complex with ACTL-1 and PIK-1.

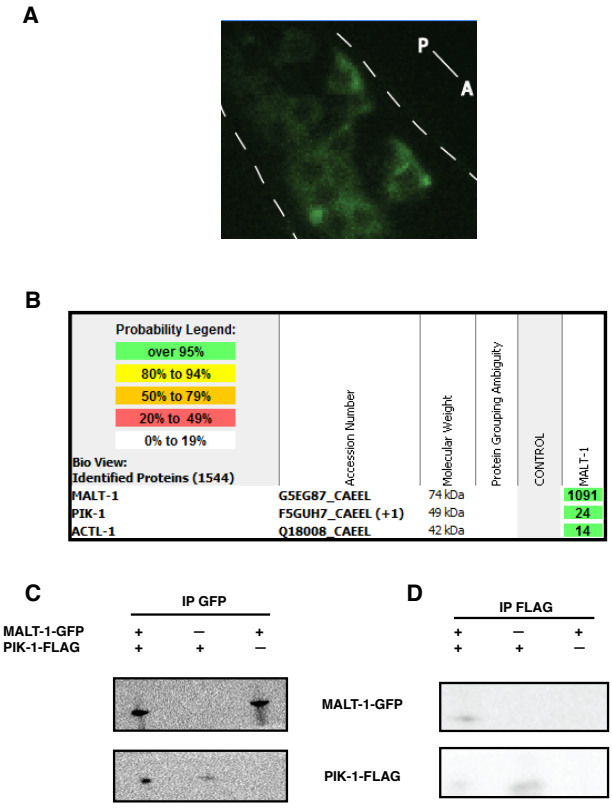

Figure 2.5 MALT-1 physically interacts with ACTL-1 and PIK-1. (A) MALT-1::GFP localizes diffusely in the cytoplasm of neurons. Tail neurons are shown. (B) Identification of proteins co-immunoprecipitating with MALT-1::GFP by mass spectrometry suggests ACTL-1 and PIK-1 form a complex with MALT-1. Proteins immunoprecipitating with free GFP (expressed from the *unc-119* promoter) are used as a control. Values represent Total Spectrum Count, displayed in Scaffold Viewer (proteomesoftware.com). (C and D) Co-immunoprecipitation of MALT-1-GFP and PIK-1-FLAG after heterologous expression in HEK293T cells.

The similar phenotypes of *malt-1* and *pik-1* mutants suggested these proteins act in the same signaling pathway. The co-IP of MALT-1-GFP and PIK-1/IRAK support this hypothesis. To test this further, we investigated whether *malt-1* and *pik-1* mutations exhibit any phenotypic additivity. *malt-1; pik-1* double mutants did not enhance the *malt-1* Ca^{2+} signaling defect in RMG (Fig. 2.6A), suggesting MALT-1 and PIK-1 function in the same pathway.

In *C. elegans*, IL-17 signaling downstream of PIK-1/IRAK requires an IκBζ homolog called NFKI-1 (Chen et al., 2017). Overexpressing NFKI-1 suppresses

the null phenotypes of upstream signaling components, including the receptors and *pik-1*. Consistent with MALT-1 functioning upstream of IκBζ, overexpressing NFKI-1 restored 21% O_2 responses (Fig. 2.6B) and aggregation (Fig. 2.6C) to *malt-1(null)* mutants. Together, our data suggest that MALT-1 forms a signaling complex with ACTL-1 and PIK-1/IRAK at the IL-17 receptors.

Our model predicts that IL-17/ILC17.1 and MALT-1 drive the same transcriptional changes in neurons. To test whether this is the case across the whole animal, in

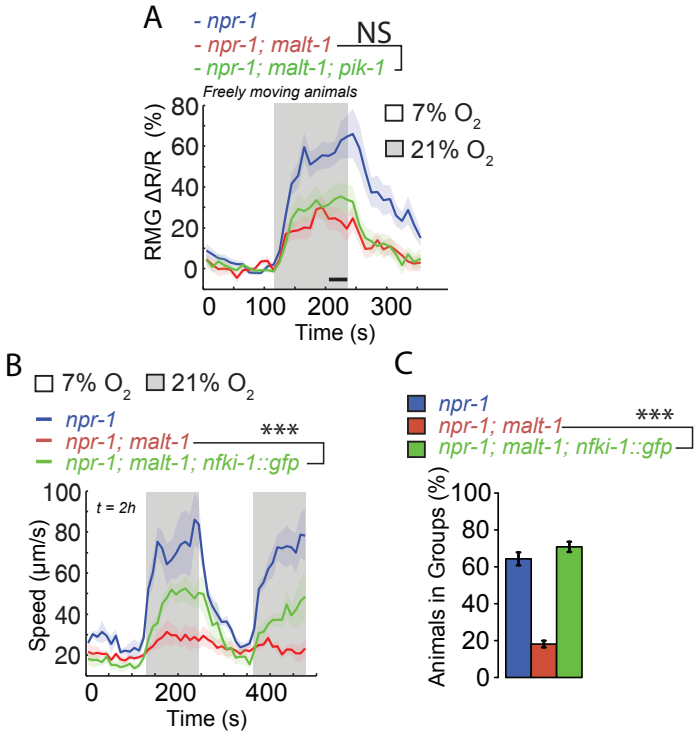

Figure 2.6 MALT1 acts like an IL-17 signaling component. (A) *malt-1* RMG Ca^{2+} transients (reported by YC2.60) are not further reduced by *pik-1* LOF (n ≥ 14). Speed (B) and aggregation (C) defects of *malt-1* are rescued by overexpressing *nfki-1* cDNA. (B) n ≥ 43 animals, N = 4 assays. *** = P < 0.001, Mann-Whitney *U* test. (C) N ≥ 4 assays. *** = P < 0.001, ANOVA with Tukey's post hoc HSD.

collaborartion with Alastair Crisp, we compared the RNA-seq profiles of *malt-1*, *nfki-1*, and *ilc-17.1* mutants to WT(*npr-1*). Around 2/3 of the genes whose expression was decreased two-fold by loss of MALT-1 were also downregulated in *nfki-1*, and/or *ilc-17.1* mutants (Fig. 2.7A). We also observed that more than half of the genes that were two-fold upregulated in *malt-1* animals were comparably changed in both *nfki-1* and *ilc-17.1* mutants (Fig. 2.7B). These

findings suggest that there is substantial overlap in the transcriptional signatures of *malt-1, nfki-1* and *ilc-17.1* mutants, and that much of the perturbation observed in *malt-1* mutants is explained by defects in IL-17 signaling. Interestingly, gene ontology and pathway annotations of the genes positively regulated by MALT-1, NFKI-1 and IL-17 revealed an enrichment for immune system molecules (Fig. 2.7D). This may indicate that MALT-1 and IL-17 are positive regulators of the immune response in *C. elegans*. Metabolic processes were over-represented among the genes negatively regulated by this pathway, but the implications of this are not clear (Fig. 2.7E).

We also explored the consequence of MALT-1, NFKI-1 or ILC-17.1 overexpression, in order to identify genes that are consistently regulated by this pathway. The expression of 7 genes was significantly increased in all three overexpression conditions, and reciprocally regulated in all three mutants (Fig. 2.7C). Again, several of these genes are related to immunity (Fig. 2.7F). It will be interesting to verify whether these genes are effectors of IL-17 signaling, and what their role is in the organism. It will be especially important to identify the genes that are regulated in neuronal tissue.

Paracaspase activity promotes O_2 responses

To test if MALT-1 signaling activity involves protease function, we changed the catalytic cysteine residue in the active site to alanine. This mutant has been established as a paracaspase-dead model in mice (Gewies et al., 2014). The C374A mutation abolished the ability of *malt-1* cDNA to rescue our mutant phenotype (Fig. 2.8A), indicating that MALT-1 functions as a protease in the *C. elegans* nervous system.

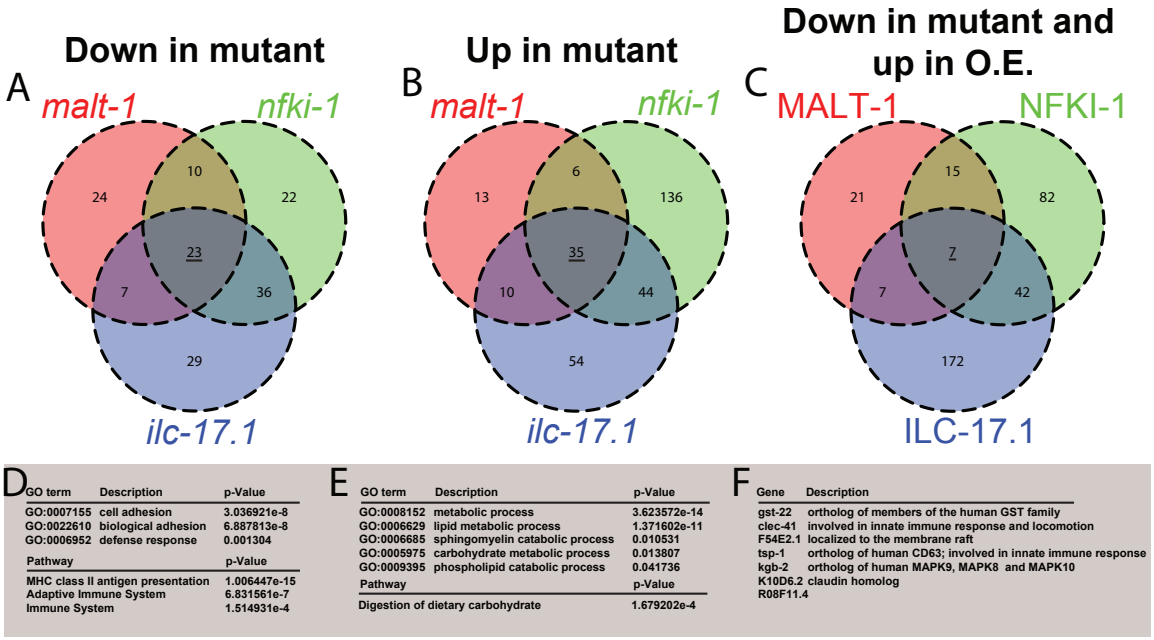

D

GO term	Description	p-Value
GO:0007155	cell adhesion	3.036921e-8
GO:0022610	biological adhesion	6.887813e-8
GO:0006952	defense response	0.001304

Pathway	p-Value
MHC class II antigen presentation	1.006447e-15
Adaptive Immune System	6.831561e-7
Immune System	1.514931e-4

E

GO term	Description	p-Value
GO:0008152	metabolic process	3.623572e-14
GO:0006629	lipid metabolic process	1.371602e-11
GO:0006685	sphingomyelin catabolic process	0.010531
GO:0005975	carbohydrate metabolic process	0.013807
GO:0009395	phospholipid catabolic process	0.041736

Pathway	p-Value
Digestion of dietary carbohydrate	1.679202e-4

F

Gene	Description
gst-22	ortholog of members of the human GST family
clec-41	involved in innate immune response and locomotion
F54E2.1	localized to the membrane raft
tsp-1	ortholog of human CD63; involved in innate immune response
kgb-2	ortholog of human MAPK9, MAPK8 and MAPK10
K10D6.2	claudin homolog
R08F11.4	

Figure 2.7 Transcriptional fingerprints of *malt-1, nfki-1 and ilc-17.1* mutants. The total number of genes that are downregulated (A) and upregulated (B) two-fold or more in *malt-1;npr-1, ilc-17.1;npr-1* and *nfki-1;npr-1* conditions compared to *npr-1*. (C) The number of genes whose expression is significantly increased by overexpression of MALT-1, NFKI-1 or ILC-17.1, and is significantly reduced in the corresponding mutant condition, is shown. (D and E) Gene ontology (GO) terms and pathways significantly overrepresented among genes dysregulated in all three mutant conditions. (D) Downregulated genes, corresponding to those underlined in (A). (E) Upregulated genes, corresponding to those underlined in (B). (F) The identities and descriptions of the genes underlined in (C). MALT-1 was overexpressed pan-neuronally, NFKI-1 and ILC-17.1 were overexpressed from their endogenous promoters.

Eight substrates of mammalian MALT1 are known (Hachmann and Salvesen, 2016), four of which have homologs in *C. elegans* (Fig. 2.9B). Among these only REGE-1 (REGnasE-1) retains the arginine residue at which MALT1 cleavage occurs (Fig. 2.8B). Mammalian Regnase-1 is an RNase which inhibits the activation of IL-17 expressing T_H17 cells, by promoting the degradation of mRNA such as that encoding IκBζ (Jeltsch et al., 2014; Uehata et al., 2013). Both its RNase activity and regulatory role in the expression of immune genes are conserved in *C. elegans* (Habacher et al., 2016).

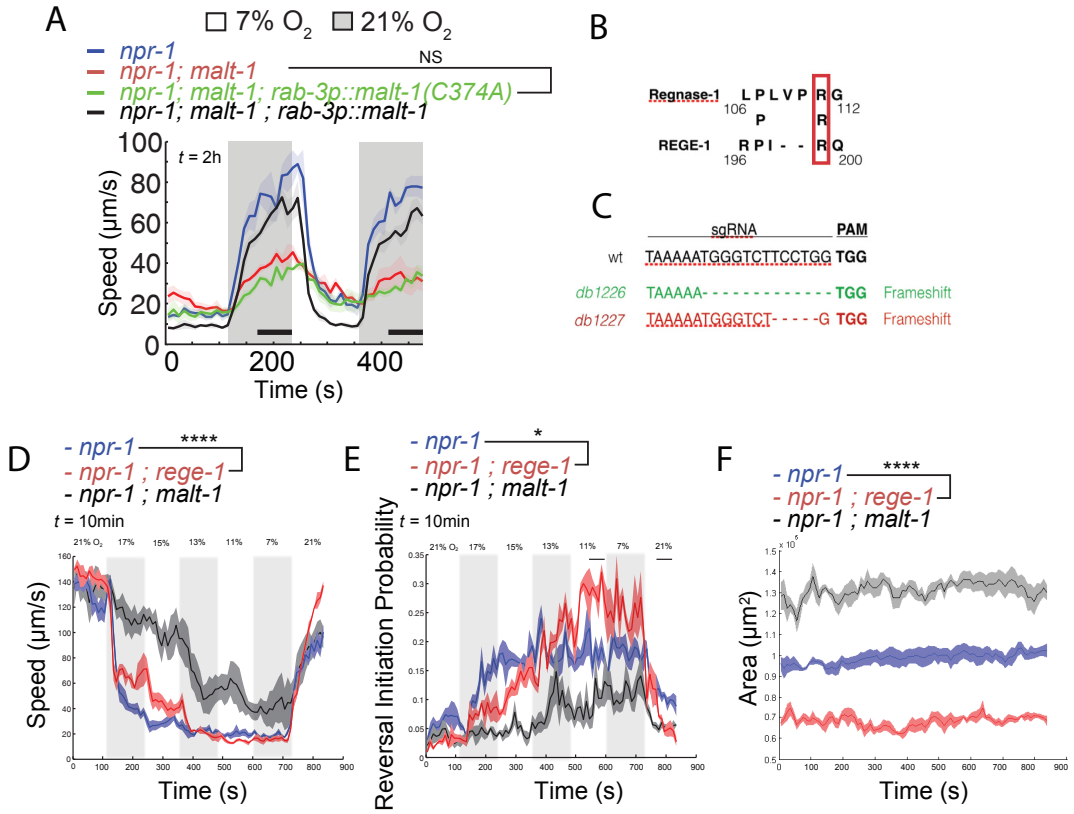

Figure 2.8 MALT-1 functions as a protease. (A) cDNA encoding a C374A mutant, expressed from the *rab-3* promoter, does not rescue the reduced speed responses of *malt-1* (n ≥ 43 animals, N = 4 assays). Data corresponding to *npr-1* and *npr-1; malt-1; rab-3p::malt-1* are same as in Fig. 2.1G, plotted here because it was obtained in parallel to the other genotypes shown. (B) Regnase-1 R111, which directs MALT1 cleavage in mammals, is conserved in *C. elegans* REGE-1. (C-F) Lesions generated by sgRNA-directed Cas9 cleavage at the *rege-1* locus (C) increase behavioural responses to 21% O_2 (D and E). *malt-1* and *rege-1* have opposite effects on body size (F). (D-F) n ≥ 57 animals, N = 4 assays. * = P < 0.05, **** = P < 0.0001, Mann-Whitney *U* test.

To test for a role in the O_2-escape circuit we generated frameshift mutations in the *rege-1* locus using CRISPR-Cas9 (Fig. 2.8C). *rege-1; npr-1* mutants aggregated strongly (data not shown), and exhibited sensitized responses to high O_2 compared to *npr-1* controls (Fig. 2.8D). A similar effect was seen on reversals; *rege-1* enhanced the extent to which *npr-1* animals ceased reversals after a switch to intermediate O_2 levels (Fig. 2.8E). We reasoned that if the MALT1 inhibition of Regnase1 is conserved in *C. elegans*, it might regulate other

aspects of worm physiology. We therefore looked for traits reciprocally modulated by *malt-1* and *rege-1*. Whereas disrupting *malt-1* increased body size, *rege-1* mutants are smaller than normal (Fig. 2.8E). Our data suggest paracaspase activity contributes to IL-17 signaling. It will be interesting to discover whether cleavage of REGE-1 or other, novel substrates is required.

Discussion

MALT-1 is required for IL-17 signaling

Several lines of evidence suggest MALT-1 mediates the neuromodulatory effects of IL-17. (1) *malt-1* mutants respond to 21% O_2 shortly after being picked for assay, but are unable to sustain this escape behaviour. Of the mutants characterized to date, only those affecting IL-17 signaling exhibit this phenotype. (2) We previously showed that heat-shock induced expression of IL-17 can rescue IL-17 null phenotypes within ~6h of a heat-shock pulse. Heat-shock inducted *malt-1* expression similarly restores responses within 6h.

(3) Our unbiased *in vivo* biochemical analysis of MALT-1 suggests it forms a complex with ACT1 and IRAK homologs in neurons. We previously showed that ACTL-1 and PIK-1 are IL-17 signaling components (Chen et al., 2017). In mammals, ACT1 adaptors are engaged by IL-17R activation and provide a docking surface critical for signal transduction (Chang et al., 2006; Gaffen et al., 2014). PIK-1 is the only *C. elegans* member of the IRAK family of serine-threonine kinases, which like MALT1 perform both scaffolding and enzymatic functions during NF-κB signaling (Song et al., 2009).

A high-throughput yeast two-hybrid study suggests that the ACTL-1-PIK-1 interaction is direct (Li et al., 2004), but it is not clear which is a direct binding partner of MALT-1. As all three proteins contain death domains, which participate exclusively in homotypic interactions (Park et al., 2007). It is tempting to speculate that this complex might turn out to be the first known binding partner of a paracaspase death domain.

(4) The phenotype of *malt-1; pik-1* double mutants is non-additive, consistent with MALT1 and IRAK functioning in the same pathway. (5) *malt-1(null)* phenotypes, like those of IL-17 signaling components, can be suppressed by overexpressing IκBζ/NFKI-1. (6) The transcriptional signature of *malt-1* mutants overlaps substantially with that of *ilc-17.1* and *nfki-1*. To explore this further, we aim to compare RNA-seq profiles after genetic perturbation of *ilc-17.1*, *malt-1* and *nfki-1* in the nervous system, and specifically in RMG.

MALT-1 protease activity functions to sustain O_2-responsiveness

While MALT1-ACT1-IRAK complexes likely represent a scaffolding function of MALT-1, we showed that MALT-1 protease activity is functionally essential. Therefore, as in the mammalian immune system, MALT-1 likely performs a dual function during signal transduction in the nervous system.

Whether RNA stability is regulated by *C. elegans* paracaspase activity remains an open question. In mammalian immunity, cleavage of Regnase-1 and Roquin by MALT1 prevents degradation of mRNAs important for T cell activation (Jeltsch et al., 2014; Uehata et al., 2013). By comparing exonic to intronic ratios among *C. elegans* mRNAs Habacher et al. (2016) identified a subset of transcripts that may be post-transcriptionally regulated by Regnase-1/*rege-1*. It would be interesting to quantify levels of these mRNAs in the absence of MALT-1.

The ACT1/MALT1/IRAK/IκBζ cascade is required in and beyond RMG

Although expressed broadly in the nervous system, the phenotypic effects of disrupting *malt-1* were surprisingly specific. General locomotion patterns and sensory neuron responses were largely unaffected by *malt-1* knockout. Instead, RMG output appears to be a major site of MALT-1 modulation. Ca^{2+} responses in RMG, but not URX, neurons are dependent on *malt-1*. Our finding that the responsiveness of URX and BAG neurons to sensory stimuli is not dependent on

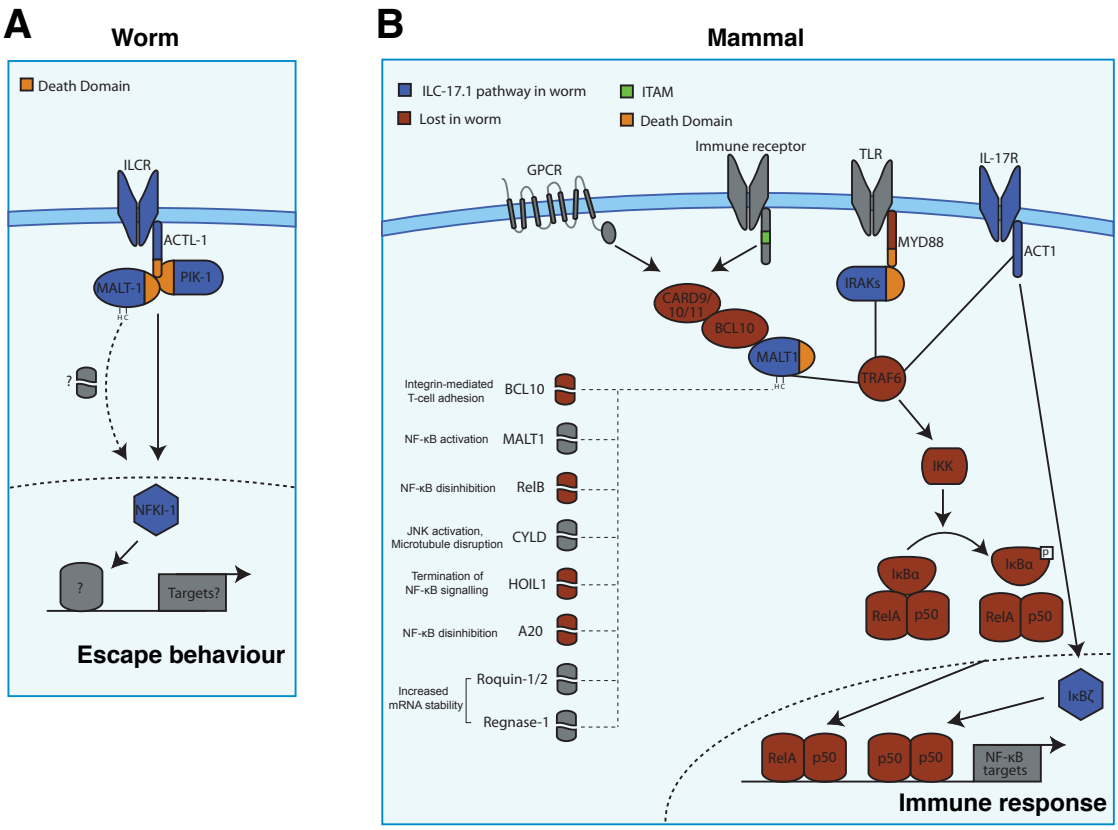

Figure 2.9 Malt1 signaling in *C. elegans* neurons and the mammalian immune system. (A) Activation of nematode IL-17Rs engages ACT1-like adaptors, which recruit IRAK and MALT1 homologs (Chen et al., 2017). The ACT1-IRAK-MALT1 signalosome serves a scaffolding function to activate IκBζ/NFKI-1 by an unknown mechanism. IκBζ, probably by cooperating with another transcriptional regulator, orchestrates changes in the RMG transcriptome that result in increased neuronal output. MALT1-mediated cleavage of an unknown substrate positively regulates IκBζ signaling. (B) Multiple pathways converge to regulate mammalian NF-κB-mediated immune responses. CBM signalosomes form in response to stimulation of GPCRs (non-immune cells) or ITAM-containing receptors (immune cells) such as BCRs or TCRs (Jaworski and Thome, 2015). MALT1, IRAKs and Act1 signal downstream of non-overlapping immune receptors, but all promote NF-κB mobilization via recruitment of the E3 ubiquitin ligase TRAF6 and subsequent activation of the IKK complex (Gaffen, 2009; Wu and Arron, 2003). IκBζ is an atypical member of the IκB family which functions in the nucleus to promote the transcription of a second-wave of NF-κB targets (Yamamoto et al., 2004). Although still poorly characterized, IκBζ appears to be particularly important in mediating the effects of IL-17 (Johansen et al., 2015). MALT1 paracaspase activity provides an additional layer of regulation to the NF-κB pathway by controlling protein degradation directly (RelB cleavage) or indirectly (through CYLD, CYLD, HOIL1), and by regulating mRNA stability (Regnase-1 and Roquin) (Hachmann et al., 2012).

malt-1 supports the hypothesis that its requirement is greatest in neurons modulated by IL-17 or other neuromodulatory cytokines.

Our cell-specific rescue experiments support a role for MALT-1 in neurons additional to RMG. Previous work in the lab reported that this is likely also the case for ACTL-1, PIK-1 and NFKI-1, which are also broadly expressed. It is possible that the ACT1/IRAK/MALT1/IκBζ cascade mediates signaling from other, as yet unknown, receptors within the O_2 escape circuit. It will be interesting to discover under what conditions this pathway is required in other circuits.

Neuromodulation: a novel function for paracaspase

Paracaspases are highly conserved across bilaterian species, but the function responsible for this conservation is unknown. The absence of Rel homology domains in *C. elegans* (Sullivan et al., 2009) raises the possibility that an NF-κB-independent mechanism may contribute (Staal et al., 2016). Our study presents one potential explanation (Fig. 2.9). It will be important to investigate the role of paracaspases a) across diverse species, to determine whether IL-17/ IκBζ signaling is a theme or an exception, and b) in the mammalian brain, to establish whether its expression there reflects a function in cytokine-mediated neuromodulation.

Given its role in automimmunity and cancer, inhibiting MALT1 protease activity is considered a promising therapeutic avenue (Demeyer et al., 2016). In order to understand potential side-effects of paracaspase inhibitors it will be important to more fully characterize the functions of MALT1 outside the immune system. In this study I describe for the first time a physiological role for paracaspase in neurons.

Materials and Methods

C. elegans strains

A full list of strains is provided in the Appendix. Worms were maintained on nematode growth medium (NGM) at room temperature (20˚C) unless stated otherwise, with OP50 *E. coli* as a food source.

Mapping mutant alleles

To localize causal variants we used Hawaiian SNP-based mapping in combination with WGS, following the methods of (Davis et al., 2005) and (Minevich et al., 2012). To facilitate phenotyping, we used the AX288 [*lon-2*(*e678*) *npr-1*(*ad609*)] strain for mapping; *the npr-1* null allele confers stronger aggregation than the CB4856 Hawaiian strain typically used for mapping. AX288 was constructed by backcrossing *lon-2 npr-1(ad609)* 16 times into CB4856. For each mutant, 40-60 recombinant F2 animals were singled, and their progeny scored for aggregation. Genomic DNA from aggregating and non-aggregating F3 lines was pooled. SNP genotyping was performed either by *Dra* I restriction digest or WGS. Library preparation and HiSeq WGS were performed by the CRI Genomics Core Facility (Cancer Research UK Cambridge Institute). In collaboration with Geoff Nelson, I ran the Cloudmap pipeline on the public galaxy server to identify genomic intervals harbouring the causal mutation.

Protein alignment

Protein sequences were obtained from UniProt, and aligned using Clustal Omega. Percentage identity was viewed in Jalview using default settings. Domain annotations were obtained from InterPro and UniProt.

Molecular Biology

Gateway cloning

Most *C. elegans* expression constructs were generated using MultiSite Gateway Recombination (Invitrogen). The following Entry clones were a gift from Changchun Chen: *rab-3p*, *npr-1p*, *flp-5p*, *gcy-32p, hsp-16.41p*, *gfp::unc-54utr*,

SL2::mCherry, mCherry. *C. elegans* gDNA and cDNA was isolated using DNeasy Blood and Tissue (Qiagen) and RevertAid First Strand cDNA synthesis (Thermo Scientific) kits respectively. Phusion polymerase (NEB) was used to amplify *malt-1* and its promoter. The following primers were used:
To amplify the *malt-1* promoter (4kb): ggggACAACTTTGTATAGAAAAGTTGctgc cggtggattccaacatattg and
ggggACTGCTTTTTTGTACAAACTTGtctgaaattggggttcaagaaatttatttttgatttttaaaata
To amplify the *malt-1* ORF (gDNA):
ggggACAAGTTTGTACAAAAAAGCAGGCTtttcagaaaaatgaacacaaacttggcggagttc and ggggACCACTTTGTACAAGAAAGCTGGGTActgtagacatttgattcttgtaatcaa aatatgaccaatatc
To amplify *malt-1* cDNA:
ggggACAAGTTTGTACAAAAAAGCAGGCTtttcagaaaaatgaacacaaacttggcggagttc and ggggACCACTTTGTACAAGAAAGCTGGGTATTACTGTAGACATTTGATTC TTGTAATCAAAATATGACCAATATCAACATTC

Gibson assembly
sgRNAs were cloned downstream of the *rpr-1* promoter using Gibson Assembly (NEB) as described in (Chen et al., 2013). To target the *F22D3.6* locus we expressed gatcaggtatccaccgtag. To target the *rege-1* locus we expressed TAAAAATGGGTCTTCCTGG. The primers used to amplify these sequences for insertion into *E*coRI-cut expression plasmids were
gcgcgtcaagttgtGgatcaggtatccaccgtagGTTTTAGAGCTAGAA and
TTCTAGCTCTAAAACctacggtggatacctgatcCacaacttgacgcgc for *malt-1*, and
gcgcgtcaagttgtGTAAAAATGGGTCTTCCTGGGTTTTAGAGCTAGAA and
TTCTAGCTCTAAAACCCAGGAAGACCCATTTTTACacaacttgacgcgc for *rege-1.*
For HEK293T cell expression *malt-1* cDNA was cloned into a modified pcDNA4 vector, with EGFP inserted between *Nar* I and *Xba* I sites. To amplify *malt-1* cDNA for Gibson Assembly into *Not* I- and *Eco* RV- cut plasmid we used TAGTCCAGTG TGGTGGAATTCTGCAGCCACCatgaacacaaacttggcggagttacctg and CCTGCCC

TCGATGGCCCTGTCGCTctgtagacatttgattcttgtaatcaaaatatgaccaatatcaacattcttc. PIK-1-FLAG was a gift from Changchun Chen.

Site-directed mutagenesis

The Q5 Site-Directed Mutagenesis Kit (NEB) was used to create C734A mutant cDNA, with the following primers: TCTTGATGTCgcCAGAAAATTTGTTCCATATG and gcgcgtcaagttgtGCCTGACGACGAGTTGTGCTGTTTTAGAGCTAGAA.

***C. elegans* Microinjection**

Expression constructs were injected at 50 ng/µl, with the exception of CRISPR-Cas9 mixes that were prepared as previously described (Chen et al., 2013): 30ng ng/µl *eft-3::cas9*, 100 ng/µl sgRNA, 30ng ng/µl cc::GFP.

Behavioural assays

All behavioural assays were performed at room temperature (20˚C).

Aggregation assays

Aggregation was assayed as previously described (de Bono and Bargmann, 1998). 60 young adults per assay were picked onto plates seeded with 100 µl OP50 48h previously. Animals were left undisturbed for 2h before scoring, which was performed blind to genotype. The % of animals in groups was calculated, with a group defined as 3 or more animals in contact with one another.

Locomotion assays

Aerotaxis was performed as previously described (Laurent et al., 2015; Fenk and de Bono, 2015) with minor modifications. 15-25 young adults per assay were picked onto plates seeded with 20 µl OP50 14-18h previously. [O_2] was controlled using a microfluidic system. Gas mixes, bubbled through H_2O, were delivered to a PDMS chamber at a rate of 1.4ml/min using a PHD 2000 Infusion syringe pump (Harvard Apparatus). Video recordings were taken at 2fps with

FlyCapture software, using a Point Grey Grasshopper camera mounted on a Leica MZ6 microscope. Speed and reversals were measured using Zentracker (https://github.com/wormtracker/zentracker). For measuring *ilc-17.1*-like phenotypes, worms were left undisturbed for 2h on assay plates prior to recording. In Fig. 2.1E, assays were performed using a manifold setup described in Chapter V.

Heat-shock

We observed leaky expression from the *hsp-16.41* promoter in animals grown at room temperature. For this reason animals were kept at 15˚C until the time of heatshock (late L4). To induce heat-shock, parafilm-wrapped plates were submerged in a 34˚C water bath for 30 min, and then recovered at room temperature until the time of assay.

Light microscopy

Worms were immobilized in 25mM sodium azide on 2% agarose pads. Samples were imaged by spinning disk confocal laser microscopy as previously described (Chen et al., 2014). Z stacks were acquired using an Andor Ixon EMCCD on a Nikon Eclipse Ti inverted microscope. Average intensity images were generated in Image J.

Calcium Imaging

Worms expressing cameleon (YC2.60 and YC3.60) were recorded using a Nikon AZ100 microscope fitted with ORCA-Flash4.0 digital cameras (Hamamatsu). Excitation light was provided from an Intensilight C-HGFI (Nikon), through a 438/24nm filter and an FF458DiO2 dichroic (Semrock). Emission light was split using a TwinCam dual camera adaptor (Cairn Research) and passed through CFP (483/32nm) and YFP (542/27) filters, and a DC/T510LPXRXTUf2 dichroic. We acquired movies using NIS-Elements, with exposure time set to 100ms.

Ca^{2+} imaging in freely moving animals

Single young adults were transferred to peptone-free agar plates spotted with 4 µl of concentrated OP50 food in M9 buffer. A 2x AZ-Plan Fluor objective lens (Nikon) was used with 2x zoom.

Ca^{2+} imaging in immobilized animals

4-8 young adults were transferred to peptone-free agar plates, and immobilized on a 2µl patch of concentrated OP50 in M9 buffer using Dermabond adhesive. Animals were immobilized so as to leave the nose exposed. The same 2x objective lens was used as above, with 4x zoom.

Immunoprecipitation from *C. elegans*

Lysis buffer was prepared with 50mM HEPES (pH 7.4), 1mM EGTA, 1mM $MgCl_2$, 100 mM KCl, 10% glycerol, 0.05% Tergitol type-NP40(Sigma-Aldrich), 1mM DTT, 0.1M PMSF with 1 complete EDTA-free proteinase inhibitor cocktail tablet (Roche Applied Science) per 12ml (Zanin et al., 2011). Worms were washed twice in M9 and once in ice-cold lysis buffer, then pelleted at 2000-3000 rpm at 4˚C. After snap-freezing in LN_2, worm pellets were broken into small pieces in preparation for cryogenic grinding. Samples were pulverized using a Freezer/Mill (SPEX SamplePrep). Crude extract was clarified at 4°C for 10 min at 20,000*g,* and again for 20 min at 100,000*g* with a TLA-100 rotor (Beckman Coulter). For immunoprecipitation, samples were incubated with 30µl GFP-Trap (ChromoTek) for 4h at 4°C, then washed 6 times with 100mM/300mM KCl. Protein was eluted in SDS-sample buffer (90°C for 5min).

Immunoprecipitation from HEK293T cells

HEK293T cells were cultured in DMEM with high glucose (GlutaMax, Life Technologies) and 10% FBS. Cells were transfected with 1µl plasmid using *trans*IT (Mirus) in Opti-MEM (Life Technologies). After 48h cells were washed twice in PBS and lysed in 1% CHAPS buffer (50 mM Hepes pH 7.4, 150 mM NaCl, 1% CHAPS, 1 mM PMSF with complete EDTA-free proteinase inhibitor

cocktail (Roche Applied Science). After clarification at 4°C for 30min (14,000 rpm) lysate was incubated with 10µl GFP-Trap (ChromoTek)/ANTI-FLAG M2 Affinity Gel (Sigma Aldrich) for 3h. Beads were washed four times with 150mM NaCl and 1% CHAPS, then eluted in SDS-sample buffer (90°C for 5min).

Immunoblotting

After SDS-PAGE using 4-12% Bis-Tris gels (Life Technologies), protein was transferred to nitrocellulose membrane (0.45 micrometers, 7 x 8.4 cm, Bio-Rad) using a Trans-Blot semi-dry transfer cell (Bio-Rad). Membranes were blocked with 5% milk for 1h, then incubated with primary and secondary antibodies (gifts from S Shao) for 1h each. Unbound antibody was washed away with PBST (3 washes, 5min each), and Amersham ECL reagent (GE Healthcare Life Sciences) used for detection.

Mass spectrometry

Samples were separated by SDS-PAGE, using 4-12% Bis-Tris gels (Life Technologies). Bands were excised after 30min staining in Colloidal Coomassie (Thermo Fisher Scientific), followed by 3h washing in H_2O. Proteolysis, Orbitrap-mass spectrometry and MASCOT database searching were performed by the LMB Biological Mass Spectrometry & Proteomics Laboratory.

RNA-seq

RNA preparation

10 Gravid adults were left to lay eggs for 2h on an OP50 lawn seeded 24h previously, before being picked away. 8-10 plates were used per replicate, and all genetics backgrounds were prepared in parallel. Once animals reached late L4 stage, they were washed twice in M9 and frozen in LN_2. 1ml Qiazol Lysis Regaent (Qiagen) and 300-400µl 0.7mm Zirconia beads (BioSpec) were added to worm pellets in preparation for mechanical disruption. Samples were disrupted with a TissueLyser (Qiagen), using 1min at maximum power followed by 1min on ice (repeated 4 times). RNA was extracted using the RNeasy Plus Universal Mini

Kit (Qiagen), following the manufacturer's instructions with the exception that 1-Bromo-3-chloropropane (Sigma, B673) was used instead of chloroform.

Library preparation, sequencing and analysis

Libraries were prepared and sequenced by the CRI, using TruSeq stranded mRNA kit with polyA capture for mRNA (Illumina) and the HiSeq 4000 platform (Illumina, with 50bp read length, SE). Transcript quantification and differential expression was performed by Alastair Crisp; reads were aligned to the *C. elegans* genome using TopHat v2.1.0, and assembled using Cufflinks v2.2.1.

GO and pathway enrichment

GO enrichment was obtained from modMine (Smith et al., 2012), using default settings (biological process, Holm-Bonferroni test correction, $P < 0.05$). Pathway enrichment ($P < 0.05$) was also performed on modMine, using data from KEGG and Reactome, with Holm-Bonferroni test correction. Because little or no GO/pathway enrichment was found using *C. elegans* annotations, *Drosophila* orthologs were used instead. *C. elegans* gene descriptions were obtained from SimpleMine.

Contributions

C Chen isolated *db699* and *db897* after EMS-mutagenesis of *npr-1* and helped with mapping. G Nelson analysed WGS data to identify *malt-1* mutations, and helped find a workaround for CloudMap file size limits. JM Skehel and colleagues in the LMB Mass Spectrometry facility performed proteomics analysis. The CRI prepared DNA/RNA libraries and performed sequencing, and A Crisp analyzed RNA-seq data.

References

Beattie, E.C., Stellwagen, D., Morishita, W., Bresnahan, J.C., Keun Ha, B., Zastrow, Von, M., Beattie, M.S., and Malenka, R.C. (2002). Control of Synaptic Strength by Glial TNFα. Science *295*, 2282–2285.

Bretscher, A.J., Busch, K.E., and de Bono, M. (2008). A carbon dioxide avoidance behavior is integrated with responses to ambient oxygen and food in Caenorhabditis elegans. Proc Natl Acad Sci USA *105*, 8044–8049.

Busch, K.E., Laurent, P., Soltesz, Z., Murphy, R.J., Faivre, O., Hedwig, B., Thomas, M., Smith, H.L., and de Bono, M. (2012). Tonic signaling from O2 sensors sets neural circuit activity and behavioral state. Nat Neurosci *15*, 581–591.

Chang, S.H., Park, H., and Dong, C. (2006). Act1 Adaptor Protein Is an Immediate and Essential Signaling Component of Interleukin-17 Receptor. J Biol Chem *281*, 35603–35607.

Chen, C., Fenk, L.A., and de Bono, M. (2013). Efficient genome editing in Caenorhabditis elegans by CRISPR-targeted homologous recombination. Nucleic Acids Res *41*, e193–e193.

Chen, C., Itakura, E., Nelson, G.M., Sheng, M., Laurent, P., Fenk, L.A., Butcher, R.A., Hegde, R.S., and de Bono, M. (2017). IL-17 is a neuromodulator of Caenorhabditis elegans sensory responses. Nature *542*, 43–48.

Chen, C., Itakura, E., Weber, K.P., Hegde, R.S., and de Bono, M. (2014). An ER Complex of ODR-4 and ODR-8/Ufm1 Specific Protease 2 Promotes GPCR Maturation by a Ufm1-Independent Mechanism. PLoS Genet *10*, e1004082–13.

Cheung, B.H.H., Arellano-Carbajal, F., Rybicki, I., and de Bono, M. (2004). Soluble Guanylate Cyclases Act in Neurons Exposed to the Body Fluid to Promote C. elegans Aggregation Behavior. Curr Biol *14*, 1105–1111.

Cheung, B.H.H., Cohen, M., Rogers, C., Albayram, O., and de Bono, M. (2005). Experience-Dependent Modulation of C. elegans Behavior by Ambient Oxygen. Curr Biol *15*, 905–917.

Coornaert, B., Baens, M., Heyninck, K., Bekaert, T., Haegman, M., Staal, J., Sun, L., Chen, Z.J., Marynen, P., and Beyaert, R. (2008). T cell antigen receptor stimulation induces MALT1 paracaspase–mediated cleavage of the NF-κB inhibitor A20. Nat Immunol *9*, 263–271.

Davis, M.W., Hammarlund, M., Harrach, T., Hullett, P., Olsen, S., and Jorgensen, E.M. (2005). BMC Genomics *6*, 118–11.

de Bono, M., and Bargmann, C.I. (1998). Natural Variation in a Neuropeptide Y Receptor Homolog Modifies Social Behavior and Food Response in. Cell *94*, 679–689.

Demeyer, A., Staal, J., and Beyaert, R. (2016). Targeting MALT1 Proteolytic Activity in Immunity, Inflammation and Disease: Good or Bad? Trends Mol Med *22*, 135–150.

Dierlamm, J., Murga Penas, E.M., Bentink, S., Wessendorf, S., Berger, H., Hummel, M., Klapper, W., Lenze, D., Rosenwald, A., Haralambieva, E., et al. (2008). Gain of chromosome region 18q21 including the MALT1 gene is associated with the activated B-cell-like gene expression subtype and increased BCL2 gene dosage and protein expression in diffuse large B-cell lymphoma. Haematologica *93*, 688–696.

Fenk, L.A., and de Bono, M. (2015). Environmental CO 2inhibits Caenorhabditis elegansegg-laying by modulating olfactory neurons and evokes widespread changes in neural activity. Proc Natl Acad Sci USA *112*, E3525–E3534.

Frézal, L., and Félix, M.-A. (2015). C. elegans outside the Petri dish. eLife *4:e05849*.

Gaffen, S.L. (2009). Structure and signalling in the IL-17 receptor family. Nat Rev Immunol *9*, 556–567.

Gaffen, S.L., Jain, R., Garg, A.V., and Cua, D.J. (2014). The IL-23–IL-17 immune axis: from mechanisms to therapeutic testing. Nat Rev Immunol *14*, 585–600.

Gewies, A., Gorka, O., Bergmann, H., Pechloff, K., Petermann, F., Jeltsch, K.M., Rudelius, M., Kriegsmann, M., Weichert, W., Horsch, M., et al. (2014). Uncoupling Malt1 Threshold Function from Paracaspase Activity Results in Destructive Autoimmune Inflammation. Cell Rep *9*, 1292–1305.

Goshen, I., Kreisel, T., Ounallah-Saad, H., Renbaum, P., Zalzstein, Y., Ben Hur, T., Levy-Lahad, E., and Yirmiya, R. (2007). A dual role for interleukin-1 in hippocampal-dependent memory processes. Psychoneuroendocrinology *32*, 1106–1115.

Gray, J.M., Karow, D.S., Lu, H., Chang, A.J., Chang, J.S., Ellis, R.E., Marletta, M.A., and Bargmann, C.I. (2004). Oxygen sensation and social feeding mediated by a C. elegans guanylate cyclase homologue. Nature *430*, 317–322.

Habacher, C., Guo, Y., Venz, R., Kumari, P., Neagu, A., Gaidatzis, D., Harvald, E.B., Færgeman, N.J., Gut, H., and Ciosk, R. (2016). Ribonuclease-Mediated Control of Body Fat. Dev Cell *39*, 359–369.

Hachmann, J., and Salvesen, G.S. (2016). The Paracaspase MALT1. Biochimie *122*, 324–338.

Hachmann, J., Snipas, S.J., van Raam, B.J., Cancino, E.M., Houlihan, E.J., Poreba, M., Kasperkiewicz, P., Drag, M., and Salvesen, G.S. (2012). Mechanism and specificity of the human paracaspase MALT1. Biochem J *443*, 287–295.

Hulpiau, P., Driege, Y., Staal, J., and Beyaert, R. (2015). MALT1 is not alone after all: identification of novel paracaspases. Cell Mol Life Sci *73*, 1103–1116.

Jabara, H.H., Ohsumi, T., Chou, J., Massaad, M.J., BSc, H.B., Megarbane, A., Chouery, E., Mikhael, R., Gorka, O., Gewies, A., et al. (2013). A homozygous mucosa-associated lymphoid tissue 1 (MALT1) mutation in a family with combined immunodeficiency. J Allergy Clin Immunol *132*, 151–158.

Jaworski, M., and Thome, M. (2015). The paracaspase MALT1: biological function and potential for therapeutic inhibition. Cell Mol Life Sci *73*, 459–473.

Jeltsch, K.M., Hu, D., Brenner, S., Zöller, J., Heinz, G.A., Nagel, D., Vogel, K.U., Rehage, N., Warth, S.C., Edelmann, S.L., et al. (2014). Cleavage of roquin and regnase-1 by the paracaspase MALT1 releases their cooperatively repressed targets to promote TH17 differentiation. Nat Immunol *15*, 1079–1089.

Johansen, C., Mose, M., Ommen, P., Bertelsen, T., Vinter, H., Hailfinger, S., Lorscheid, S., Schulze-Osthoff, K., and Iversen, L. (2015). IκBζ is a key driver in the development of psoriasis. Proc Natl Acad Sci USA *112*, E5825–E5833.

Katz, P.S., and Lillvis, J.L. (2014). ScienceDirect Reconciling the deep homology of neuromodulation with the evolution of behavior. Curr Opin Neurobiol *29*, 39–47.

Kerr, R., Lev-Ram, V., Baird, G., Vincent, P., Tsien, R.Y., and Schafer, W.R. (2000). Optical Imaging of Calcium Transients in Neurons and Pharyngeal Muscle of *C. elegans*. Neuron *26*, 583–594.

Kim, K., and Li, C. (2004). Expression and regulation of an FMRFamide-related neuropeptide gene family in *Caenorhabditis elegans*. J Comp Neurol *475*, 540–550.

Klei, L.R., Hu, D., Panek, R., Alfano, D.N., Bridwell, R.E., Bailey, K.M., Oravecz-Wilson, K.I., Concel, V.J., Hess, E.M., Van Beek, M., et al. (2016). MALT1 Protease Activation Triggers Acute Disruption of Endothelial Barrier Integrity via CYLD Cleavage. Cell Rep *17*, 221–232.

Laurent, P., Soltesz, Z., Nelson, G.M., Chen, C., Arellano-Carbajal, F., Levy, E., and de Bono, M. (2015). Decoding a neural circuit controlling global animal state in C. elegans. eLife *4*, e04241.

Lewitus, G.M., Konefal, S.C., Greenhalgh, A.D., Pribiag, H., Augereau, K., and Stellwagen, D. (2016). Microglial TNF-α Suppresses Cocaine-Induced Plasticity and Behavioral Sensitization. Neuron *90*, 483–491.

Li, S., Armstrong, C.M., Bertin, N., Ge, H., Milstein, S., Boxem, M., Vidalain, P.-O., Han, J.-D.J., Chesneau, A., Hao, T., et al. (2004). A Map of the Interactome Network of the Metazoan C. elegans. Science *303*, 540–543.

Macosko, E.Z. (2009). The Neural Circuitry Of Social Behavior In C. elegans. Student Theses and Dissertations Paper 119.

Marder, E. (2012). Neuromodulation of Neuronal Circuits: Back to the Future. Neuron *76*, 1–11.

Marin, I., and Kipnis, J. (2013). Learning and memory ... and the immune system. Learn Mem *20*, 601–606.

McAllister-Lucas, L.M. (2001). Bimp1, a MAGUK Family Member Linking Protein Kinase C Activation to Bcl10-mediated NF-kappa B Induction. J Biol Chem *276*, 30589–30597.

McKinnon, M., Rozmus, J., Fung, S.-Y., Hirschfeld, A.F., Del Bel, K.L., Thomas, L., Marr, N., Martin, S.D., Marwaha, A.K., Priatel, J.J., et al. (2014). Combined immunodeficiency associated with homozygous MALT1 mutations. J Allergy Clin Immunol *133*, 1458–1462.e7.

Minevich, G., Park, D.S., Blankenberg, D., Poole, R.J., and Hobert, O. (2012). CloudMap: A Cloud-Based Pipeline for Analysis of Mutant Genome Sequences. Genetics *192*, 1249–1269.

Ngo, V.N., Davis, R.E., Lamy, L., Yu, X., Zhao, H., Lenz, G., Lam, L.T., Dave, S., Yang, L., Powell, J., et al. (2006). A loss-of-function RNA interference screen for molecular targets in cancer. Nature *441*, 106–110.

Park, H.H., Lo, Y.-C., Lin, S.-C., Wang, L., Yang, J.K., and Wu, H. (2007). The Death Domain Superfamily in Intracellular Signaling of Apoptosis and Inflammation. Annu Rev Immunol *25*, 561–586.

Punwani, D., Wang, H., Chan, A.Y., Cowan, M.J., Mallott, J., Sunderam, U., Mollenauer, M., Srinivasan, R., Brenner, S.E., Mulder, A., et al. (2015). Combined Immunodeficiency Due to MALT1 Mutations, Treated by Hematopoietic Cell Transplantation. J Clin Immunol *35*, 135–146.

Qiao, Q., Yang, C., Zheng, C., Fontán, L., David, L., Yu, X., Bracken, C., Rosen, M., Melnick, A., Egelman, E.H., et al. (2013). Structural Architecture of the CARMA1/Bcl10/MALT1 Signalosome: Nucleation-Induced Filamentous Assembly. Mol Cell *51*, 766–779.

Rogers, C., Persson, A., Cheung, B., and de Bono, M. (2006). Behavioral Motifs and Neural Pathways Coordinating O2 Responses and Aggregation in C. elegans. Curr Biol *16*, 649–659.

Ruefli-Brasse, A.A., French, D.M., and Dixit, V.M. (2003). Regulation of NF-B–Dependent Lymphocyte Activation and Development by Paracaspase. Science *302*, 1581–1584.

Ruland, J., Duncan, G.S., Wakeham, A., and Mak, T.W. (2003). Differential Requirement for Malt1 in T and B Cell Antigen Receptor Signaling. Immunity *19*, 749–758.

Sawcer, S., Hellenthal, G., Pirinen, M., Spencer, C.C.A., Patsopoulos, N.A., Moutsianas, L., Dilthey, A., Su, Z., Freeman, C., Hunt, S.E., et al. (2011). Genetic risk and a primary role for cell-mediated immune mechanisms in multiple sclerosis. Nature *476*, 214–219.

Schneider, H., Pitossi, F., Balschun, D., Wagner, A., Del Rey, A., and Besedovsky, H.O. (1998). A neuromodulatory role of interleukin-1. Proc Natl Acad Sci USA *95*, 7778–7783.

Smith, R.N., Aleksic, J., Butano, D., Carr, A., Contrino, S., Hu, F., Lyne, M., Lyne, R., Kalderimis, A., Rutherford, K., et al. (2012). InterMine: a flexible data warehouse system for the integration and analysis of heterogeneous biological data. Bioinformatics *28*, 3163–3165.

Song, K.W., Talamas, F.X., Suttmann, R.T., Olson, P.S., Barnett, J.W., Lee, S.W., Thompson, K.D., Jin, S., Hekmat-Nejad, M., Cai, T.Z., et al. (2009). The kinase activities of interleukin-1 receptor associated kinase (IRAK)-1 and 4 are redundant in the control of inflammatory cytokine expression in human cells. Mol Immunol *46*, 1458–1466.

Staal, J., Driege, Y., Borghi, A., Hulpiau, P., Lievens, L., Gul, I., Sundararaman, S., Goncalves, A., Dhondt, I., Braeckman, B., et al. (2016). The CARD-CC/Bcl10/paracaspase signaling complex is functionally conserved since the last common ancestor of planulozoa. bioRxiv doi: 10.1101/046789.

Sullivan, J.C., Wolenski, F.S., Reitzel, A.M., French, C.E., Traylor-Knowles, N., Gilmore, T.D., and Finnerty, J.R. (2009). Two Alleles of NF-κB in the Sea Anemone Nematostella vectensis Are Widely Dispersed in Nature and Encode Proteins with Distinct Activities. PLoS ONE *4*, e7311–e7312.

Sun, L., Deng, L., Ea, C.-K., Xia, Z.-P., and Chen, Z.J. (2004). The TRAF6 Ubiquitin Ligase and TAK1 Kinase Mediate IKK Activation by BCL10 and MALT1 in T Lymphocytes. Mol Cell *14*, 289–301.

Taghert, P.H., and Nitabach, M.N. (2012). Peptide Neuromodulation in Invertebrate Model Systems. Neuron *76*, 82–97.

Uehata, T., Iwasaki, H., Vandenbon, A., Matsushita, K., Hernandez-Cuellar, E., Kuniyoshi, K., Satoh, T., Mino, T., Suzuki, Y., Standley, D.M., et al. (2013). Malt1-Induced Cleavage of Regnase-1 in CD4+ Helper T Cells Regulates Immune Activation. Cell *153*, 1036–1049.

Uren, A.G., ORourke, K., Aravind, L., Teresa Pisabarro, M., Seshagiri, S., Koonin, E.V., and Dixit, V.M. (2000). Identification of Paracaspases and Metacaspases: Two Ancient Families of Caspase-like Proteins, One of which Plays a Key Role in MALT Lymphoma. Mol Cell *6*, 961–967.

Vezzani, A., and Viviani, B. (2015). Neuromodulatory properties of inflammatory

cytokines and their impact on neuronal excitability. Neuropharmacology *96*, 70–82.

Wester, J.C., and McBain, C.J. (2014). ScienceDirect Behavioral state-dependent modulation of distinct interneuron subtypes and consequences for circuit function. Curr Opin Neurobiol *29*, 118–125.

Wu, H., and Arron, J.R. (2003). TRAF6, a molecular bridge spanning adaptive immunity, innate immunity and osteoimmunology. BioEssays *25*, 1096–1105.

Yamamoto, M., Yamazaki, S., Uematsu, S., Sato, S., Hemmi, H., Hoshino, K., Kaisho, T., Hirotaka, K., Takeuchi, O., Takeshige, K., et al. (2004). Regulation of Toll/IL-1-Receptor- Mediated Gene Expression by the Inducible Nuclear Protein IκBζ. Nature *430*, 218–222.

Zanin, E., Dumont, J., Gassmann, R., Cheeseman, I., Maddox, P., Bahmanyar, S., Carvalho, A., Niessen, S., Yates, J.R., III, Oegema, K., et al. (2011). Affinity Purification of Protein Complexes in C. elegans. Methods Cell Biol *106*, 289–322.

3

Control of neuronal Ca^{2+} homeostasis by a CAMTA transcription factor

Introduction

The excitability of neurons and circuits is not fixed, but can vary with experience and animal state. For example, many sensory systems change the dynamic range of their responses according to their current environment, enabling them to encode a range of potential stimuli efficiently (Barlow, 1961; Rieke and Rudd, 2009). Maintaining the appropriate balance between excitation and inhibition is important for circuits to function properly. Deranged activity can have long-term destabilizing effects on neural networks. Insufficient activity levels can impede neuronal development and plasticity (Ganguly and Poo, 2013) whereas excitotoxic signaling can promote epileptic states and a host of neurological disorders (Bezprozvanny, 2009; Wolfart and Laker, 2015). Uncontrolled Ca^{2+} rises can damage mitochondria and trigger cell death (Kass and Orrenius, 1999). Failure to control intracellular Ca^{2+} accumulation is thought to be a critical step in the onset of progressive neurodegenerative diseases such as Alzheimer's and spinocerebellar ataxias (Berridge, 2010; Kasumu and Bezprozvanny, 2010).

To prevent the establishment of these extreme states, homeostatic mechanisms keep neuronal activity close to an optimal setpoint (Davis, 2006). In response to sustained changes in activity, synaptic strength and membrane excitability are stabilized by negative feedback mechanisms (Temporal et al., 2014; Turrigiano, 2017; Turrigiano et al., 1998). Many of the mechanisms that compensate for perturbation of cell-intrinsic activity or synaptic transmission rely on Ca^{2+}-triggered transcriptional remodeling (Goold and Nicoll, 2010; Ibata et al., 2008) since most neuronal responses alter Ca^{2+} levels (Berridge et al., 2000).

One class of Ca^{2+}-responsive transcription factors are the CAMTAs (calmodulin-binding transcription activators) (Bouche, 2002). This family of transcription factors is characterized by a unique DNA binding domain (CG-1), an immunoglobin-like fold similar to those found in non-specific DNA-binding/dimerization domains of other transcription factors (IPT/TIG), ankyrin repeats, and a calmodulin (CaM)-binding region that includes multiple IQ motifs

(Fig. 3.1 G and H). Most CAMTAs also encode both nuclear localisation and export signals (NLS/NES) (Finkler et al., 2007).

In plants, CAMTAs provide a link between Ca^{2+}/CaM signaling and transcriptional responses to biotic/abiotic stress (Doherty et al., 2009; Du et al., 2009). Mammals encode two CAMTA proteins that are enriched in heart and brain tissue (Song et al., 2006). Loss of CAMTA1 in the nervous system induces degeneration of cerebellar Purkinje cells, ataxia onset, and defects in hippocampal-dependent memory formation (Bas-Orth et al., 2016; Long et al., 2014). A variety of neurological disorders, including intellectual disability, attention deficit hyperactivity disorder (ADHD), cerebellar ataxia, and reduced memory performance have been reported in individuals with lesions in the human *CAMTA1* gene (Huentelman et al., 2007; Shinawi et al., 2014; Thevenon et al., 2012). Mechanistically however, little is known about the origin of these neurobehavioural phenotypes.

In a small number of specific contexts, the physiological role of CAMTAs has been well characterized. During cardiac growth, mammalian CAMTA2 is critical for signal-dependent transcriptional reprogramming (Song et al., 2006). Additionally, *Drosophila* CAMTA plays an important role in terminating photoreceptor activation by promoting rhodopsin degradation (Han et al., 2006). Otherwise however, the physiological functions of CAMTAs in the nervous system are poorly understood.

I show here that the *C. elegans* ortholog of CAMTA, CAMT-1, acts broadly in the nervous system to control neuronal excitability. A variety of behaviours are dependent on CAMT-1, and Ca^{2+} imaging in different neurons reveals that *camt-1* mutants respond abnormally to sensory stimuli. By dissecting its role in acclimation to ambient O_2 conditions, we propose that CAMT-1 regulates multiple adaptive drives within the same neural circuit.

Results

CAMT-1 functions broadly to control *C. elegans* behaviour

Changes in ambient O_2 conditions reset the behavioural state of aggregating *C. elegans* strains feeding on a bacterial food lawn (Laurent et al., 2015). *npr-1* animals exhibit behavioural quiescence in 7% O_2 but immediate and sustained arousal in 21% O_2. A high-throughput effort quantified the behavioural fingerprint of >500 whole-genome sequenced mutants unable to orchestrate these behavioural states appropriately (Changchun Chen, Geoff Nelson, personal communication; Chen et al., 2017). Clustering analysis performed by Zoltan Soltesz grouped these fingerprints by similarity (Frey and Dueck, 2007).

Two mutant strains in one of the phenotypic clusters harboured premature stop codons in *camt-1*, the sole *C. elegans* CAMTA (Fig. 3.1A). In addition to being defective in their response to 21% O_2, these mutants, called *db894* and *db973,* were hyperactive in 7% O_2. Additional *camt-1* KO lines recapitulated these specific defects (Fig. 3.1B and 3.9C), supporting the hypothesis that loss of CAMTA impairs responses to ambient O_2. A WT copy of the *camt-1* genomic locus conferred to mutants enhanced responsiveness in 21% O_2, and rescued their hyperactive speed in 7% O_2 (Fig. 3.1C). These results suggest that CAMT-1 is required for *C. elegans* to respond appropriately to different O_2 levels.

I asked whether CAMT-1 is also required for behavioural responses to cues other than O_2. *C. elegans* is attracted towards a range of salts and volatile compounds (Bargmann et al., 1993; Ward, 1973). Chemotaxis towards benzaldehyde, diacetyl and NaCl was reduced in *camt-1* mutants (Fig. 3.1D). I next asked if *camt-1* was also required for aversive behaviours, such as avoidance of CO_2. In response to a rise in CO_2, WT N2 worms transiently perform omega turns, Ω-shaped body bends generated by an 180˚ reversal serve to orientate the animal away from the stimulus (Bretscher et al., 2008). *camt-1* mutants exhibited abnormally high levels of omega-turns without a CO_2 stimulus (Fig. 3.1E). N2 animals also exhibit an OFF response upon removal of a CO_2 stimulus, during

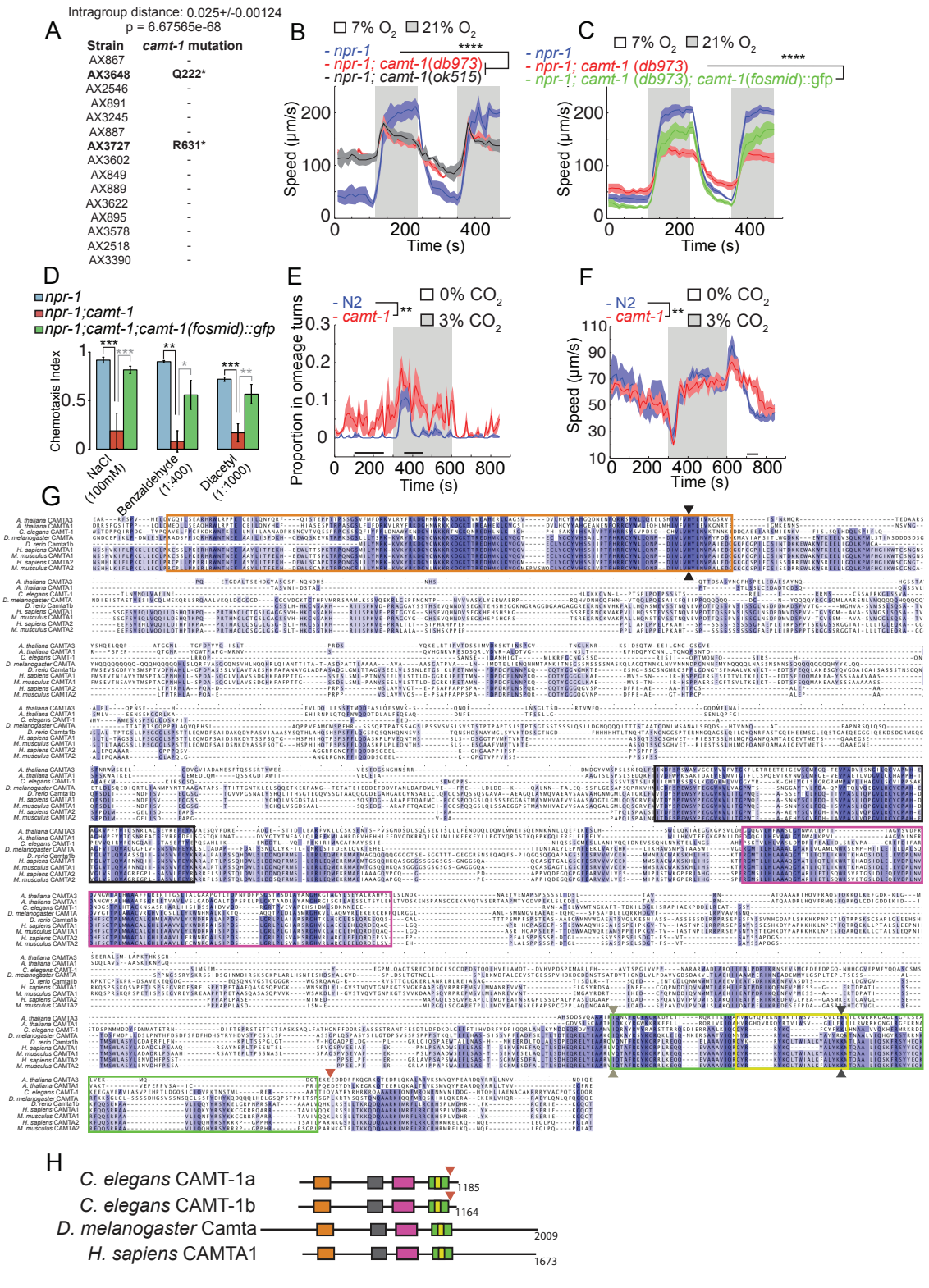

Figure 3.1 *camt-1* mutants exhibit several behavioural defects. (A) Speed of EMS-derived mutant strains at 7% O_2, 21% O_2, 1% O_2 and 3% CO_2 (C Chen). Mutants were iteratively clustered by phenotypic

which they transiently increase their speed (Fenk and de Bono, 2015). Termination of this OFF response was delayed in *camt-1* mutants, suggesting that speed responses to cues other than O_2 are also modulated by *camt-1*.

In humans, CAMTA transcription factors are expressed in many brain regions (Huentelman et al., 2007). We generated a reporter to map the expression pattern of CAMT-1 in *C. elegans*. To retain as much endogenous regulatory information as possible, we recombineered GFP immediately prior to the *camt-1* stop codon on a fosmid including >10 kb of flanking sequences 5' of the initiation codon and 3' of the stop codon for *camt-1*. This reporter was functional (Fig. 3.1C) and was expressed broadly and specifically in the nervous system (Fig. 3.2A). We observed CAMT-1 expression in dye-filled sensory neurons (Fig. 3.2B), motor neurons of the ventral cord (Fig. 3.2A), the URX O_2 sensing neurons and the RMG hub interneurons (Fig. 3.2C and D), and most cholinergic neurons (Fig. 3.2E).

similarity using affinity propagation (Z Soltesz). The phenotypic group shown contains two strains bearing lesions in *camt-1* (G Nelson). (B) *camt-1* mutants exhibit altered locomotory responses to 21% O_2 and hyperactive movement at 7% O_2. (C) A WT copy of the *camt-1* genomic locus rescues the speed defects of *camt-1* mutants. (D - F) *camt-1* mutants show chemotaxis defects (D), an increased frequency of omega turns both in the presence and absence of a CO_2 stimulus (E), and a prolonged locomotory OFF response after removal of CO_2 (F). For chemotaxis, average and SEM are shown, using ANOVA with Tukey's post hoc HSD, N ≥ 4, * = P < 0.05, ** = P < 0.01, *** = P < 0.001. For speed/omega turns, I plot average (line) and SEM (shaded regions), n ≥ 25 animals, N ≥ 3. ** = P < 0.01, **** = P < 0.0001, Mann-Whitney *U* test. Black bars indicate time points used for statistical tests. (E) and (F) were performed in 7% O_2. (G and H) Sequence alignment (G) and domain organization (H) of CAMTA proteins, highlighting the conserved CG-1 DNA binding domain (orange), the IPT/TIG Domain (black), Ankyrin repeats (purple), putative CaM-binding domain (yellow) and IQ region (green). Black arrowheads point to CG-1 histidine (H190 in *C. elegans*, see Fig. 3.9A), light grey arrowheads point to IQ1 isoleucine (I1803 in *Drosophila*, see (Han et al., 2006)), dark grey arrowheads point to CaM-binding domain lysine (K907 in *Arabidopsis*, see (Du et al., 2009)), and red arrowheads point to the site of insertion of a premature stop codon in *db1214* (see below). Residue colour intensity indicates % identity. Domain predictions are based on Uniprot and Calmodulin Target Database (http://calcium.uhnres.utoronto.ca/ctdb/ctdb/home.html).

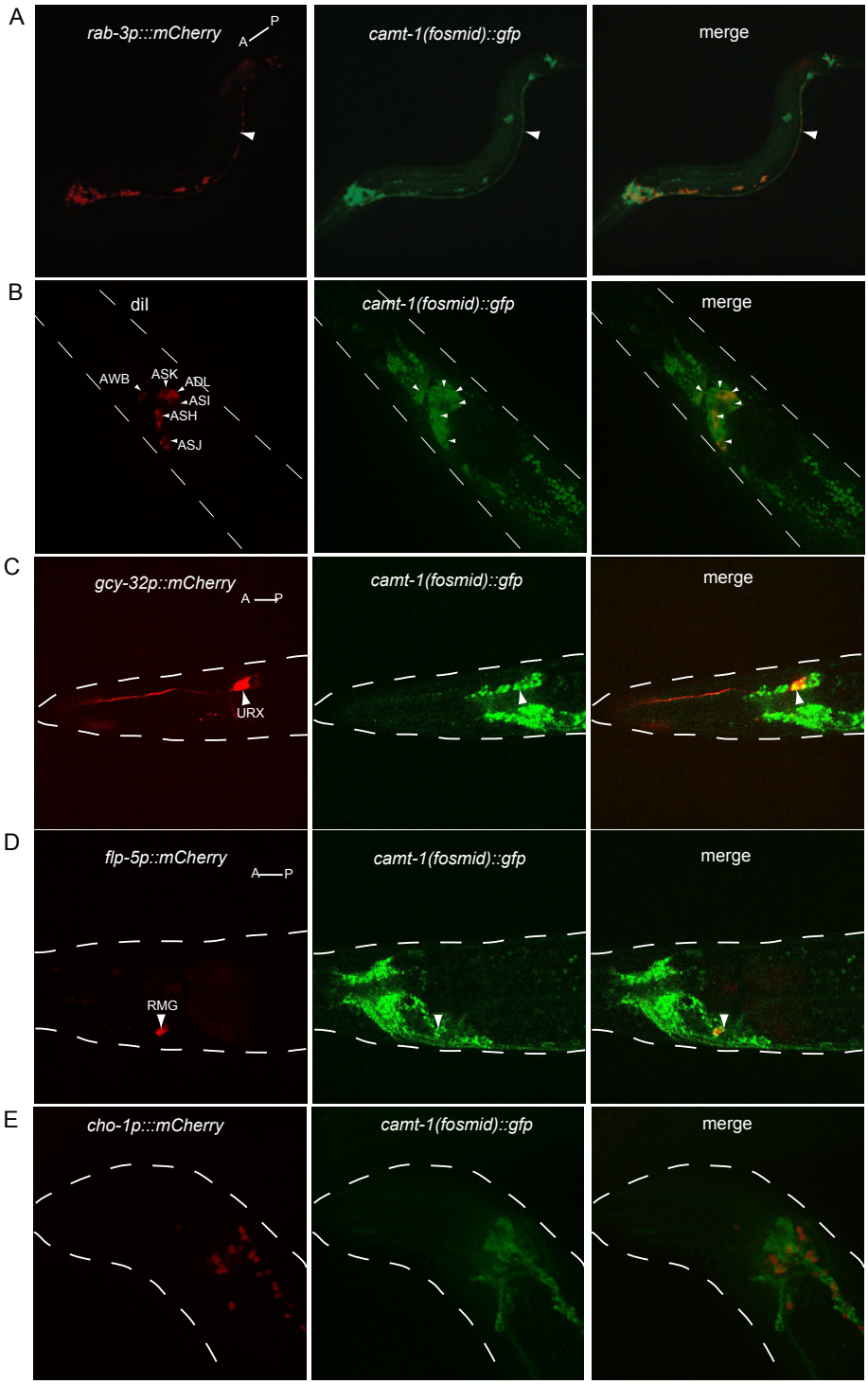

Figure 3.2 CAMT-1 is expressed widely and specifically in the nervous system. C-terminally GFP-tagged CAMT-1, driven from its endogenous regulatory sequences, colocalizes with (A) a *rab-3p::mcherry* reporter expressed in most neurons, including motor neurons of the ventral cord (white arrowhead), (B) DiI-filled amphid neurons, (C) URX O_2-sensors visualized using *gcy-32p::mcherry*, (D) RMG visualized using *flp-5p::mcherry* and (E) cholinergic neurons visualized using a *cho-1p::mcherry* reporter.

Calcium-dependent changes in gene expression are known to be important for both development and function of the nervous system (West et al., 2002). To elcudiate if CAMT-1 activity was required during development, we expressed *camt-1* cDNA from a heatshock-inducible promoter. Without heat-shock, this

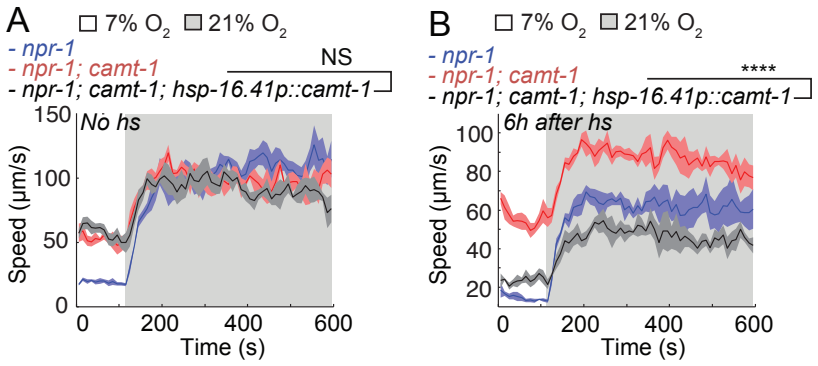

Figure 3.3 Inducing CAMT-1 expression in L4 animals can rescue mutant phenotypes. (A) A *hsp-16.41p::camt-1* transgene does not rescue the hyperactive locomotion of *camt-1* mutants without heat-shock. (B) Heat-shock induced expression of CAMT-1 in L4 animals rescues *camt-1* O_2-evoked responses. Plotted are average speed (line) and SEM (shaded regions), n ≥ 50 animals, N = 4 assays. **** = P < 0.0001, Mann-Whitney *U* test.

transgene did not rescue the hyperactivity phenotype of *camt-1* mutants (Fig. 3.3A). However, inducing *camt-1* expression specifically in late L4s/ young adults was sufficient to rescue the phenotype, indicating that CAMT-1 is not required developmentally (Fig. 3.3B).

We limited *camt-1* cDNA expression to different subsets of neurons to find out where it is required to promote aerotaxis. As expected, pan-neuronal expression rescued mutant phenotypes (Fig. 3.4C). Interestingly neuronal *camt-1* overexpression reduced speed at 7% O_2 even beyond *npr-1* levels, suggesting that speed is correlated with CAMT-1 levels. Restricting expression to O_2 sensory neurons or RMG did not, however, substantially restore behaviour (Fig. 3.4A and B).

The *camt-1* locus is predicted to encode 2 alternatively spliced CAMTA proteins. Our fosmid reporter and rescue experiments above specifically tagged or

expressed the longer a isoform. We found that rescue conferred by the shorter b isoform was comparable to that obtained by the a isoform (Fig. 3.4D). It is therefore unclear if there are functional differences between the two isoforms, although it is possible that they are differentially expressed.

CAMT-1 dampens sensory neuron signaling

To test whether disrupting *camt-1* altered sensory responses we recorded stimulus-evoked Ca^{2+} levels in O_2- and CO_2-sensing neurons with Yellow Cameleon (YC2.60/3.60). URX activity tracks environmental O_2 levels, and tonic

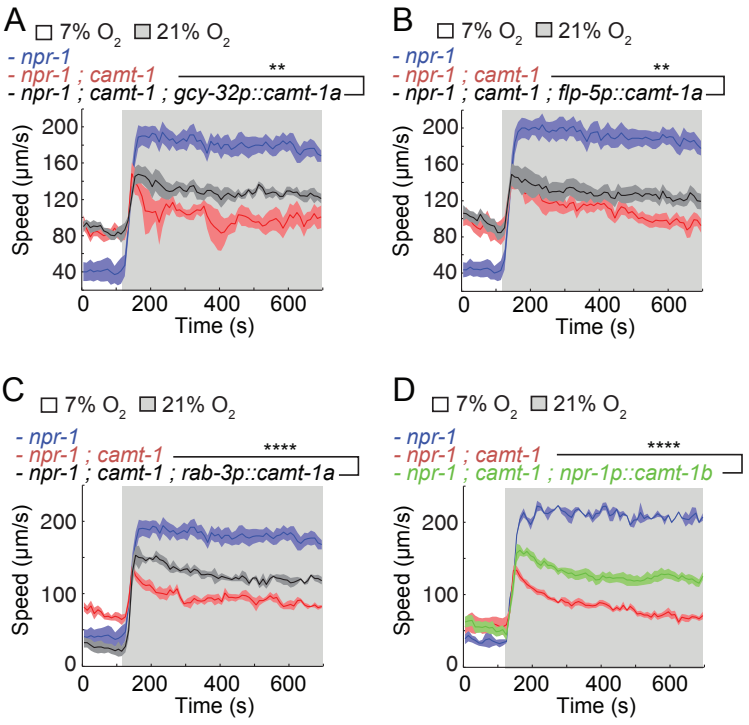

Figure 3.4 CAMT-1 likely acts in multiple neurons. Defective responses of *camt-1* mutants to 21% O_2 are only partially rescued by expression of the longest CAMT-1 isoform (CAMT-1a) in O_2-sensing neurons (A), or RMG (B). (C) Pan-neuronal expression of CAMT-1a restores responsiveness to 21% O_2 and low speed in 7% O_2. (D) Pan-neuronal expression of the shorter CAMT-1b isoform also rescues the mutant's speed defect in 21% O_2. Average speed (line) and SEM (shaded regions) are plotted, n ≥ 59 animals, N ≥ 4 assays. ** = P < 0.01, **** = P < 0.0001, Mann-Whitney *U* test.

signaling from URX to RMG drives high locomotory activity at 21% O_2 (Busch et al., 2012). AFD and BAG neurons are CO_2 sensors, and BAG drives omega turns when CO_2 levels rise (Bretscher et al., 2011; Fenk et al., 2015). We found that Ca^{2+} levels in URX, AFD and BAG were significantly elevated in *camt-1* mutants

across all O_2/CO_2 conditions, suggesting that *camt-1* dampens the excitability of these sensory neurons (Fig. 3.5A, C, E). Remarkably, we observed the converse phenotype, dramatically reduced Ca^{2+} levels, when we overexpressed *camt-1* cDNA specifically in WT O_2 sensors or in BAG neurons (Fig. 3.5B, D).

To express YC2.60 in O_2 sensors we used the *gcy-37* promoter (Fig. 3.5A and B). *gcy-37* encodes one of 5 atypical soluble guanylate cyclases expressed in the AQR, PQR and URX neurons, at least two of which are molecular O_2 sensors. We investigated whether CAMT-1 altered expression from the *gcy-37* promoter,

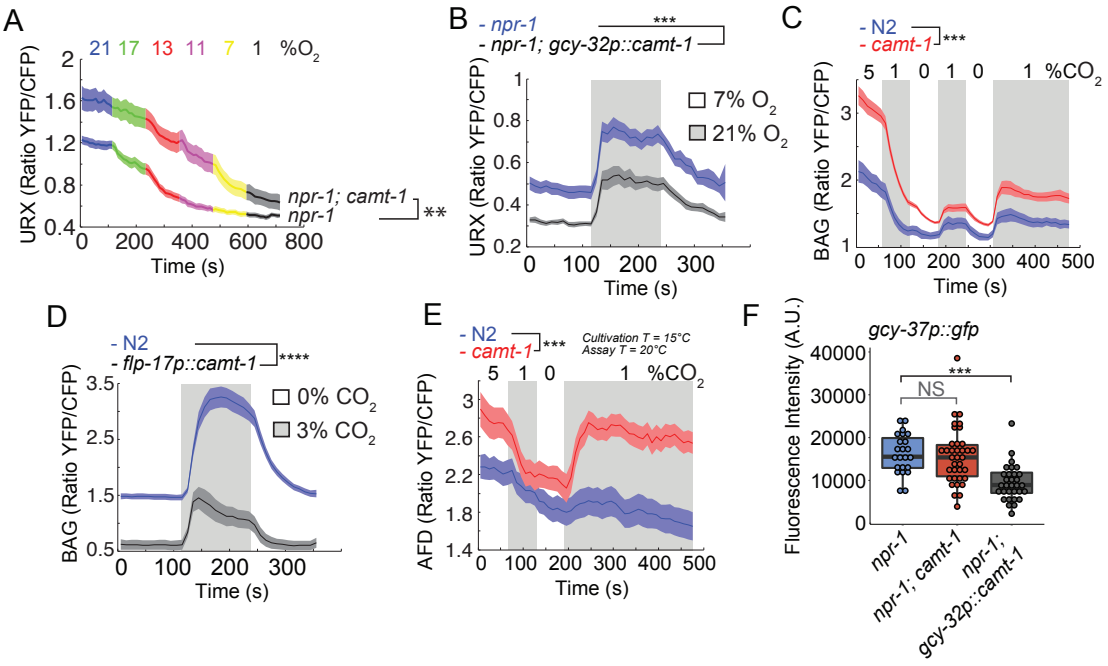

Figure 3.5 CAMT-1 negatively regulates sensory neuron activity. The URX O_2-sensing neurons and the BAG and AFD CO_2 sensors have enhanced Ca^{2+} levels in *camt-1* mutants across a range of stimulus intensities (A, C, E). Conversely, overexpressing *camt-1* cDNA in O_2 sensing or BAG neurons strongly reduces Ca^{2+} levels (B and D). YFP/CFP ratios in URX were reported by YC2.60 driven from the *gcy-32* promoter (A and B), in BAG by YC3.60 driven from the *flp-17* promoter (C and D) and in AFD by YC3.60 driven from the *gcy-8* promoter (E). (F) Quantification of GFP expression driven from the *gcy-37* promoter suggests that YC2.60 expression levels are not significantly affected by disrupting *camt-1,* but are reduced when CAMT-1 is overexpressed. For speed and omega turns, I plot the average (line) and SEM (shaded regions). (A) n ≥ 15. (B) n ≥ 17. (C) n ≥ 18. (D) n ≥ 20. (E) n ≥15. (F) n ≥ 23. ** = P < 0.01, *** = P < 0.001, **** = P < 0.0001, Mann-Whitney *U* test (YFP/CFP ratios) or ANOVA with Tukey's post hoc HSD (GFP quantification). Black bars indicate timepoints used for statistical test.

by quantifying the expression of a *gcy-37p::GFP* transgene in WT, *camt-1* and CAMT-1 overexpression strains. We found that GFP levels were reduced by CAMT-1 overexpression, but unaltered by loss of CAMT-1 (Fig. 3.5F). Although YC2.60 is a ratiometric sensor, we cannot exclude the possibility that its reduced expression in animals overexpressing CAMT-1 contributes to the reduced baseline YFP/CFP ratio. An alternative hypothesis is that CAMT-1 overexpression inhibits expression not only of *gcy-37*, but also of *gcy-35* and *gcy-36*, which are required for O_2-evoked Ca^{2+} responses in URX.

CAMT-1 promotes RMG interneuron responsiveness

RMG hub interneurons integrate inputs from multiple sensory stimuli, including food, pheromones and O_2, and drive the change in locomotory state associated with a switch from 7% to 21% O_2 (Laurent et al., 2015; Macosko et al., 2009). The O_2-evoked responses in RMG depend on URX: URX ablation abolishes these responses. Unexpectedly, we found that at 7% O_2, baseline Ca^{2+} in RMG was higher in *camt-1* animals than controls, whereas Ca^{2+} responses to 21% O_2 were strongly reduced in *camt-1* mutants, despite CAMT-1 loss dramatically increasing URX Ca^{2+} responses (Fig. 3.6A). Since these observations were made in immobilized animals, we confirmed them by imaging freely moving animals. RMG responses were elevated in freely moving *camt-1* mutants in 7% O_2, but the amplitude of response to 21% O_2 was decreased (Fig. 3.6B and C). Whether the RMG phenotype reflects a homeostatic response to hyperactivation by URX, or altered input into RMG from other neurons is unclear. However, our analysis of URX and RMG physiology is consistent with *camt-1* mutants showing reduced locomotory activity at 21% O_2 due to defective RMG responsiveness.

CAMT-1 regulates experience-dependent plasticity

The URX-RMG circuit acclimates to previous O_2 experience. Long-term exposure to 21% O_2 enhances URX and RMG responsiveness to subsequent 21% O_2 input (Fenk and de Bono, 2017), while cultivation in 7% O_2 shifts the dynamic range of URX towards lower O_2 concentrations (Emmanuel Busch, unpubl.).

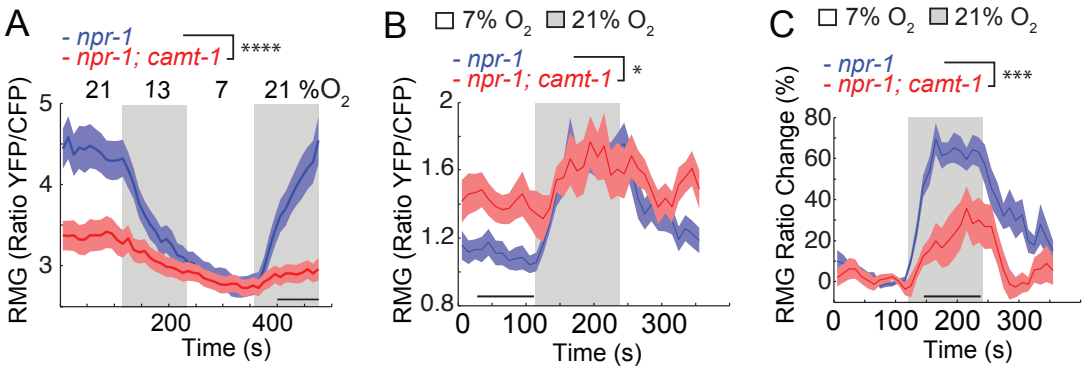

Figure 3.6 CAMT-1 promotes RMG responsiveness. The amplitude of Ca^{2+} responses to 21% O_2 are decreased in camt-1 mutants, in both immobilized (A, n ≥ 28) and freely moving animals (B and C, n ≥ 15) expressing YC2.60 in RMG. (B) Shown are the absolute YFP/CFP ratio (left) and % change (right). camt-1 mutants have both elevated Ca^{2+} levels at 7% O_2 (A) and a smaller response amplitude when shifted to 21% (A and B). Plotted are average YFP/CFP ratios (line) and SEM (shaded regions). * = P < 0.05, *** = P < 0.001, **** = P < 0.0001, Mann-Whitney U test. Black bars indicate time points used for statistical test.

The increased sensitivity of *camt-1* mutants to low O_2 concentrations suggested CAMT-1 may regulate experience-dependent plasticity in the O_2 circuit. Consistent with this, we found that *camt-1* mutants grown at 7% O_2 showed increased tonic Ca^{2+} levels in both URX and RMG neurons when animals were kept at 7% O_2, whereas *npr-1* animals showed no significant shift. A simple interpretation is that CAMT-1 counteracts an increase in URX excitability following long periods of low activity. By contrast, *camt-1* mutants acclimated to 7% O_2 showed a decrease in tonic Ca^{2+} levels at 21% O_2 (Fig. 3.7A and B). Thus, while CAMT-1 helps set the excitability of the O_2 circuit, its effects are complex.

The decreased URX response to 21% O_2 in animals cultivated at 7% O_2 might reflect negative feedback loops that prevent excitotoxicity in this neuron. More specifically, transiently exposing *camt-1* animals cultivated in 7% O_2 to room air while preparing them for imaging could reduce URX excitability relative to WT. To test this, we kept animals reared at 7% O_2 inside an air-tight chamber during assay setup. Under these conditions we found that the amplitude of the URX response to 21% O_2 was similar in *npr-1* and *npr-1; camt-1* animals (Fig. 3.7C).

To explore whether CAMT-1 altered the dynamic range of URX, we plotted the relative change in the YFP/CFP ratio, instead of the ratio itself. In *npr-1* animals URX is most responsive to O_2 concentrations around 13% and shows little or no response to lower concentrations (Oda et al., 2016). We found that loss of CAMT-1 shifted the dynamic range of URX towards lower O_2 concentrations (Fig. 3.7D and E). Thus, as well as being a negative regulator of URX Ca^{2+} signaling,

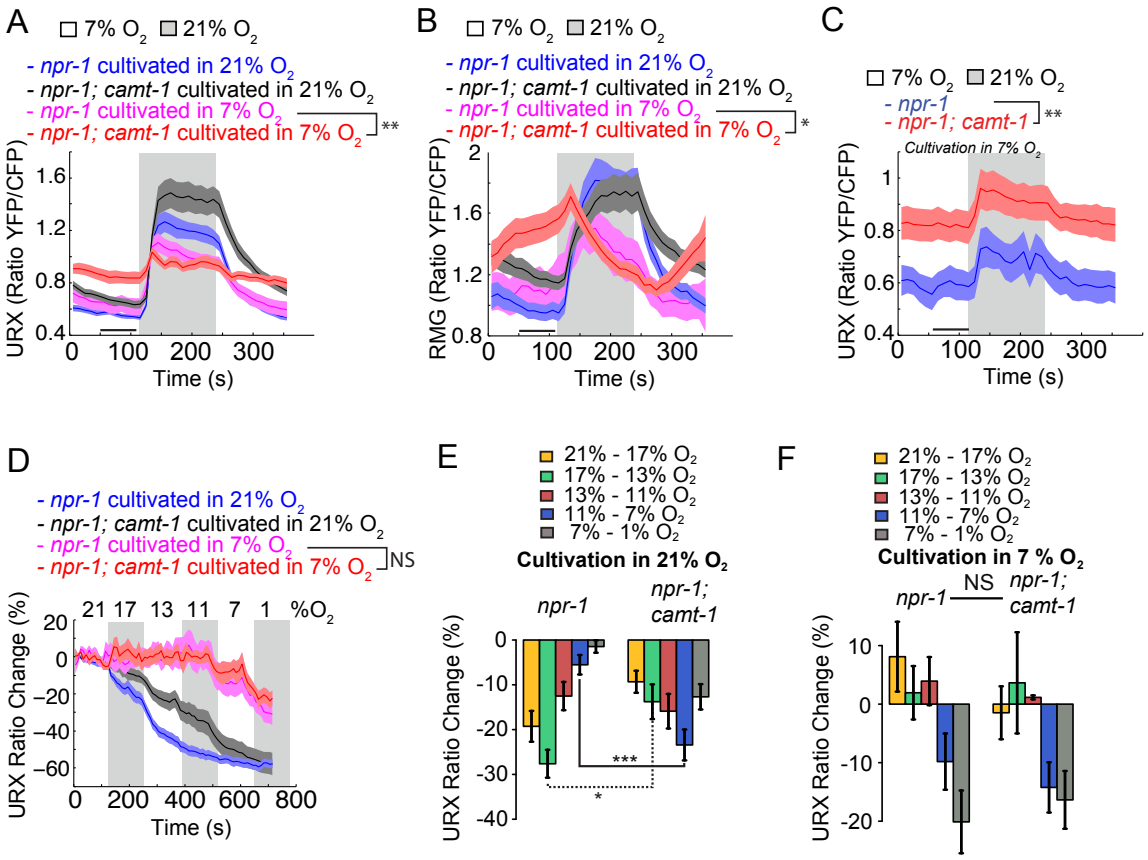

Figure 3.7 CAMT-1 controls acclimation to previous O_2 conditions. In *camt-1* mutants reared in 7% O_2, Ca^{2+} levels in URX and RMG are elevated, but responsiveness to 21% O_2 is decreased (A and B). Preventing any exposure to 21% O_2 before recording eliminates the difference in response amplitude between *npr-1* and *npr-1; camt-1*, but does not eliminate enhanced activity at 7% O_2 (C). *camt-1* shifts the dynamic range of URX towards lower O_2 levels in worms reared in 21% O_2, but has little effect on the dynamic range of animals reared in 7% O_2 (D-F). (D) % change in YFP/CFP ratio relative to the average ratio at 21% O_2. (E and F) Maximum % change in YFP/CFP during each stimulus. Plotted are the average (represented by the lines in A-D and coloured bars in E and F) and SEM (represented by the shaded regions in A-E and error bars is F and G). Data from Fig. 3.5A is replotted in D-F to show relative rather than absolute change. (A) n ≥ 17. (B) n ≥ 14. (C) n ≥ 11. (D) n ≥ 10. (E) n ≥ 15. (F) n ≥ 11. * = P < 0.05, ** = P < 0.01, *** = P < 0.001, Mann-Whitney *U* test. Black bars indicate timepoints used for statistical test.

CAMTA activity keeps URX tuned to O_2 concentrations approaching 21% in animals acclimated to 21% O_2. We found that the shape of the URX dose-response curve in animals grown at 7% O_2 was not altered by *camt-1* (Fig. 3.7D and F). Therefore, CAMT-1 is required to shift the dynamic range of URX from low to high O_2 concentrations during adaptation to 21% O_2.

To complement our imaging data, we compared behavioural responses to O_2 in animals acclimated to 21% and 7% O_2. *npr-1* animals reared in 7% O_2 exhibited enhanced speed in 21% O_2 and increased basal speed when returned to 7% O_2. Loss of CAMT-1 dramatically enhanced elevated speed in 7% O_2 (Fig. 3.8A). This finding is consistent with a model in which the homeostatic drive of the 21% O_2-escape circuit to become more excitable during long-term sensory deprivation is restricted by CAMT-1.

Together, our data suggest that multiple plastic features of the 21% O_2-escape circuit are controlled by CAMT-1. As well as tuning the dynamic range of URX close to 21% O_2, CAMT-1 counteracts the homeostatic upregulation of the excitiability/output of unknown downstream neurons.

Hyperactive URX Ca^{2+} signaling in *camt-1* mutants is driven by sensory transduction but not synaptic input

To examine if altered URX function in *camt-1* mutants predominantly reflected altered sensory responses or altered synaptic input, I tested the effect of mutations that disrupt these processes. O_2 sensation in URX requires a pair of soluble guanylate cyclasses, GCY-35 and GCY-36. I made a *camt-1*; *gcy-36* double mutant to test the effect on URX of disrupting *camt-1* when O_2 sensing is defective. I found that disrupting *camt-1* did not enhance the speed of *gcy-36* animals, suggesting that the effect of CAMT-1 depends on sensory transduction (Fig. 3.8A and B). Similarly, *camt-1* did not affect URX activity in *gcy-36* null animals reared at 7% O_2, indicating that in the absence of sensory input CAMT-1 does not increase neuronal activity (Fig. 3.8C). We note that in animals

acclimated to 21%, CAMT-1 loss was sufficient to increase Ca^{2+} signaling in URX. However, we attribute this to residual O_2 sensation after *gcy-36* knockout, given that the speed and URX activity of *camt-1;gcy-36* animals was altered by previous O_2 experience. A requirement for sensory input supports a model in which CAMT-1 negatively regulates the potentiation of URX responses.

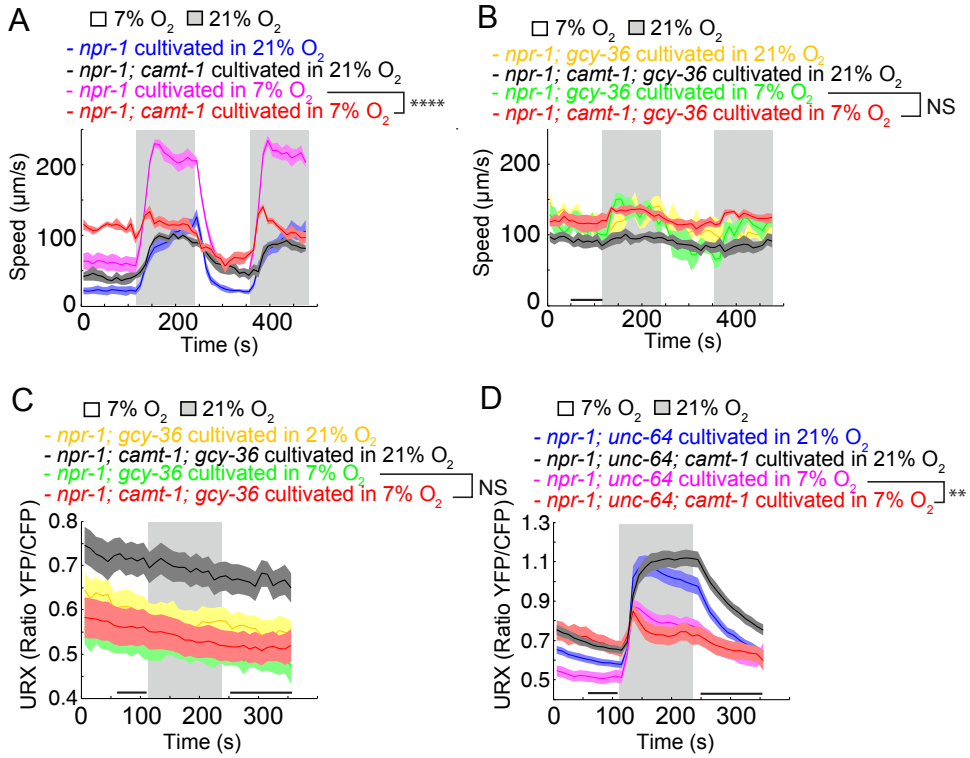

Figure 3.8 *camt-1* induced URX hyperactivity is dependent on O_2 sensation but not synaptic communication.

(A) Disrupting *camt-1* impairs speed responses to 21% O_2 and induces locomotory hyperactivity at 7% O_2 to an even greater extent in animals reared in 7% O_2. (B-C) *camt-1* phenotypes are dependent on GCY-36. All assays were performed in parallel. (B) *camt-1* loss does not induce hyperactive locomotion in *gcy-36* mutants (n ≥ 40 animals, N ≥ 3 assays). (C) In the absence of sensory input, URX does not signal hyperactively in *camt-1* mutants (n ≥ 17). Although *camt-1* loss increases Ca^{2+} levels in *gcy-36* mutants reared in 21% O_2, it does not do so in *gcy-36* mutants reared at 7% O_2. This difference indicates that *gcy-36* mutants retain some O_2-sensing capacity. (D) *unc-64* does not block elevated baseline Ca^{2+} levels in URX induced by *camt-1* loss (n ≥ 37). For speed and YFP/CFP ratios, average (line) and SEM (shaded regions) are plotted. Black bars indicate timepoints used for statistical tests. ** = P < 0.01, **** = P < 0.0001, Mann-Whitney *U* test.

As *camt-1* is expressed in many neurons, URX hyperactivity may be secondary to dysfunction elsewhere. To reduce synaptic and dense core vesicle input to

URX we used an *unc-64* (syntaxin) mutant. We found that *camt-1*-induced hyperactivity in URX was not abolished by *unc-64* mutation (Fig. 3.8D). This finding is consistent with *camt-1* having a cell autonomous function in URX. However, as the *unc-64(e246)* allele is a hypomorph (null mutants are dead) we cannot rule out a role for synaptic transmission (Saifee et al., 1998). In addition, gap junction communication from RMG is not affected by *unc-64* and may drive augmented URX signaling.

Differing requirements for DNA- and CaM-binding domains of CAMT-1

In our aggregation screen we isolated a point mutation in *camt-1* (H190P) that lies in the CG-1 DNA-binding domain. Histidine 190 is absolutely conserved among CAMTA proteins from plant to human (Fig. 3.1G). H190P cDNA did not rescue the *camt-1* phenotype, indicating that this residue is necessary for CAMTA activity (Fig. 3.9A).

The requirement of H190 suggests that the DNA-binding activity of CAMT-1 is important for its function. To test whether CAMT-1 functions in the nucleus, I have generated strains to investigate (i) the sub-cellular localization of CAMT-1 protein (Fig. 3.9D) and (ii) its functionality when restricted to the nucleus (Fig. 3.9E).

In plants and flies, the function of CAMTA proteins depends on its CaM-binding ability (Du et al., 2009; Han et al., 2006). Mapping of the CaM-binding region in *Drosophila* and *Arabidopsis* identified an isoleucine within the first IQ motif (IQ1) necessary for photoreceptor deactivation, and a single lysine residue within the CaM-binding domain necessary for growth and disease resistance respectively. Both residues are conserved in *C. elegans* (Fig. 3.1G). To test the requirement of IQ1 in *C. elegans* I mutated the analogous isoleucine residue in CAMT-1. I found that I962N mutant *camt-1* cDNA rescued behavioural responsiveness at least as well as WT cDNA (Fig. 3.9B). Although I have not yet tested the requirement of the conserved lysine within the CaM-binding domain, I observed that deleting

183 amino acids, encompassing the entire CaM-binding region, did not reduce rescuing capacity (data not shown). One interpretation of this is that CaM-biding is not essential for CAMT-1 function. However overexpressing a functional DNA-binding region may mask any regulatory requirement for CaM-binding. Given that *camt-1* overexpression has a strong effect in Ca^{2+} imaging assays, single-copy experiments will be a more informative test.

I generated lesions in the predicted CaM-binding region of the endogenous *camt-1* locus by CRISPR-Cas9. *db1214* encodes a premature stop codon close to the C terminus of *camt-1* (Fig. 3.1G and H), and reduced responsiveness to 21% O_2 (Fig. 3.9C). Besides the IQ region, this allele is predicted to remove a putative NLS, which is also missing from the CAMT-1b isoform and therefore seems not to be essential for function (Fig. 3.4D). Any conclusions over the role of CAMTA CaM-binding however, will require more precise disruptions of the endogenous locus.

A candidate approach to elucidate cellular pathways dysregulated by *camt-1*

Cell-intrinsic disruption of membrane conductance or of endoplasmic reticulum (ER) stores might contribute to perturbations in Ca^{2+} homeostasis. We searched our collection of non-aggregating strains for mutations that affect ion channels or ER Ca^{2+} flux. Initially I focused on genes with an enrichment of upstream CGCG motifs, which could plausibly be direct transcriptional targets of CAMTA.

A missense mutation in the RCK domain of the BK channel SLO-1 disrupted behavioural responses to 21% O_2 (Isabel Beets, personal communication). BK channels provide an important route of repolarizing current in neurons, so we wondered if *slo-1* mutants phenocopy *camt-1* (Elkins et al., 1986; Salkoff et al., 2006). URX responses to 21% O_2 in *slo-1* mutants were at least as strong as WT, but basal Ca^{2+} levels at 7% were unchanged (Fig. 3.10D). Additionally,

although *slo-1* reduced speed in 21% O_2, activity at 7% O_2 was normal (Fig. 3.10 C).

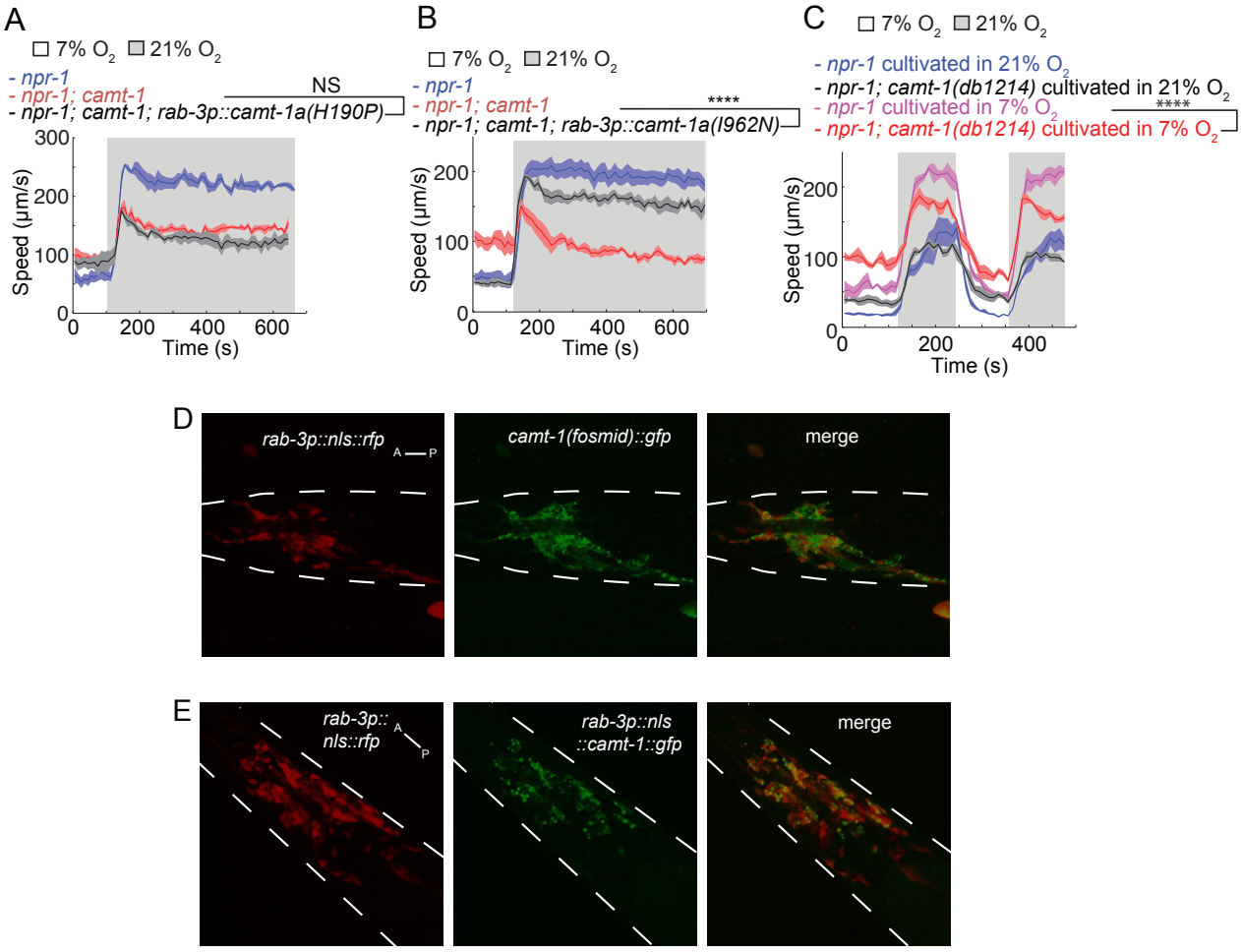

Figure 3.9 Mutational domain analysis and localization of CAMT-1. (A) cDNA encoding CAMT-1(H190P) does not rescue mutant speed defects in 7% or 21% O_2, n ≥ 44 animals, N = 4 assays. (B) IQ1 disruption using cDNA encoding CAMT-1(I962N) restores behaviour close to WT levels, n ≥ 37 animals, N ≥ 3 assays. (C) Deletion of 117 amino acids from the C terminus of CAMT-1, encoded by *db1214*, disrupts appropriate control of behavioural state after cultivation in 7% and 21% O_2, n ≥ 34 animals, N = 4 assays. **** = P < 0.0001, Mann-Whitney *U* test. (D) *in vivo* co-expression of CAMT-1::GFP and nuclear-localized neuronal RFP. (E) *in vivo* co-expression of nuclear-localized CAMT-1::GFP and nuclear-localized neuronal RFP.

I also identified a premature stop codon in *T06D8.9*, an uncharacterized gene homologous to store operated calcium entry regulatory factor (SARAF). SARAF is an ER membrane protein that is enriched in the immune and nervous systems

and maintains intracellular Ca^{2+} homeostasis during store operated calcium entry (SOCE) (Palty et al., 2012). The causality of the *T06D8.9* mutation had not been tested, so I generated CRISPR-Cas9 induced breaks in the *T06D8.9* locus. I found that SARAF loss did not have any noticeable effect on behavioural responses to 21% O_2 (Fig. 3.10B). Interestingly, *T06D8.9* upstream sequence drove expression only in two unidentified neurons in the head (Fig. 3.10A).

As SLO-1 or SARAF dyfunction were unlikely to explain hyperactive URX signaling in *camt-1* mutants, direct investigation of the contribution of cell membrane/ER currents will require pharmacological manipulation or localized indicators.

RMG responsiveness to 21% O_2 is promoted by IL-17 signaling (Chen et al., 2017). I explored whether transcriptional changes driven by IL-17 might be dependent on or modulated by CAMT-1. An IκBζ-like protein, NFKI-1, mediates the effects of IL-17 in RMG: in *nfki-1* mutants, RMG responses to 21% O_2 are reduced compared to control. Unexpectedly, overexpressing CAMT-1 restored aggregation behaviour to *nfki-1* mutants, increased their locomotory activity at 21% O_2 (Fig. 3.10E and F), and also rescued their enhanced escape of CO_2 (Fig. 3.10G). I am now using RNA-seq to compare the transcriptional profiles of *camt-1* and *nfki-1* mutants, to provide more direct insight into the relationship between CAMTA-dependent transcription and neuronal gene expression.

Transcriptome-wide analysis of CAMT-1 function

To explore the relationship between CAMTA activity and gene expression, in collaboration with Alastair Crisp, we transcriptionally profiled *camt-1* mutant and CAMT-1 overexpression strains. We found that a large number of genes were dysregulated in these conditions (Fig. 3.11A). Interestingly, many more genes were positively regulated by CAMT-1 than negatively regulated. We defined genes that were consistently positively regulated by CAMT-1 as those whose expression was both decreased by its absence, and increased by its

overexpression (Fig. 3.11A). Among this group, molecules involved in neurotransmitter and ion transport were significantly over-represented, consistent with a role for CAMT-1 in controlling neuronal activity (Fig. 3.11B).

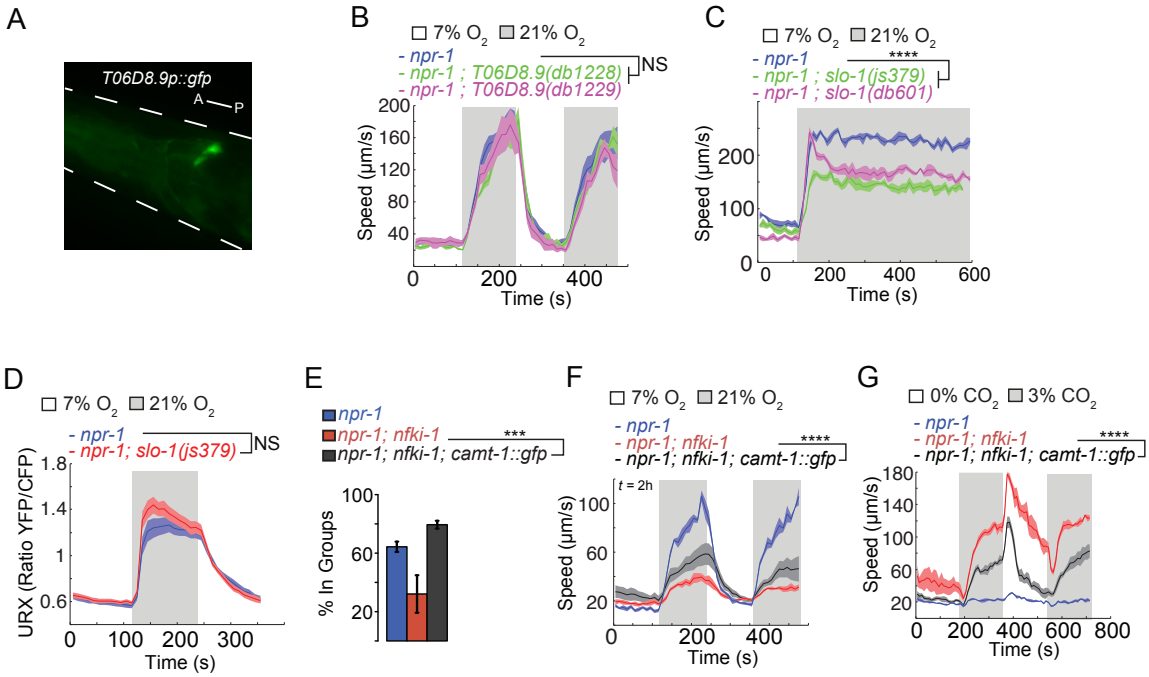

Figure 3.10 CAMT-1 overexpression overrides defects in IκBζ signaling. (A) GFP driven by 1.7Kb of T06D8.9 is expressed in the head. (B) Two independent CRISPR-Cas9 induced cuts in the *T06D8.9* locus (both encoding frameshifts) respond well to 21% O_2, n ≥ 34 animals, N = 4 assays. Missense (*db601*) and nonsense (*js379*) mutations in *slo-1* reduce speed responses to 21% O_2, n ≥ 51 animals, N ≥ 4 assays. (D) URX Ca^{2+} responses in *slo-1*(*js379)* mutants are at least as large as WT in response to 21% O_2. (E-G) 21% aggregation (E, N ≥ 4), O_2-avoidance (F, n ≥ 105 animals, N = 4 assays), and CO_2-avoidance (G, n ≥ 66 animals, N ≥ 4 assays) phenotypes of *nfki-1* mutants are significantly rescued by overexpression of a fosmid encoding CAMT-1. **** = P < 0.0001, Mann-Whitney *U* test. *** = P < 0.001, ANOVA with Tukey's HSD.

Discussion

I show that the sole *C. elegans* ortholog of CAMTA transcription factors is expressed specifically and widely in the nervous system. My data suggest that CAMT-1 regulates the excitability of multiple neurons. By modulating the dynamic range of O_2 sensors and the amplitude of downstream responses, CAMT-1

A

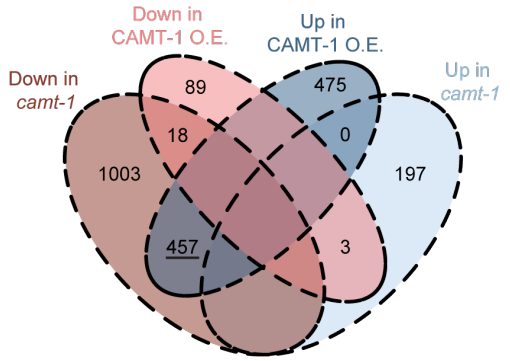

B

Down in *camt-1* and up in CAMT-1 O.E.

GO term	Description	p-Value	Matches
GO:0006508	proteolysis	6.869976e-43	96
GO:0019538	protein metabolic process	6.369207e-13	115
GO:0006334	nucleosome assembly	1.932960e-7	20
GO:0006333	chromatin assembly or disassembly	2.064707e-6	20
GO:0065004	protein-DNA complex assembly	3.330400e-6	20
GO:0071103	DNA conformation change	5.605419e-5	21
GO:0043170	macromolecule metabolic process	9.546235e-5	139
GO:0006836	neurotransmitter transport	2.928255e-4	16
GO:0006470	protein dephosphorylation	0.001826	13
GO:0008592	regulation of Toll signaling pathway	0.006684	6
GO:0055085	transmembrane transport	0.009666	28
GO:0006461	protein complex assembly	0.023465	23

Pathway	p-Value	Matches
Organic cation transport	1.343552e-28	15
Transport of glucose and other sugars, bile salts and organic acids, metal ions and amine compounds	1.991227e-12	15
SLC-mediated transmembrane transport	1.688548e-7	17
Transmembrane transport of small molecules	8.271223e-7	19

Figure 3.11 Transcriptional remodeling by CAMT-1. (A) The total number of genes that are dysregulated in *camt-1* mutant or CAMT-1 pan-neuronal overexpression (O.E.) conditions are shown. All changes shown are two-fold or greater. (B) Gene ontology (GO) terms and pathways significantly overrepresented among the 457 genes (underlined in A) that are down regulated in *camt-1* mutants and upregulated in CAMT-1 overexpression.

maintains Ca^{2+} balance within a neural circuit that governs navigation in O_2 gradients.

CAMT-1 functions broadly in the adult nervous system

What role might a broadly expressed transcription factor play in the nervous system? Our data suggest that CAMT-1 is not required to specify neural cell fate. I did not observe overt defects in *C. elegans* neuroanatomy using dye filling or pan-neuronal fluorescent reporters, and the promoters we used to drive Ca^{2+} indicators, which also serve as cell fate markers, were expressed appropriately. Moreover, expressing CAMT-1 selectively in adults, using the heat-shock promoter, could rescue at least some *camt-1* mutant defects. These data suggest CAMT-1 is more likely to regulate neuronal function than development.

camt-1 mutants have defective behavioural responses to O_2, CO_2, and gustatory and olfactory cues. Where I have carried out Ca^{2+} imaging studies, I identified defects at the sensory neuron level: The URX, BAG and AFD O_2 and/or CO_2 sensors signalled hyperactively in *camt-1* mutants. Together our behavioural and

physiological data suggest that CAMT-1 is required broadly in the nervous system.

Drosophila and mouse mutants in CAMTA are viable, suggesting they have a largely intact nervous system (Han et al., 2006; Long et al., 2014). Studies of these mutants have focused on anatomically localized neuronal functions of CAMTAs. *Drosophila* CAMTA is required to terminate the light response in photoreceptors, but may also be important in other neurons (Eddison et al., 2012). Mammalian CAMTAs have been implicated only in the function of cerebellar and hippocampal cells (Bas-Orth et al., 2016; Long et al., 2014), but appear to be expressed widely in the brain (Huentelman et al., 2007). A prediction of our findings in that in *C. elegans* the function of many neurons is modified by CAMT-1. It will be interesting to discover if the same is true in other organisms.

CAMTA maintains balance within the URX-RMG circuit.
At 21% O_2, RMG activity is driven by tonic signaling from URX (Busch et al., 2012; Laurent et al., 2015). Surprisingly however, in *camt-1* mutants the larger Ca^{2+} response evoked in URX by 21% O_2 is associated with a substantially reduced response in RMG.

URX signals hyperactively in *camt-1* mutants even when synaptic input is disrupted, consistent with a cell-autonomous defect. The *unc-64* hypomorph reduces synaptic and peptidergic transmission but leaves gap-junction communication unaffected. URX forms gap-junctions only with RMG (wormweb.org), suggesting that CAMT-1 functions in either URX or RMG (or a neuron connected by gap-junctions to RMG). This conclusion carries the caveat that some synaptic transmission likely persists in the hypomorphic *unc-64* mutants we studied. My results lead to three models, although I cannot rule out the possibility that URX and RMG abnormalities are secondary to dysfunction elsewhere.

1) CAMT-1 functions cell-autonomously in URX to inhibit its responsiveness to elevated O_2 levels; in *camt-1* mutants, hyperactive signaling from URX leads to decreased RMG excitability (Fig. 3.12A). On the one hand this might seem surprising, as within physiologic ranges RMG responses are potentiated by sustained activity in URX (Fenk and de Bono, 2017). However, in other systems, overexcitation is known to engage mechanisms that depress synaptic strength (by reducing pre-synaptic release or downregulating post-synaptic receptors) (De Gois et al., 2005; Evers et al., 2010; Hu et al., 2010) or reducing the intrinsic excitability of post-synaptic targets. Above a certain threshold of sensory signaling, inhibition of interneuron responses could be advantageous for preventing runaway potentiation and maintaining behavioural control. The thermotaxis circuit in *C. elegans* is regulated by a similar principle. Moderate stimulation of thermosensory AFD neurons drives activation of AIY, but strong Ca^{2+} increases in AFD inhibit AIY responses (Kuhara et al., 2011).

2) CAMT-1 functions cell-autonomously in RMG to promote responsiveness to input from URX; the primary result of *camt-1* loss is chronic inactivity in RMG, which drives URX hypersensitivity (Fig. 3.12B). RMG signaling promotes URX activity in 21% O_2, suggesting the existence of a positive feedback loop (Laurent et al., 2015). To maintain excitation-inhibition balance, it is common for brain circuits to incorporate both positive and negative feedback control mechanisms, the relative influence of which shift depending on activity state (Dehorter et al., 2017; McCormick et al., 2015). During odor adaptation in *C. elegans*, negative peptidergic feedback from AIA interneurons controls AWC sensory neuron signaling (Chalasani et al., 2010). This model predicts that long-term blockade of RMG activity releases URX from similar inhibitory regulation.

3) CAMT-1 serves different functions in URX and RMG. The finding that CAMTA2 is a coactivator for the homeodomain protein Nkx2-5 during hypertrophic signaling, raises the possibility that it may also cooperate with other

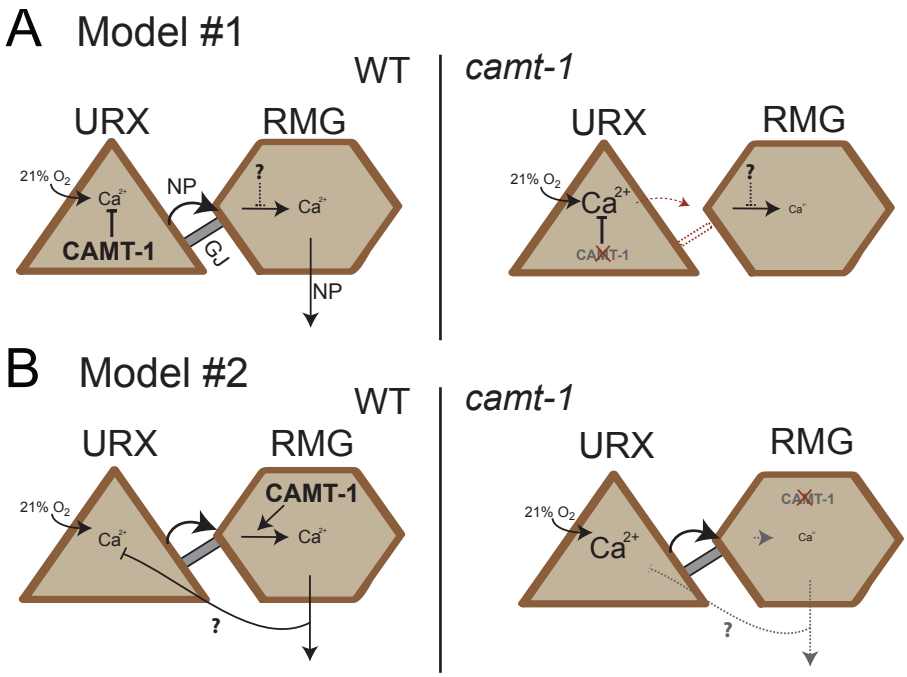

Figure 3.12 Two models for activity-dependent feedback within the URX-RMG circuit. URX communicates with RMG via neuropeptides (NP) and gap-junctions (GJ). In 21% O_2, tonic signaling from URX drives activity in RMG. Release of neuropeptides from RMG influences the activity of downstream neurons and sustains high speed (Laurent et al., 2015). Neurosecretion from RMG is thought to potentiate RMG responsiveness (Fenk and de Bono, 2017), and promote URX excitability (Laurent et al., 2015). Our data suggest that additional negative feedback mechanisms exist within this circuit. (A) Increased Ca^{2+} activity in URX drives depression of transmission from URX to RMG, either by downregulation of synaptic release/gap-junction current from URX or inhibition of Ca^{2+} responses in RMG. (B) In addition to positive feedback, RMG exerts negative feedback control over URX activity. When RMG activity is chronically low, loss of inhibitory signals from RMG cause URX to become hyperexcitable. Two alternative models that are not depicted are (i) signal-dependent functions of CAMT-1 allow it to have qualitatively distinct effects in different neurons or (ii) input from other neurons in which CAMT-1 functions generate the disconnect between URX and RMG activity.

transcription factors in a signal-dependent manner (Song et al., 2006). One possibility is that CAMTA activity is regulated by signal(s) that vary between URX and RMG. A prediction of this model would be that protein-protein interactions of CAMT-1 would be different, or differentially influential, in URX and RMG.

In support of cell-autonomous role in URX, overexpressing CAMT-1 specifically in O_2 sensing neurons (URX, AQR and PQR) reduces Ca^{2+} readout and/or *gcy-*

37 expression. However, an additional role in RMG or other downstream neurons is suggested by the finding that CAMT-1 overexpression is sufficient to overcome a defect in IκBζ signaling, which specifically promotes the responsiveness of RMG to input from URX (Chen et al., 2017). This observation is intriguing as it raises the possibility that CAMT-1 could promote IL-17 induced transcriptional remodeling in RMG.

CAMT-1 expression in O_2 sensors or RMG alone is insufficient to rescue mutant defects. This suggests it functions in multiple neurons within the circuit that drives O_2 avoidance. To pinpoint these cells, cell-specific disruption of *camt-1* will be essential.

It is curious that *camt-1* mutants exhibit hyperactive locomotion in 7% O_2 and yet show reduced responsiveness to 21% O_2. Our dose-response analysis indicates that CAMT-1 keeps the dynamic range of URX neurons tuned to near 21% O_2, a function that likely contributes to the control of these behavioural states.

Control of homeostatic plasticity by CAMT-1

A sustained change in activity induces changes in the circuit that governs behavioural responses to 21% O_2. After long-term cultivation at 7% O_2, the Ca^{2+} responses evoked in URX and RMG neurons by 21% O_2 are reduced, but behavioural responses are enhanced. This suggests that homeostatic mechanisms function to compensate for reduced Ca^{2+} levels in URX/RMG, and upregulate responsiveness downstream.

Our analysis of *camt-1* mutants reared in 7% O_2 and 21% O_2 raise two hypotheses. The first hypothesis is that CAMT-1 is involved in remodeling the dynamic range of URX in response to sustained stimulation. Our data suggest that CAMT-1 ensures URX excitability is dampened at lower O_2 concentrations. Thus, disrupting CAMT-1 locks URX neurons in a state of hypersensitivity to low

O_2, and reduces its ability to tune its dynamic range to concentrations approaching 21% when they become prevailing.

A second hypothesis is that the homeostatic drive to increase activity/excitability in neurons downstream of RMG after the circuit has been quiescent for some time is limited by CAMT-1. We propose this based on the observation that the *camt-1* mutant phenotype at 21% O_2 is exacerbated after acclimation at 7% O_2. To further explore the role of CAMT-1 in controlling homeostatic compensation for reduced URX/RMG activity, it will be important to identify the neurons/ processes that drive this phenomenon.

Mechanistic insights into CAMT-1 function

The DNA-binding specificity of CAMTAs in mammals, flies and plants is encoded by their CG-1 domains (da Costa e Silva, 1994; Han et al., 2006; Song et al., 2006). Based on the requirement for a conserved histidine residue within its CG-1 domain (H190), we predict that CAMT-1 also functions as a transcription factor. Our preliminary studies do not provide clear indication of where CAMT-1 localizes subcellularly, but it will be important to discover whether CAMT-1 functions in the nucleus and whether its localization is activity-dependent.

The role of Ca^{2+} signaling and CaM-binding in regulating CAMTA activity remains a matter of debate. Although the CaM-binding domain promotes CAMTA-mediated transcription in flies and plants, it has no noticeable impact on the function of mouse CAMTA2 (Du et al., 2009; Han et al., 2006; Song et al., 2006). We have been unable to detect a requirement for IQ motifs for CAMT-1. However, perturbation of CaM-binding domains when CAMT-1 is expressed at physiological levels will provide a more rigorous insight into their function.

Finally, our RNA profiling has begun to reveal the transcriptional landscapes promoted by CAMT-1. It is clear that CAMT-1 is a regulator of many genes. Our data suggest that it functions in an activity-dependent manner, so identifying

those that link it to the control of neuronal Ca^{2+} signaling will be an important future goal.

Conclusion

CAMTA transcription factors are highly conserved across multicellular organisms (Finkler et al., 2007). A spectrum of neurological phenotypes, including neurodegeneration and reduced memory performance (Bas-Orth et al., 2016; Huentelman et al., 2007), have been attributed to their dysfunction, but their physiological role is not well understood.

Here, I show that disrupting CAMTA in *C. elegans* leads to increased excitability in many neurons. I speculate that similar increased activity may drive the development of ataxia in mice and humans (Long et al., 2014; Thevenon et al., 2012). My study also suggests CAMT-1 controls activity-dependent plasticity. Interestingly, CAMTA gene expression is induced by synaptic activity and during formation of long-term memory formation (Lakhina et al., 2015; Pruunsild et al., 2017), suggesting that CAMTA transcription factors may be employed by many neurons to tune adaptive changes in their dynamic range. Several outstanding questions remain: how is neural gene expression altered by CAMT-1? Is CAMT-1 function modified by changing levels of Ca^{2+}?

Materials and methods

C. elegans maintenance, microinjection, heat-shock, light microscopy, protein alignment and RNA-seq were performed as described in Chapter 2.

Strains

RB746 *camt-1*(*ok515*), and OH10689 *otIs355[rab-3p(prom1)::2xNLS::TagRFP]* were obtained from the CGC which is funded by NIH Office of Research Infrastructure Programs (P40 OD010440). Strains generated in this study are listed in the Appendix.

Molecular Biology

Fosmid recombineering

We obtained a clone containing the *camt-1* locus from the *C. elegans* fosmid library (Source BioScience). To insert GFP immediately prior to the termination codon of the longest *camt-1* splice variant (*T05C1.4a*) we followed the protocol of (Tursun et al., 2009). The primers used to amplify the recombineering cassette from pBALU1 were:
ATCATCCATGGGACCAATTGAAACCGCCGTATGGTTGCGGAACACTTGCAA
TGAGTAAAGGAGAAGAACTTTTCAC and
aaaccaataaaaaaaatcggcatcttctaaaagtgacaccggggcaaTTATTTGTATAGTTCATC
CATGCCATG. To generate transgenic lines, we injected a mix of 50 ng/µl fosmid DNA and 50 ng/µl co-injection marker (cc::RFP).

Gateway cloning

We amplified gDNA corresponding to the *camt-1* pomoter (3.5Kb) with ggggACAACTTTGTATAGAAAAGTTG aagttacagtaatctcctatctcgtgctttataatatg and ggggACTGCTTTTTTGTACAAACTTGtagttcatcatcatcatcatattgaaaatgtgg, primers, gDNA corresponding to the *T06D8.9* promoter (1.7Kb) with GGGGACAACTTTGTATAGAAAAGTTGTGCTTCTTCAAATCGTCCCAGC and GGGGACTGCTTTTTTGTACAAACTTGCTGAAAAAAGAAACTAACAATTAGGA ATTTTGAACG primers, and cDNA corresponding to *camt-1* (*T05C1.4b*) with ggggACAAGTTTGTACAAAAAAGCAGGCTtttcagaaaaATGAATAATTCAGTCAC TCGTCTTCTTTTCAAACGACTGCTGAC and ggggACCACTTTGTACAAGAAAGCTGGGTATTATGCAAGTGTTCCGCAACCAT ACGGCG primers. We were unable to amplify *camt-1* cDNA corresponding to the longer *T05C1.4a* splice variant so we generated it by site-directed mutagenesis of *T05C1.4b* cDNA (see below).

Site-directed mutagenesis

In all cases we used the Q5 Site-Directed Mutagenesis Kit (NEB).

To convert *T05C1.4b* cDNA to *T05C1.4a* we used primers gtcatactcaacatctaATTGCGGAAAATGCATGC and catcatcaatatttacaTTATTACGATTTTGTCGCATAAAATTC. To remove the stop codon from *camt-1* cDNA for C-terminal GFP fusion we used TACCCAGCTTTCTTGTACAAAG and TGCAAGTGTTCCGCAACC. To generate H190P cDNA we used GGACAATGCTTGGTACAAAAACGATGG and GGACAATGCTTGGTACAAAAACGATGG, and for I962N cDNA: GCAATGGTCAaCCAACGAGCC and TGCTTCGTAGACGTCTCG. To add an N-terminal NLS cgcaaagtaccggtagaaaaaATGAATAATTCAGTCACTCGTC and tttcttctttggagcggtcatTTTTCTGAAAAGCCTGCTTTTTTG were used. To add a second NLS, we used cgcaaagtaccggtagaaaaaATGACCGCTCCAAAGAAG and tttcttctttggagcggtcatTTTTCTGAAAAGCCTGCTTTTTTG.

Gibson assembly

As in chapter 2, sgRNAs were cloned downstream of the *rpr-1* promoter using Gibson Assembly (NEB) following the protocol of (Chen et al., 2013). To target the *camt-1* locus by CRISPR-Cas9 we delivered a gattgtgaagaactcgccg guide, and to target the*T06D8.9* we delivered a GGTGCCTTCACCCCAAAGG guide. 100 ng/µl sgRNA was co-injected with 30ng/µl *eft-3::cas9* and 30ng ng/µl injection marker (cc::GFP).

Behaviour and Ca^{2+} imaging

Aerotaxis assays and neural imaging were performed as described in Chapter 2. Unless otherwise indicated Ca^{2+} imaging was performed in immobilized animals. We used a gas-tight hypoxia chamber to grow animals at 7% O_2. '21% O_2-reared worms' were grown in parallel outside the chamber. As indicated in the text, to prevent any exposure to room air before Ca^{2+} imaging, animals were immobilized on assay plates within a custom-made portable gas-tight container inside the 7% O_2 chamber. Chemotaxis assays were performed as previously described

(Bargmann et al., 1993) with minor modifications. 9cm assay plates were made with 2% Bacto Agar, 1mM $CaCl_2$, 1mM $MgSO_4$ and 25mM K_2HPO_4 pH 6. Test and control circles of 3cm diameter were marked on opposite sides of the assay plate, equidistant from a starting point where >50 animals were placed to begin the assay. For olfactory assays, 1µl odorant in ethanol or 1µl ethanol, and 1µl NaN_3, was added to each circle. For gustatory assays, an agar plug containing 100mM NaCl was added the night before and removed prior to assay. Assays were allowed to proceed for 30-60min, after which point plates were moved to 4°C. Chemotaxis index was calculated as (number of animals in test circle – number of animals in control circle) / total number of animals that have left starting point.

Contributions

EMS mutants were isolated by C Chen, their whole genome sequence characterized by G Nelson. C Chen and Z Soltesz carried preliminary behavioural analysis, as indicated in the text. I Beets mapped *db601*. The CRI prepared RNA libraries and performed sequencing, and Alastair Crisp analyzed RNA-seq data.

References

Bargmann, C.I., Hartwieg, E., and Horvitz, H.R. (1993). Odorant-Selective Genes and Neurons Mediate Olfaction in C. elegans. Cell *74*, 515–527.

Barlow, H.B. (1961). Possible Principles Underlying the Transformations of Sensory Messages. Sensory Communication, Ed W.Rosenblith Ch , MIT Press, Cambridge, Mass 217–234.

Bas-Orth, C., Tan, Y.-W., Oliveira, A.M.M., Bengtson, C.P., and Bading, H. (2016). The calmodulin-binding transcription activator CAMTA1 is required for long-term memory formation in mice. Learn Mem *23*, 313–321.

Bernander, O., Douglas, R.J., Martin, K., and Koch, C. (1991). Synaptic background activity influences spatiotemporal integration in pyramidal cells. Proc Natl Acad Sci USA *15*, 11569–11573.

Berridge, M.J. (2010). Calcium Signalling and Alzheimer's Disease. Neurochem Res *36*, 1149–1156.

Berridge, M.J., Lipp, P., and Bootman, M.D. (2000). THE VERSATILITY AND UNIVERSALITY OF CALCIUM SIGNALLING. Nat Rev Mol Cell Biol *1*, 11–21.

Bezprozvanny, I. (2009). Calcium signaling and neurodegenerative diseases. Trends Mol Med *15*, 89–100.

Bouche, N. (2002). A Novel Family of Calmodulin-binding Transcription Activators in Multicellular Organisms. J Biol Chem *277*, 21851–21861.

Bretscher, A.J., Busch, K.E., and de Bono, M. (2008). A carbon dioxide avoidance behavior is integrated with responses to ambient oxygen and food in Caenorhabditis elegans. Proc Natl Acad Sci USA *105*, 8044–8049.

Bretscher, A.J., Kodama-Namba, E., Busch, K.E., Murphy, R.J., Soltesz, Z., Laurent, P., and de Bono, M. (2011). Temperature, Oxygen, and Salt-Sensing Neurons in C. elegans Are Carbon Dioxide Sensors that Control Avoidance Behavior. Neuron *69*, 1099–1113.

Busch, K.E., Laurent, P., Soltesz, Z., Murphy, R.J., Faivre, O., Hedwig, B., Thomas, M., Smith, H.L., and de Bono, M. (2012). Tonic signaling from O2 sensors sets neural circuit activity and behavioral state. Nat Neurosci *15*, 581–591.

Chalasani, S.H., Kato, S., Albrecht, D.R., Nakagawa, T., Abbott, L.F., and Bargmann, C.I. (2010). Neuropeptide feedback modifies odor-evoked dynamics in Caenorhabditis elegans olfactory neurons. Nat Neurosci *13*, 615–621.

Chen, C., Fenk, L.A., and de Bono, M. (2013). Efficient genome editing in Caenorhabditis elegans by CRISPR-targeted homologous recombination. Nucleic Acids Res *41*, e193–e193.

Chen, C., Itakura, E., Nelson, G.M., Sheng, M., Laurent, P., Fenk, L.A., Butcher, R.A., Hegde, R.S., and de Bono, M. (2017). IL-17 is a neuromodulator of Caenorhabditis elegans sensory responses. Nature *542*, 43–48.

da Costa e Silva, O. (1994). CG-1, a parsley light-induced DNA-binding protein. Plant Mol Biol *25*, 921–924.

Davis, G.W. (2006). Homeostatic Control of Neural Activity: From Phenomenology to Molecular Design. Annu Rev Neurosci *29*, 307–323.

De Gois, S., Schäfer, M.K.-H., Defamie, N., Chen, C., Ricci, A., Weihe, E., Varoqui, H., and Erickson, J.D. (2005). Homeostatic scaling of vesicular glutamate and GABA transporter expression in rat neocortical circuits. J Neurosci *25*, 7121–7133.

Dehorter, N., Marichal, N., Marín, O., and Berninger, B. (2017). Tuning neural circuits by turning the interneuron knob. Curr Opin Neurobiol *42*, 144–151.

Destexhe, A., and Paré, D. (1999). Impact of Network Activity on the Integrative Properties of Neocortical Pyramidal Neurons In Vivo. J Neurophysiol *81*, 1531–1547.

Doherty, C.J., Van Buskirk, H.A., Myers, S.J., and Thomashow, M.F. (2009). Roles for Arabidopsis CAMTA Transcription Factors in Cold-Regulated Gene Expression and Freezing Tolerance. Plant Cell *21*, 972–984.

Du, L., Ali, G.S., Simons, K.A., Hou, J., Yang, T., Reddy, A.S.N., and Poovaiah, B.W. (2009). Ca2+/calmodulin regulates salicylic-acid-mediated plant immunity. Nature *457*, 1154–1158.

Eddison, M., Belay, A.T., Sokolowski, M.B., and Heberlein, U. (2012). A Genetic Screen for Olfactory Habituation Mutations in Drosophila: Analysis of Novel Foraging Alleles and an Underlying Neural Circuit. PLoS ONE *7*, e51684–10.

Elkins, T., Ganetzky, B., and Wu, C.-F. (1986). A Drosophila mutation that eliminates a calcium-dependent potassium current. Proc Natl Acad Sci USA *83*, 8415–8419.

Evers, D.M., Matta, J.A., Hoe, H.-S., Zarkowsky, D., Lee, S.H., Isaac, J.T., and Pak, D.T.S. (2010). Plk2 attachment to NSF induces homeostatic removal of GluA2 during chronic overexcitation. Nat Neurosci *13*, 1199–1207.

Fenk, L.A., and de Bono, M. (2015). Environmental CO 2inhibits Caenorhabditis elegansegg-laying by modulating olfactory neurons and evokes widespread changes in neural activity. Proc Natl Acad Sci USA *112*, E3525–E3534.

Fenk, L.A., and de Bono, M. (2017). A memory of recent oxygen experience switches pheromone valence in C. elegans. bioRxiv doi:10.1101/107524

Finkler, A., Ashery-Padan, R., and Fromm, H. (2007). CAMTAs: Calmodulin-binding transcription activators from plants to human. FEBS Lett *581*, 3893–3898.

Frey, B.J., and Dueck, D. (2007). Clustering by Passing Messages Between Data Points. Science *315*, 972–976.

Ganguly, K., and Poo, M.-M. (2013). Activity-Dependent Neural Plasticity from Bench to Bedside. Neuron *80*, 729–741.

Goold, C.P., and Nicoll, R.A. (2010). Single-Cell Optogenetic Excitation Drives Homeostatic Synaptic Depression. Neuron *68*, 512–528.

Han, J., Gong, P., Reddig, K., Mitra, M., Guo, P., and Li, H.-S. (2006). The Fly CAMTA Transcription Factor Potentiates Deactivation of Rhodopsin, a G Protein-Coupled Light Receptor. Cell *127*, 847–858.

Hobert, O. (2016). A map of terminal regulators of neuronal identity in Caenorhabditis elegans. Wiley Interdiscip Rev Dev Biol *5*, 474–498.

Hu, J.-H., Park, J.M., Park, S., Xiao, B., Dehoff, M.H., Kim, S., Hayashi, T., Schwarz, M.K., Huganir, R.L., Seeburg, P.H., et al. (2010). Homeostatic Scaling Requires Group I mGluR Activation Mediated by Homer1a. Neuron *68*, 1128–1142.

Huentelman, M.J., Papassotiropoulos, A., Craig, D.W., Hoerndli, F.J., Pearson, J.V., Huynh, K.D., Corneveaux, J., Hanggi, J., Mondadori, C.R.A., Buchmann, A., et al. (2007). Calmodulin-binding transcription activator 1 (CAMTA1) alleles predispose human episodic memory performance. Hum Mol Genet *16*, 1469–1477.

Ibata, K., Sun, Q., and Turrigiano, G.G. (2008). Rapid Synaptic Scaling Induced by Changes in Postsynaptic Firing. Neuron *57*, 819–826.

Kass, G.E., and Orrenius, S. (1999). Calcium Signaling and Cytotoxicity. Environ Health Perspect *107*, 25–35.

Kasumu, A., and Bezprozvanny, I. (2010). Deranged Calcium Signaling in Purkinje Cells and Pathogenesis in Spinocerebellar Ataxia 2 (SCA2) and Other Ataxias. Cerebellum *11*, 630–639.

Kuhara, A., Ohnishi, N., Shimowada, T., and Mori, I. (2011). Neural coding in a single sensory neuron controlling opposite seeking behaviours in Caenorhabditis elegans. Nat Commun *2*, 355–359.

Lakhina, V., Arey, R.N., Kaletsky, R., Kauffman, A., Stein, G., Keyes, W., Xu, D., and Murphy, C.T. (2015). Genome-wide Functional Analysis of CREB/Long-Term Memory-Dependent Transcription Reveals Distinct Basal and Memory Gene Expression Programs. Neuron *85*, 330–345.

Laurent, P., Soltesz, Z., Nelson, G.M., Chen, C., Arellano-Carbajal, F., Levy, E., and de Bono, M. (2015). Decoding a neural circuit controlling global animal state in C. elegans. eLife *4*, e04241.

Long, C., Grueter, C.E., Song, K., Qin, S., Qi, X., Kong, Y.M., Shelton, J.M., Richardson, J.A., Zhang, C.L., Bassel-Duby, R., et al. (2014). Ataxia and Purkinje cell degeneration in mice lacking the CAMTA1 transcription factor. Proc Natl Acad Sci USA *111*, 11521–11526.

Macosko, E.Z., Pokala, N., Feinberg, E.H., Chalasani, S.H., Butcher, R.A., Clardy, J., and Bargmann, C.I. (2009). A hub-and-spoke circuit drives pheromone attraction and social behaviour in C. elegans. Nature *458*, 1171–1175.

McCormick, D.A., McGinley, M.J., and Salkoff, D.B. (2015). ScienceDirect Brain state dependent activity in the cortex and thalamus. Curr Opin Neurobiol *31*,

133–140.

Oda, S., Toyoshima, Y., and de Bono, M. (2016). Modulation of sensory information processing by a neuroglobin in *C. elegans*. arXiv:1608.03477.

Palty, R., Raveh, A., Kaminsky, I., Meller, R., and Reuveny, E. (2012). SARAF Inactivates the Store Operated Calcium Entry Machinery to Prevent Excess Calcium Refilling. Cell *149*, 425–438.

Pruunsild, P., Bengtson, C.P., and Bading, H. (2017). Networks of Cultured iPSC-Derived Neurons Reveal the Human Synaptic Activity-Regulated Adaptive Gene Program. Cell Rep *18*, 122–135.

Reiff, D.F. (2005). In Vivo Performance of Genetically Encoded Indicators of Neural Activity in Flies. J Neurosci *25*, 4766–4778.

Rieke, F., and Rudd, M.E. (2009). The Challenges Natural Images Pose for Visual Adaptation. Neuron *64*, 605–616.

Saifee, O., Wei, L., and Nonet, M.L. (1998). The *Caenorhabditis elegans unc-64* Locus Encodes a Syntaxin That Interacts Genetically with Synaptobrevin. Mol Biol Cell *9*, 1235–1252.

Salkoff, L., Butler, A., Ferreira, G., Santi, C., and Wei, A. (2006). High-conductance potassium channels of the SLO family. Nat Rev Neurosci *7*, 921–931.

Shinawi, M., Coorg, R., Shimony, J.S., Grange, D.K., and Al-Kateb, H. (2014). Intragenic CAMTA1deletions are associated with a spectrum of neurobehavioral phenotypes. Clin Genet *87*, 478–482.

Song, K., Backs, J., McAnally, J., Qi, X., Gerard, R.D., Richardson, J.A., Hill, J.A., Bassel-Duby, R., and Olson, E.N. (2006). The Transcriptional Coactivator CAMTA2 Stimulates Cardiac Growth by Opposing Class II Histone Deacetylases. Cell *125*, 453–466.

Temporal, S., Lett, K.M., and Schulz, D.J. (2014). Activity-Dependent Feedback Regulates Correlated Ion Channel mRNA Levels in Single Identified Motor Neurons. Curr Biol *24*, 1899–1904.

Thevenon, J., Lopez, E., Keren, B., Heron, D., Mignot, C., Altuzarra, C., Béri-Dexheimer, M., Bonnet, C., Magnin, E., Burglen, L., et al. (2012). Intragenic CAMTA1rearrangements cause non-progressive congenital ataxia with or without intellectual disability. J Med Genet *49*, 400–408.

Turrigiano, G.G. (2008). The Self-Tuning Neuron: Synaptic Scaling of Excitatory Synapses. Cell *135*, 422–435.

Turrigiano, G.G. (2017). The dialectic of Hebb and homeostasis. Phil Trans R Soc B *372*, 20160258–7.

Turrigiano, G.G., Leslie, K.R., Desai, N.S., Rutherford, L.C., and Nelson, S.B. (1998). Activity-dependent scaling of quantal amplitude in neocortical neurons. Nature *391*, 892–896.

Tursun, B., Cochella, L., Carrera, I., and Hobert, O. (2009). A Toolkit and Robust Pipeline for the Generation of Fosmid-Based Reporter Genes in C. elegans. PLoS ONE *4*, e4625–16.

Ward, S. (1973). Chemotaxis by the Nematode Caenorhabditis elegans: Identification of Attractants and Analysis of the Response by Use of Mutants. Proc Natl Acad Sci USA *70*, 817–821.

Wark, B., Lundstrom, B.N., and Fairhall, A. (2007). Sensory adaptation. Curr Opin Neurobiol *17*, 423–429.

West, A.E., Griffith, E.C., and Greenberg, M.E. (2002). Regulation of transcription factors by neuronal activity. Nat Rev Neurosci *3*, 921–931.

Wilson, R.I. (2013). Early Olfactory Processing in Drosophila: Mechanisms and Principles. Annu Rev Neurosci *36*, 217–241.

Wolfart, J., and Laker, D. (2015). Homeostasis or channelopathy? Acquired cell type-specific ion channel changes in temporal lobe epilepsy and their antiepileptic potential. Front Physiol *6*, 1178–23.

4

Translation initiation factors eIF3k and eIF3l specifically regulate the responsiveness of RMG neurons

Introduction

Global or transcript-specific changes in translation efficiency underlie a range of physiological and stress-induced changes in organismal state (Buffington et al., 2014; Piccirillo et al., 2014; Ron, 2002). As the rate-limiting factors in protein synthesis, the dynamic, multi-subunit complexes that mediate translation initiation are a particularly important regulatory hub during gene expression (Gebauer and Hentze, 2004).

Typically, mechanisms that reconfigure translational profiles in response to environmental change converge on the same key components of the translation machinery. eIF2 and the cap-binding eIF4E govern a reduction in translation during metabolic stress (Baird and Wek, 2012; Pause et al., 1994), and alleviate protein-folding overload in the ER (Ron, 2002; Scheuner et al., 2001). Interestingly, general inhibition of protein synthesis is often accompanied by preferential, non-canonical translation of a small subset of transcripts. During T-cell activation for example, mRNAs encoding pro-inflammatory cytokines are sequestered in stress granules as translation is globally shutdown, before being specifically upregulated following antigen-restimulation (Piccirillo et al 2014). Once secreted, cytokines themselves control the translation of specific mRNAs. For example, IL-17 stimulates the translation of transcripts encoding Regnase-1 and IκBζ (Dhamija et al., 2013). In the nervous system, changes in translation dictate activity levels and drive the formation of long term memory (Buffington et al., 2014). Transcript-specific translational upregulation increases network excitability and lowers the threshold for the late phase of long-lasting synaptic potentiation (L-LTP) (Costa-Mattioli et al., 2007; Zhu et al., 2011).

Recently, the giant (800 kDa) eukaryotic initiation factor 3 (eIF3) complex has emerged as another source of mRNA-specificity during translation initiation (Cate, 2017; Lee et al., 2015). eIF3 is composed of 13 subunits (a-m, Fig. 4.1D), and binds the 40S ribosomal subunit and other initiation factors to serve a broad scaffolding function during initiation (des Georges et al., 2015; Hinnebusch,

2006; Siridechadilok et al., 2005). By binding secondary structure in the 5' UTR of mRNA, it also mediates the preferential translation or degradation of specific endogenous transcripts (Lee et al., 2015). Additionally, eIF3 possesses N^6-methyladenosine- and 5' cap-binding activity, which allows specialized mRNAs to be translated independent of eIF4E (Lee et al., 2016; Meyer et al., 2015) .

Although all 13 subunits are conserved across most eukaryotes, a core eIF3 complex of only 5 subunits (a, b, c, g and i) is defined by its sufficiency in budding yeast (Phan et al., 1998). Interestingly, distinct eIF3 subcomplexes exist (Shah et al., 2016; Zhou et al., 2005). Subcomplexes defined by the presence of eIF3e remodel the metabolic proteome in fission yeast without being required for general translation, suggesting that qualitatively different eIF3 assemblies promote different translatomes (Shah et al., 2016). Additionally, polysome profiling and functional studies have described a role for eIF3h in regulating the translation of developmentally important genes (Choudhuri et al., 2013; Kim, 2004; Ray et al., 2008). Together, these findings support the hypothesis that one important function of non-core subunits is to regulate the translation efficiency of specific sets of mRNAs.

eIF3k and eIF3l sit next to eIF3e on the extremities of the complex, however their role remains uncharacterized (des Georges et al., 2015). The formation of a functional pre-initiation complex on the internal ribosome entry site (IRES) of hepatitis C virus (HCV) RNA requires most eIF3 subunits (Sun et al., 2011). However, eIF3k:eIF3l dimers are dispensable for 40S recruitment (Masutani et al., 2007) and are easily dissociated from the eIF3 complex even when the assembly is stabilized by IRES-binding, suggesting they do not play a critical role in the eIF3-IRES interaction (Zhou et al., 2008). It is likely, therefore, that they have a regulatory role in eIF3 complex stability, perhaps in specific contexts.

The α-helical PCI (proteasome, COP9, Initiation factor 3) domains of eIF3k and eIF3l are conserved in both multicellular and unicellular organisms (Meleppattu et

al., 2015), and have paralogs in two other large intracellular assemblies: the 26S proteasome lid and the COP9 signallosome (CSN). These function in ubiquitylation-mediated protein degradation (Pick et al., 2009). It seems therefore likely that PCI proteins play an evolutionarily ancient role in protein homeostasis by regulating the stability or activity of complexes required for protein synthesis and turnover (Bhattacharyya et al., 2014).

In *C. elegans*, eIF3k and eIF3l are not essential for viability or for general translation (Cattie et al., 2016). However, their absence has been shown to confer resistance to ER stress, extend lifespan and reduce programmed cell death (Cattie et al., 2016; Huang et al., 2012). Here, we show that their function in specific neurons is required for behavioural responses. Our study demonstrates a novel role for non-core eIF3 subunits in regulating neuronal responsiveness to sensory input.

Results

C. elegans eIF3 subunits l and k promote high speed in 21% O_2

I mapped the causal lesion in the non-aggregating mutant *db1015* to a nonsense mutation in *eif-3.L* (Fig. 4.1A). A WT copy of the *eif-3.L* genomic locus was sufficient to restore speed responses to the *db1015* animas (Fig. 4.1B), and their defective avoidance of 21% O_2 was recapitulated by an independent nonsense mutation in *eif-3.L* (Fig. 4.1C). Therefore *C. elegans* eIF3l is required for avoidance of high ambient O_2.

All 13 eIF3 subunits are conserved from nematode to human (des Georges et al., 2015; Smith et al., 2016). KO of any but the -k and -l subunits induces lethality or sterility in *C. elegans* (Cattie et al., 2016). I identified a splice site mutation in *eif-3.K* among the collection of EMS-derived non-aggregating mutants (Fig. 4.1E-G). Moreover, two independent CRISPR/Cas9-induced frameshift mutations in *eif-3.K* disrupted avoidance of 21% O_2 (Fig. 4.1H). To confirm that loss of EIF-

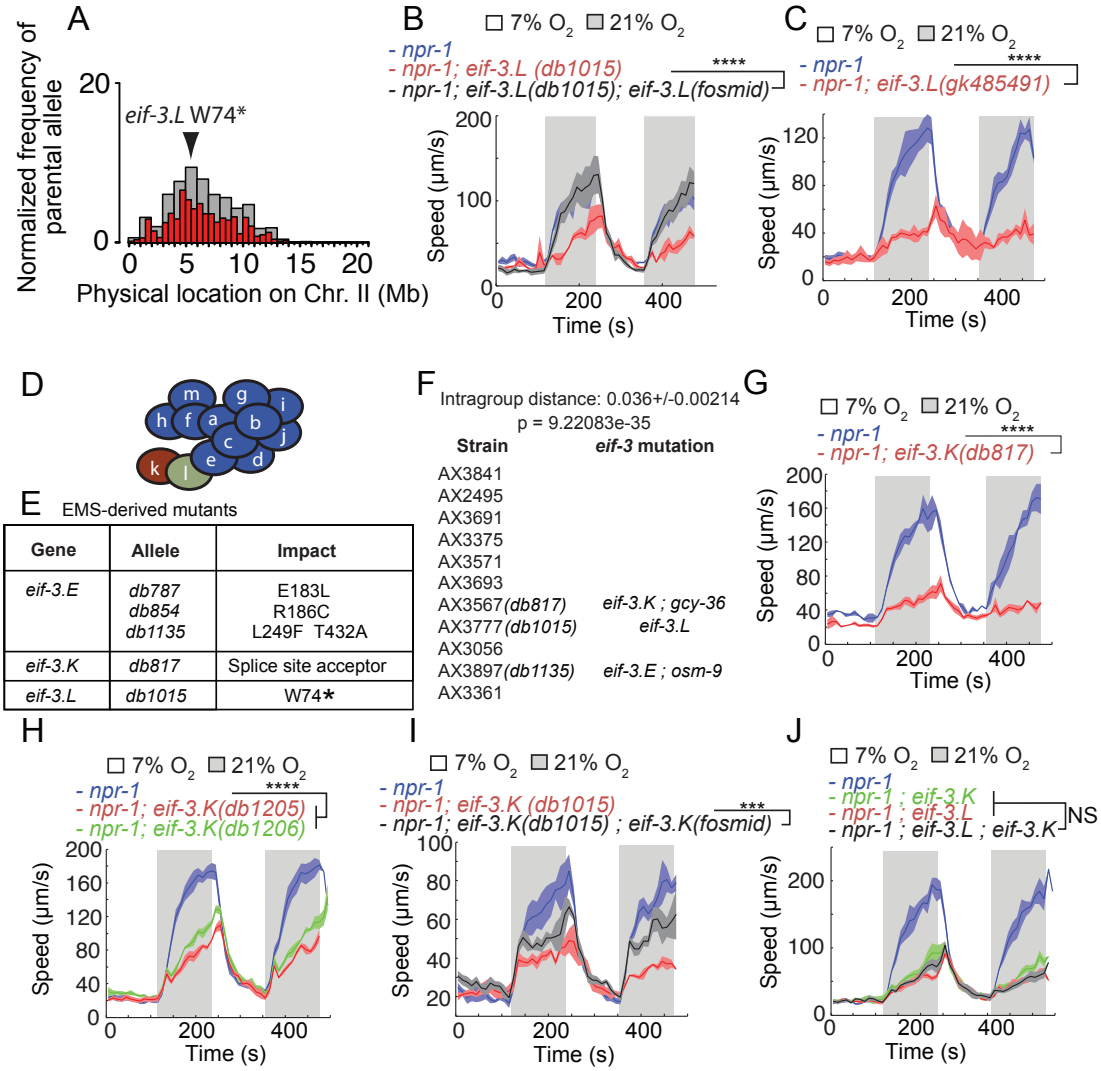

Gene	Allele	Impact
eif-3.E	*db787* *db854* *db1135*	E183L R186C L249F T432A
eif-3.K	*db817*	Splice site acceptor
eif-3.L	*db1015*	W74*

Figure 4.1 EIF-3.K and EIF-3.L promote avoidance of 21% O_2. (A) WGS-based CloudMap Hawaiian Variant Mapping of a non-aggregating strain (AX3777) isolated by EMS-based mutagenesis. The genomic region surrounding a nonsense mutation in *eif-3.L* (W74*) is associated with loss of aggregation. The aerotaxis defect of *db1015* mutants is rescued by a fosmid including the *eif-3.L* locus (B) and recapitulated by an independent nonsense mutation in *eif-3.L* (C), n ≥ 30 animals, N ≥ 3 assays. (D) eIF3k and l reside at the periphery of the 13-subunit eIF3 complex (Zhou et al., 2008; des Georges et al., 2015). (E) Among a collection of EMS-derived non-aggregating mutants, five encode protein-coding changes in the EIF-3 complex, two of which are predicted to be high impact. (F) Iterative clustering by similarity using affinity propagation shows that three of these mutants exhibit similar behavioural fingerprints (Z Soltesz and C Chen). (G-I) EIF-3.K promotes aerotaxis. Mutations in *eif-3.K* generated by EMS (F, n ≥ 32 animals, N ≥ 2 assays) or CRISPR/Cas9 (G - showing two independent frameshift deletions, n ≥ 50 animals, N= 4 assays) reduce speed in 21% O_2. A fosmid including the *eif-3.K* locus restores behaviour to an *eif-3.K* mutant (H, n ≥ 34 animals, N = 4 assays). (J) The aerotaxis phenotypes of *eif-3.K* and *eif-3.L* mutants are not additive, n ≥ 43 animals, N ≥ 3 assays. Average speed (line) and SEM (shaded regions) are plotted. *** = P < 0.001 **** = P < 0.0001, Mann-Whitney *U* test.

3.K was responsible, I rescued the defect by providing a WT version of EIF-3.K to the mutant (Fig. 4.1I).

To extend my analysis I also looked for hypomorphic in essential *eif-3* subunits. Although multiple mutations in *eif-3.E* were isolated in the aggregation screen, I have so far been unable to demonstrate that any are causal (Fig. 4.1E). Interestingly, the behavioural fingerprint of one *eif-3.E* mutant, AX3897, clustered with that of *eif-3.K* and *eif-3.L* mutants (Fig. 4.1F), although it must be noted that the strains used for behavioural clustering were not outcrossed, and therefore contained many EMS-induced background mutations. We mapped the region associated with loss of aggregation in AX3897 to a lesion in *osm-9*, which encodes a well-studied TRPV channel (data not shown). Therefore, whether the mutation of *eif-3.E* in this strain has any effect on aggregation awaits further investigation.

eIF3k and l are mutually dependent on one another for insertion into the eIF3 complex (Smith et al., 2016; 2013). Consistent with loss of either subunit being sufficient to abolish the function of the other, I found that the aerotaxis phenotypes of *eif-3.L* and *eif-3.K* were not additive (Fig. 4.1J).

eIF3 subunits function in RMG hub neurons

To test whether EIF-3 subunits impinge upon the URX-RMG circuit, I compared Ca^{2+} responses in URX and RMG neurons during exposure to 21% O_2 in *npr-1* and *npr-1; eif-3.K/L* animals. I found that non-essential *eif-3* mutants displayed reduced activity in RMG, whereas Ca^{2+} levels in URX O_2 sensory neurons were not reduced (Fig. 4.2A and B). To confirm that defective Ca^{2+} signaling was associated with reduced RMG output, I used a *flp-5* transcriptional reporter as a readout of neurosecretion. It has previously been shown that transcription of *flp-5* in RMG is coupled to its release (Laurent et al., 2015). Consistent with reduced neuropeptide secretion from RMG, expression of *flp-5p::gfp* was reduced in *eif-3.L* mutants (Fig. 4.2C).

To test whether EIF-3.L functions in RMG to promote responsiveness to 21% O_2, I expressed cDNA encoding EIF-3.L in RMG (and ASG, PVT, I4 and M4, which are not known to affect aerotaxis) using the *flp-5* promoter (Kim and Li, 2004; 2017). This transgene fully rescued the speed defect of *eif-3.L* mutants in 21%

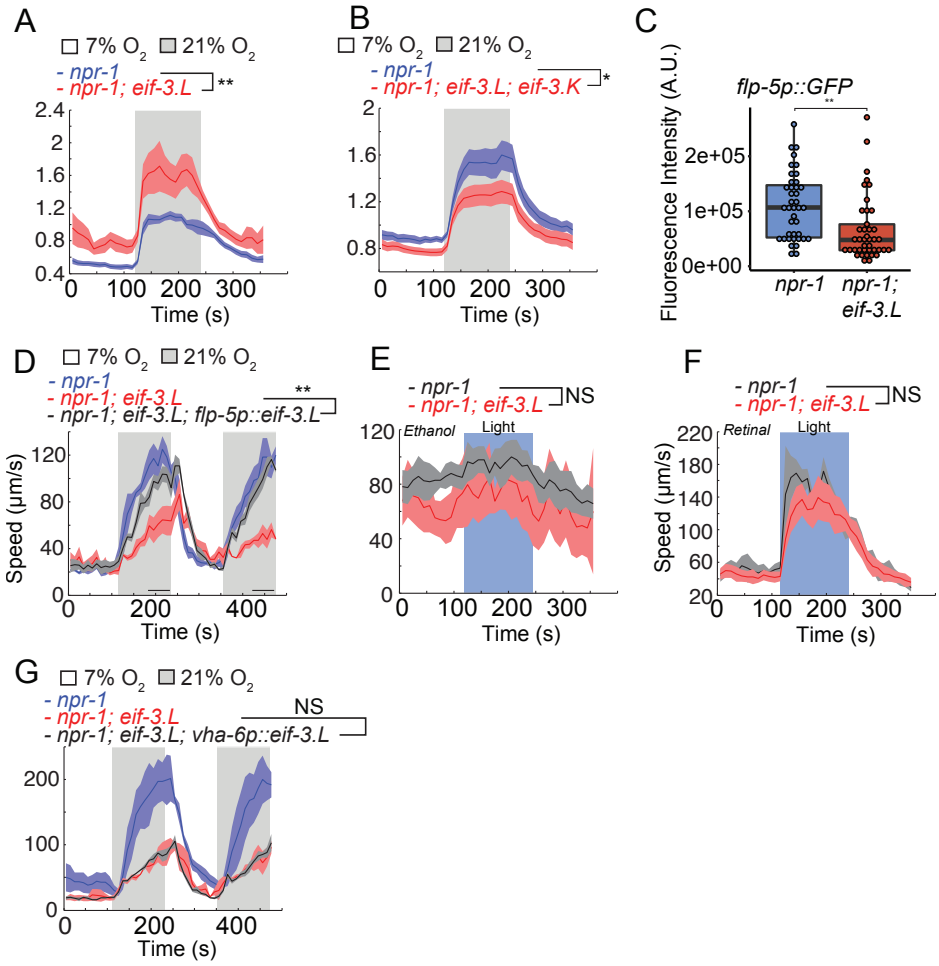

Figure 4.2 EIF-3.L functions in RMG neurons. Ca^{2+} levels are reduced in RMG (YC2.60) in *eif-3.L* mutants (B, n ≥ 22, immobilized animals) but not in URX (A, n ≥ 9, freely moving animals). (C) Loss of EIF-3.L reduces the expression of a *flp-5p::gfp* transgene in RMG, n ≥ 40. (D) Directing EIF-3.L expression to RMG using the *flp-5* promoter rescues the 21% O_2 avoidance defect of *eif-3.L* mutants, n ≥ 23 animals, N ≥ 4 assays. (E and F) ChR2-mediated activation of RMG is sufficient to induce *npr-1*-like high speed in *eif-3.L* mutants (F), dependent on the presence of all-*trans* retinal (E), n ≥ 17 animals, N ≥ 3 assays. (G) Intestine-specific expression of EIF-3.L is not sufficient to rescue the reduced speed of *eif-3.L* mutants in 21% O_2, n ≥ 25 animals, N ≥ 3 assays. Average speed/ratios (line) and SEM (shaded regions) are plotted. * = P < 0.05, ** = P < 0.01, Mann-Whitney *U* test (A, B, D-H), or unpaired t-test (C).

O_2 (Fig. 4.2D). Consistent with there being no defects in the ability of downstream neurons to respond to RMG in the absence of EIF-3.L, artificial activation of RMG using channeldrhodopsin (ChR2) was sufficient to evoke high speed in *eif-3.L* mutants (Fig. 4.2F).

A recent study showed that the enhanced lifespan and resistance to ER stress of *eif-3.K* mutants could be rescued by tissue-specific expression of EIF-3.K either in the nervous system or in the intestine (Cattie et al., 2016). I restricted EIF-3.L to the intestine to test whether its expression there is also able to promote behavioural responses. I found however that gut-specific expression of EIF-3.L had no effect on the reduced speed of *eif-3.L* mutants in 21% O_2 (Fig. 4.2G). Together, my data show that EIF-3.L is required specifically in RMG to mediate avoidance of 21% O_2. I expect the same to be true for EIF-3.K, although this awaits confirmation.

eIF3k and L regulate a range of physiological features

To map the expression pattern of EIF-3.K and .L I generated C-terminally tagged fosmid reporters. Consistent with previous reports (Cattie et al., 2016; Huang et al., 2012), EIF-3.K::GFP and EIF-3.L::GFP were constitutively expressed in all tissues (Fig. 4.3A and B). Previous studies have implicated non-essential EIF-3 subunits in programmed cell death and ER homeostasis, suggesting that they regulate diverse aspects of physiology (Cattie et al., 2016; Huang et al., 2012). I found that chemotaxis towards the attractive odorant diacetyl was dependant on both EIF-3.K and EIF-3.L, indicating that they control behaviours unrelated to O_2 sensing (Fig. 4.3C). Unexpectedly, the defective chemotaxis of an *eif-3.K ; eif-3.L* double mutant was stronger than that of either single mutant, suggesting that the two subunits may in fact fulfill partially distinct roles (Fig. 4.3C).

Additionally, I found that body fat levels were modulated by EIF-3.L; intestinal lipid levels were increased in *npr-1; eif-3.L* animals compared to *npr-1* controls

(Fig. 4.3E). It is interesting to note that a role for O_2-sensing neurons in stimulating fat loss has recently been described (Witham et al., 2016), although many explanations could account for altered lipid stores.

I observed that *eif-3.K* and *.L* mutants have a flat body posture when quiescent (Fig. 4.3D), a phenotype associated with lethargus (Iwanir et al., 2013; Schwarz et al., 2012). If this preliminary observation can be confirmed, it may indicate that *eif-3.K/L* mutants have globally decreased levels of neural activity.

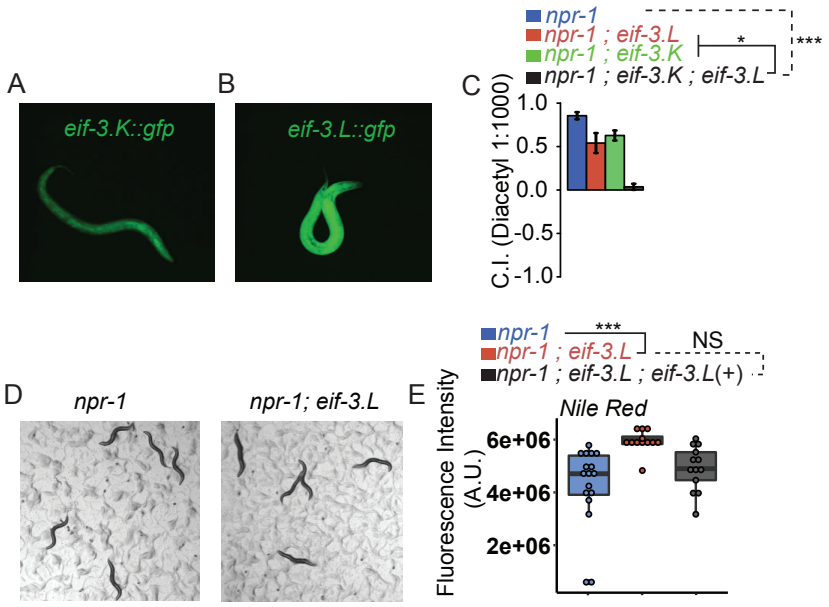

Figure 4.3 Broad expression and function of EIF-3.K and EIF-3.L. (A and B) Fosmid reporters expressing C-terminally tagged EIF-3.K::GFP (A) and EIF-3.L::GFP (B) are constitutively expressed throughout the animal. (C) *eif-3.K* and *eif-3.L* mutants display decreased chemotaxis towards diacetyl, N ≥ 4. These phenotyes are additive. (D) *eif-3.L* mutants appear to have unusually flat body posture when quiescent. (E) Fixative-based Nile Red staining is reduced in the intestine of *eif-3.L* mutants, n ≥ 12. * = P < 0.05, *** = P < 0.001, ANOVA with Tukey's post hoc HSD.

Decreased bulk translation does not recapitulate the loss of EIF-3.K and EIF-3.L

I considered the possibility that a general reduction in translation might account for the reduced behavioural responsiveness of *eif-3.K* and *eif-3.L* mutants. To test this, I used mutants that are known to reduce translational rates in *C. elegans*: *ife-2* and *ife-4,* which disrupt eIF4E function, and *gcn-2*, an eIF2α kinase mutant (Dinkova et al., 2004; Hansen et al., 2007; Kim and Strange, 2013).

These mutations did not disrupt the 21% O_2- avoidance of *npr-1* animals, nor did they modify the phenotype of *npr-1; eif-3.L; eif-3.K* (Fig. 4.4A and B, and data not shown). This suggests that if EIF-3.L controls behaviour by regulating translation, it has a specific role that is not shared by other well-characterized translational regulators. It is also consistent with the findings of Cattie et al. (2016) who showed that the enhanced resistance to ER stress of *eif-3.K* and *eif-3.L* mutants was not recapitulated by mutants that generally reduce translation.

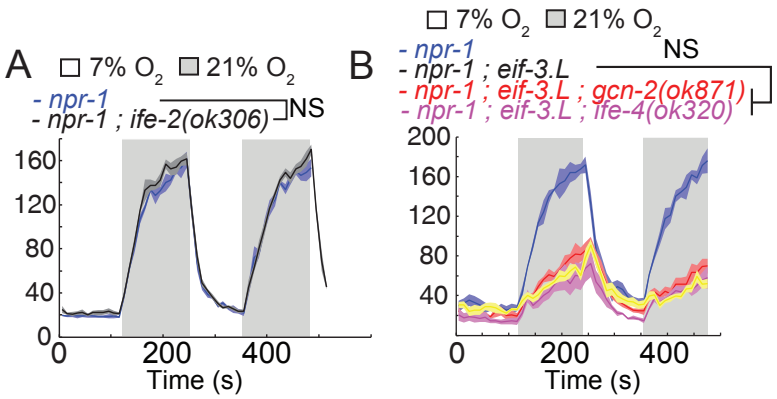

Figure 4.4 General reductions in translation do not modify avoidance of 21% O_2. (A) A deletion in the *ife-2* locus does not impair locomotory responses to high ambient O_2, n ≥ 63 animals, N = 4 assays. (B) *ife-4* or *gcn-2* do not modulate the phenotype of *eif-3.K;eif-3.L;npr-1*. Average speed/ratios (line) and SEM (shaded regions) are plotted, n ≥ 36 animals, N = 4 assays, Mann-Whitney *U* test.

The relationship between IL-17 and eIF3k/l signaling

Interestingly, like *ilc-17.1* and *nfki-1* mutants, animals lacking EIF-3.L become completely unresponsive to 21% O_2 after 2h without mechanical stimulation (Fig. 4.5B). Given the phenotypic similarity of *eif-3.K/eif-3.L* and *ilc-17.1* mutants, we considered whether eIF3k and eIF3L promote or mediate IL-17 signaling in RMG. Consistent with this, I found that the aggregation and speed phenotypes of *eif-3.L* mutants in 21% O_2 were suppressed by IκBζ/NFKI-1 overexpression (Fig. 4.5A and B).

To explore whether IL-17 and EIF-3.K/L promote the same global transcriptional state, I used RNA-sequencing to compare gene expression in *ilc-17.1*, *nfki-1*, and *eif-3.L; eif-3.K* mutants. Compared to WT (*npr-1*), the expression of 70 genes

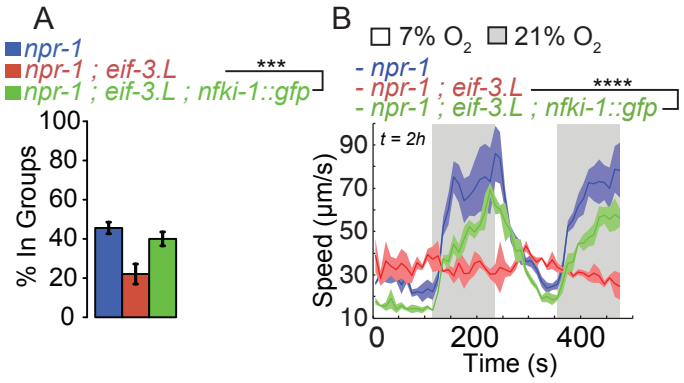

Figure 4.5 Elevated IκBζ signaling compensates for loss of EIF-3.L. Aggregation (A, N ≥ 4) and speed (B, n ≥ 41) defects of *eif-3.L* are rescued by overexpressing *nfki-1* cDNA. **** = P < 0.0001, *** = P < 0.001, ANOVA with Tukey's post hoc HSD (A) or Mann-Whitney *U* test (B).

was reduced two-fold by loss of EIF-3.K and EIF-3.L, while 204 genes were overexpressed (Fig. 4.6A and B). In collaboration with Alastair Crisp I compared this geneset to that perturbed by loss of ILC-17.1 or NFKI-1. We defined genes consistently regulated by IL-17 signaling as those whose expression was significantly altered in both *ilc-17.1* and *nfki-1* mutants. Of these, ~1/3 (44/129) were also dysregulated in *eif-3.L; eif-3.K* mutants.

We also identified a large number of genes (200) whose expression was modulated by EIF-3.K or EIF-3.L, but not significantly altered by loss of IL-17 signaling (Fig. 4.6A and B). Unsurprisingly therefore, the large range of phenotypes induced by loss of eIF3k and eIF3l in *C. elegans* is associated with widespread perturbation of the transcriptome. Together, these data define a set of transcripts regulated specifically by EIF-3.K and EIF-3.L, and a set modulated by both IL-17 signaling and non-accessory EIF-3 subunits. Whereas mainly immune system pathways were over-represented in genes down-regulated by both *eif-3.L;eif-3.K* and IL-17 signaling mutations, EIF-3.K and EIF-3.L also regulated many additional genes involved in metabolism (Fig. 4.6C and D). It will be interesting to discover which group is functionally relevant to non-core eIF3 subunit function in RMG.

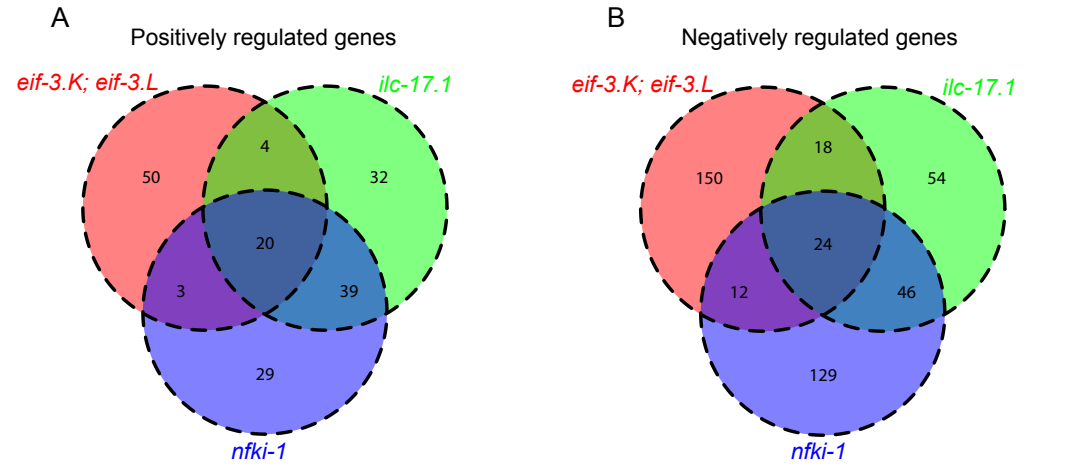

C

Positively regulated genes				Negatively regulated genes			
GO term	Description	p-Value	Matches	GO term	Description	p-Value	Matches
GO:0006629	lipid metabolic process	1.245596e-11	27	GO:0010466	negative regulation of peptidase activity	7.461984e-41	25
GO:0006334	nucleosome assembly	4.063554e-10	17	GO:0051346	negative regulation of hydrolase activity	1.554127e-35	25
GO:0008152	metabolic process	2.725364e-4	90	GO:0052547	regulation of peptidase activity	2.230837e-30	25
GO:0034622	cellular macromolecular complex assembly	5.825398e-4	17	GO:0030162	regulation of proteolysis	2.391297e-25	27
				GO:0070613	regulation of protein processing	3.242905e-25	27
GO:0006508	proteolysis	5.581997e-5	11	GO:0005975	carbohydrate metabolic process	7.669240e-11	15
GO:0006520	cellular amino acid metabolic process	2.474579e-4	7	GO:0006685	sphingomyelin catabolic process	2.454420e-4	3
GO:0019752	carboxylic acid metabolic process	0.004796	7	GO:0055114	oxidation-reduction process	9.386234e-4	12
GO:0006082	organic acid metabolic process	0.006526	7	GO:0009395	phospholipid catabolic process	9.790599e-4	3
GO:0043436	oxoacid metabolic process	0.006526	7	GO:0006684	sphingomyelin metabolic process	0.002441	3

D

Positively regulated genes			Negatively regulated genes		
Pathway	p-Value	Matches	Pathway	p-Value	Matches
megakaryocyte development and platelet production	9.107609e-14	17	Regulation of Lipid Metabolism by PPARalpha	2.736595e-34	29
MHC class II antigen presentation	3.460977e-9	9	Platelet degranulation	2.075854e-29	25
Hemostasis	2.511501e-6	17	Response to elevated platelet cytosolic Ca2+	6.081791e-29	25
Recycling of bile acids and salts	5.566536e-5	4	Fatty acid, triacylglycerol, and ketone body metabolism	1.425450e-21	29
Abacavir transmembrane transport	8.154717e-4	4			
MHC class II antigen presentation	1.837255e-16	9			
Adaptive Immune System	1.312736e-7	9	Digestion of dietary carbohydrate	1.679202e-4	3
Immune System	3.062678e-5	9			

Figure 4.6 Overlapping transcriptional changes in *eif-3.L;eif-3.K* and IL-17 signaling mutants. The total number of genes downregulated (A) and upregulated (B) in *npr-1;eif-3.L;eif-3.K, npr-1;ilc-17.1*, and *npr-1;nfki-1* animals compared to *npr-1*. Only genes that exhibit a two-fold, or greater, change are included. Gene ontology (GO) terms (C) and pathways (D) significantly overrepresented among genes regulated by *eif-3.K;eif-3.L* (red) and by all three mutants (blue) are shown.

Discussion

Translational control mechanisms are important regulators of neural circuit activity and cognition (Buffington et al., 2014). Their disruption is associated with memory defects, neurodegeneration and autism spectrum disorders (Chang et al., 2002; Kang and Schuman, 1996; O'Roak et al., 2012). Here I establish that

two accessory components of the translation initiation factor eIF3 are novel regulators of circuit state. Loss of eIF3k or eIF3l homologs reduces the responsiveness of RMG hub neurons to input from O_2 sensors, and attenuates escape of a repulsive environment. The sufficiency of EIF-3.L restricted to RMG suggests that they act cell-autonomously in neurons to control behaviour.

The major remaining question is whether eIF3k and eIF3l act analogously to other non-core eIF3 subunits to regulate the translational efficiency of specific neural mRNAs. eIF3d and eIF3e act cooperatively to remodel metabolism in *Schizosaccharomyces pombe* (Shah et al., 2016), and loss of eIF3h decreases the translation of a crystallin transcript that regulates zebrafish brain development (Choudhuri et al., 2013). However, k and l subunits are dispensable for the formation of active eIF3 complexes *in vitro* (Masutani et al., 2007), and have so far not been assigned any translational function. Like *eif3h* zebrafish morphants, *eif-3.K* and *eif-3.L* mutant nematodes exhibit WT polysome profiles (Cattie et al., 2016; Choudhuri et al., 2013). Our finding that general reduced bulk translation does not modify 21% O_2-avoidance is consistent with a model in which eIF3k and l subunits alter the translational rate of a specific subset of transcripts. Future work will aim to identify mRNAs that are (i) bound by k:l-containing eIF3 complexes and (ii) whose rate of translation is modulated by eIF3k and eIF3l.

An alternative possibility is that the neuronal function of eIF3k and eIF3l we have observed is independent of their role in translation initiation. Examples of complex promiscuity among PCI proteins have been described. For example, Rpn5 associates with both the CSN and the proteasome in *Saccharomyces cerevisiae* (Yu et al., 2011), and CIF-1 appears to fulfil the role of both Csn7 and eIF3m in *C. elegans* (Luke-Glaser et al., 2007). Additionally, the interaction of eIF3e with all three PCI complexes is conserved from plants to mammals (Alves et al., 2002; Yahalom et al., 2000; Yen et al., 2003). The structural counterparts of eIF3k:eIF3l in the CSN and 26S proteasome lid are CSN8:CSN3, and RPN12:RPN3 respectively (des Georges et al., 2015). No homolog for CSN8 has

been found in *C. elegans*, raising the possibility that it might be compensated for by EIF-3.K (Liu et al., 2013). However, EIF-3.K and EIF-3.L co-purify with EIF-3 complexes, not with the CSN (Luke-Glaser et al., 2007), and *C. elegans* homologs for all components of the 26S proteasome have been identified (Davy et al., 2013). Another relevant observation is that eIF3e was found to directly bind the L-type Ca^{2+} channel $Ca_v1.2$ and mediate its activity-dependent internalization in cortical neurons (Green et al., 2007). Therefore, although modulation of the efficiency of eIF3-mediated translation initiation remains the most plausible role for EIF-3.K and EIF-3.L in neurons, there is precedent for other scenarios.

Although EIF-3.K and EIF-3.L are broadly expressed, their effect on O_2-avoidance is associated specifically with their function in RMG neurons. It is interesting therefore, that their loss induces behavioural phenotypes reminiscent of IL-17 pathway mutants, which are also required in RMG (Chen et al., 2017). We identified a partially shared transcriptional signature of *eif-3.K*;*eif-3.L* and *ilc-17.1*/*nfki-1* mutants, which may contribute to their phenotypic overlap. Together, these observations raise the hypothesis that IL-17 signaling and non-essential eIF3 subunits cooperate to promote RMG activity. Interestingly, one way by which mammalian IL-17 achieves changes in gene expression is through the translational activation of latent inflammatory mRNAs (Dhamija et al., 2013). It is tempting to wonder, therefore, whether eIF3 subunits might mediate such a role in neurons and/or other tissues.

Materials and Methods

C. elegans maintenance, microinjection, WGS-based Hawaiian Variant Mapping, behavioural assays, Ca^{2+} imaging and RNA-seq analysis were performed as described in Chapters 2 and 3.

Strains

VC40148 *eif-3.L*(*gk485491*), KX15 *ife-2*(*ok306*), KX17 *ife-4*(*ok320*), and RB967 *gcn-2*(*ok871*) were obtained from the CGC which is funded by NIH Office of

Research Infrastructure Programs (P40 OD010440). Strains generated in this study are listed in the Appendix.

Molecular Biology

Fosmid recombineering

Clones covering the *eif-3.K* and *eif-3.L* locus were obtained from the *C. elegans* fosmid library (Source BioScience). As in Chapter 3, we followed the protocol of (Tursun et al., 2009) for C-terminal protein tagging. Clones covering the *eif-3.K* and *eif-3.L* locus were obtained from the *C. elegans* fosmid library (Source BioScience) and the GFP cassette from pBALU1 was amplified using tttcagATGTCGCCGATCTTCTGACCAGCATTCAACCCCCGTTGACTCTTATGAGTAAAGGAGAAGAACTTTTCAC with caacagaaacaagggtattataatttgaatgacagtgataattgataTTATTTGTATAGTTCATCCATGCCATG for *eif-3.K*, and AGTTGCAAGAGGTTCAGGATGTGCTCAAACGACTCGATATCCAGAAACCAATGAGTAAAGGAGAAGAACTTTTCAC with ggaaatcaaccagtcatgtttcgtttagctcaaatacttttttaaggaTCATTTGTATAGTTCATCCATGCCATG for *eif-3.L*.

Gateway cloning

We amplified cDNA corresponding to *eif-3.K* using ggggACAAGTTTGTACAAAAAAGCAGGCT tttcagaaaa atgtcgttcgagaaactgcaaaag and ggggACCACTTTGTACAAGAAAGCTGGGTA ttaaagagtcaacgggggttgaatg, and to *eif-3.L* using ggggACAAGTTTGTACAAAAAAGCAGGCTtttcagaaaaatgtctcgacgcgtggaattcgatttatcc and ggggACCACTTTGTACAAGAAAGCTGGGTAtcatggtttctggatatcgagtcgtttgagc. Although not used in this study, we also cloned the *eif-3.K* promoter region (1.3Kb upstream of the ATG) using ggggACAACTTTGTATAGAAAAGTTGaatatattaaccgttattgtttaaaatatcataatcaggtaggttc and ggggACTGCTTTTTTGTACAAACTTGcttaaaaacaaattatagcaattgaagaaaagaaactctgc, and the *eif-3.L* promoter (3.7Kb) using ggggACAACTT

TGTATAGAAAAGTTGcggttaatcaaaaaagggtgtcagaatgc and ggggACTGC TTTTTTGTACAAACTTGtactgaaagaaggtttttatattgatattatttaaatgtcaaactaaattc gaaaag.

Gibson Assembly

To target the *eif-3.K* locus for CRISPR/Cas9-mediated mutagenesis we expressed TTCTGGAAATTGGTGAAGG from the *rpr-1* promoter (Chen et al., 2013). This sequence was amplified for insertion into *Eco* RI-cut expression plasmids using gcgcgtcaagttgtGTTCTGGAAATTGGTGAAGGGTTTTAGAGCTAGAA and TTCTAGCTCTAAAACCCTTCACCAATTTCCAGAACacaacttgacgcgc.

Optogenetics

L4 animals expressing ChR2 in RMG, were picked to OP50 lawns supplemented with 100µl ChR2 cofactor (5mM all-*trans* retinal). Control animals were picked to OP50 lawns treated with 100µl ethanol. Test and controls sets were kept in the dark for 24h before being transferred to assay plates seeded with 20 µl OP50 14-18h beforehand. As described in Chapter 2, 7% O_2 was continuously delivered at 1.4ml/min using a PDMS chamber connected to a PHD 2000 Infusion syringe pump. Excitation light (11.6 mW/cm^2) was delivered from a Leica EL6000 mercury lamp and filtered using 480/40nm excitation filters fitted on a Leica M165FC microscope. Movies were recorded with a Point Grey Grasshopper camera, using FlyCapture software (2fps). Speed was measured using Zentracker software.

Nile Red staining

Fixative-based Nile Red (Sigma, N3013) staining was performed following the protocol of (Pino et al., 2013). Well-fed young adults were washed twice in M9 buffer, and once in PBS with 0.01% Triton X-100. They were then incubated in 40% isopropanol for 3 min at room temperature, and pelleted by centrifugation.

After removing the supernatant, we stained animals in dark conditions for 3h using 6µl Nile Red solution (0.5 mg/ml in acetone) per 1ml 40% isopropanol.

Light microscopy and fluorescence quantification

As in Chapter 2, animals were immobilized on 2% agarose pads using 25 mM sodium azide for spinning disk confocal laser microscopy. Z stacks were acquired using an Andor Ixon EMCCD on a Nikon Eclipse Ti inverted microscope, and converted to maximum intensity projections in Image J. Only planes containing the cell (RMG for *flp-5p::gfp* quantification) or tissue (anterior intestinal region for Nile Red quantification) were included in projections. Corrected fluorescence was calculated by: Integrated Density – (area of selected cell/region x average background intensity).

Contributions

EMS mutants were isolated by C Chen, their whole genome sequence characterized by G Nelson. C Chen and Z Soltesz carried preliminary behavioural analysis, as indicated in the text. The CRI prepared DNA/RNA libraries and performed sequencing, and Alastair Crisp analyzed RNA-seq data.

References

Alves, K.H., Bochard, V., Rety, S., and Jalinot, P. (2002). Association of the mammalian proto-oncoprotein Int-6 with the three protein complexes eIF3, COP9 signalosome and 26S proteasome. FEBS Lett *527*, 15–21.

Baird, T.D., and Wek, R.C. (2012). Eukaryotic initiation factor 2 phosphorylation and translational control in metabolism. Adv Nutr *3*, 307–321.

Bhattacharyya, S., Yu, H., Mim, C., and Matouschek, A. (2014). Regulated protein turnover: snapshots of the proteasome in action. Nat Rev Mol Cell Biol *15*, 122–133.

Buffington, S.A., Huang, W., and Costa-Mattioli, M. (2014). Translational Control in Synaptic Plasticity and Cognitive Dysfunction. Annu Rev Neurosci *37*, 17–38.

Cate, J.H.D. (2017). Human eIF3: from “blobology” to biological insight. Phil Trans R Soc B *372*, 20160176–20160179.

Cattie, D.J., Richardson, C.E., Reddy, K.C., Ness-Cohn, E.M., Droste, R., Thompson, M.K., Gilbert, W.V., and Kim, D.H. (2016). Mutations in Nonessential eIF3k and eIF3l Genes Confer Lifespan Extension and Enhanced Resistance to ER Stress in Caenorhabditis elegans. PLoS Genet *12*, e1006326–20.

Chang, R.C.-C., Suen, K.-C., Ma, C.-H., Elyaman, W., Ng, H.-K., and Hugon, J. (2002). Involvement of double-stranded RNA-dependent protein kinase and phosphorylation of eukaryotic initiation factor-2a in neuronal degeneration. J Neurochem *83*, 1215–1225.

Chen, C., Fenk, L.A., and de Bono, M. (2013). Efficient genome editing in Caenorhabditis elegans by CRISPR-targeted homologous recombination. Nucleic Acids Res *41*, e193–e193.

Chen, C., Itakura, E., Nelson, G.M., Sheng, M., Laurent, P., Fenk, L.A., Butcher, R.A., Hegde, R.S., and de Bono, M. (2017). IL-17 is a neuromodulator of Caenorhabditis elegans sensory responses. Nature *542,* 43–48.

Choudhuri, A., Maitra, U., and Evans, T. (2013). Translation initiation factor eIF3h targets specific transcripts to polysomes during embryogenesis. Proc Natl Acad Sci USA *110*, 9818–9823.

Costa-Mattioli, M., Gobert, D., Stern, E., Gamache, K., Colina, R., Cuello, C., Sossin, W., Kaufman, R., Pelletier, J., Rosenblum, K., et al. (2007). eIF2α Phosphorylation Bidirectionally Regulates the Switch from Short- to Long-Term Synaptic Plasticity and Memory. Cell *129*, 195–206.

Davy, A., Bello, P., Vaglio, P., Hitti, J., Doucette-Stamm, L., Thierry-Mieg, N., Reboul, J., Boulton, S., Walhout, A., Coux, O., et al. (2013). A protein–protein interaction map of the *Caenorhabditis elegans* 26S proteasome. EMBO Rep *2*, 821–828.

des Georges, A., Dhote, V., Kuhn, L., Hellen, C.U.T., Pestova, T.V., Frank, J., and Hashem, Y. (2015). Structure of mammalian eIF3 in the context of the 43S preinitiation complex. Nature *525*, 491–495.

Dhamija, S., Winzen, R., Doerrie, A., Behrens, G., Kuehne, N., Schauerte, C., Neumann, E., Dittrich-Breiholz, O., Michael, K., and Holtmann, H. (2013). Interleukin-17 (IL-17) and IL-1 Activate Translation of Overlapping Sets of mRNAs, Including That of the Negative Regulator of Inflammation, MCPIP1. J Biol Chem *288*, 19250–19259.

Dinkova, T.D., Keiper, B.D., Korneeva, N.L., Aamodt, E.J., and Rhoads, R.E. (2004). Translation of a Small Subset of Caenorhabditis elegans mRNAs Is Dependent on a Specific Eukaryotic Translation Initiation Factor 4E Isoform. Mol Cell Biol *25*, 100–113.

Gebauer, F., and Hentze, M.W. (2004). Molecular mechanisms of translational

control. Nat Rev Mol Cell Biol *5*, 827–835.

Green, E.M., Barrett, C.F., Bultynck, G., Shamah, S.M., and Dolmetsch, R.E. (2007). The Tumor Suppressor eIF3e Mediates Calcium-Dependent Internalization of the L-Type Calcium Channel CaV1.2. Neuron *55*, 615–632.

Hansen, M., Taubert, S., Crawford, D., Libina, N., Lee, S.-J., and Kenyon, C. (2007). Lifespan extension by conditions that inhibit translation in Caenorhabditis elegans. Aging Cell *6*, 95–110.

Hinnebusch, A.G. (2006). eIF3: a versatile scaffold for translation initiation complexes. Trends Biochem Sci *31*, 553–562.

Huang, C.-Y., Chen, J.-Y., Wu, S.-C., Tan, C.-H., Tzeng, R.-Y., Lu, P.-J., Wu, Y.-F., Chen, R.-H., and Wu, Y.-C. (2012). C. elegans EIF-3.K Promotes Programmed Cell Death through CED-3 Caspase. PLoS ONE *7*, e36584–13.

Iwanir, S., Tramm, N., Nagy, S., Wright, C., Ish, D., and Biron, D. (2013). The Microarchitecture of C. elegans Behavior during Lethargus: Homeostatic Bout Dynamics, a Typical Body Posture, and Regulation by a Central Neuron. Sleep *36*, 385–395.

Kang, H., and Schuman, E.M. (1996). A Requirement for Local Protein Synthesis in Neurotrophin-Induced Hippocampal SynapticPlasticity. Science *273*, 1402–1406.

Kim, H., and Strange, K. (2013). Changes in translation rate modulate stress-induced damage of diverse proteins. AJP: Cell Physiology *305*, C1257–C1264.

Kim, K., and Li, C. (2004). Expression and regulation of an FMRFamide-related neuropeptide gene family in *Caenorhabditis elegans*. J Comp Neurol *475*, 540–550.

Kim, T.H. (2004). Translational Regulation via 5' mRNA Leader Sequences Revealed by Mutational Analysis of the Arabidopsis Translation Initiation Factor Subunit eIF3h. Plant Cell *16*, 3341–3356.

Laurent, P., Soltesz, Z., Nelson, G.M., Chen, C., Arellano-Carbajal, F., Levy, E., and de Bono, M. (2015). Decoding a neural circuit controlling global animal state in *C. elegans*. *4*, e04241.

Lee, A.S.Y., Kranzusch, P.J., and Cate, J.H.D. (2015). eIF3 targets cell-proliferation messenger RNAs for translational activation or repression. Nature *522*, 111–114.

Lee, A.S.Y., Kranzusch, P.J., Doudna, J.A., and Cate, J.H.D. (2016). eIF3d is an mRNA cap-binding protein that is required for specialized translation initiation. Nature *536*, 96–99.

Liu, C., Guo, L.-Q., Menon, S., Jin, D., Pick, E., Wang, X., Deng, X.W., and Wei, N. (2013). COP9 Signalosome Subunit Csn8 Is Involved in Maintaining Proper Duration of the G. J Biol Chem *288*, 20443–20452.

Luke-Glaser, S., Roy, M., Larsen, B., Le Bihan, T., Metalnikov, P., Tyers, M., Peter, M., and Pintard, L. (2007). CIF-1, a Shared Subunit of the COP9/Signalosome and Eukaryotic Initiation Factor 3 Complexes, Regulates MEL-26 Levels in the Caenorhabditis elegans Embryo. Mol Cell Biol *27*, 4526–4540.

Masutani, M., Sonenberg, N., Yokoyama, S., and Imataka, H. (2007). Reconstitution reveals the functional core of mammalian eIF3. EMBO J *26*, 3373–3383.

Meleppattu, S., Kamus-Elimeleh, D., Zinoviev, A., Cohen-Mor, S., Orr, I., and Shapira, M. (2015). The eIF3 complex of Leishmania—subunit composition and mode of recruitment to different cap-binding complexes. Nucleic Acids Res *43*, 6222–6235.

Meyer, K.D., Patil, D.P., Zhou, J., Zinoviev, A., Skabkin, M.A., Elemento, O., Pestova, T.V., Qian, S.-B., and Jaffrey, S.R. (2015). 5'prime; UTR m6A Promotes Cap-Independent Translation. Cell *163*, 999–1010.

O'Roak, B.J., Vives, L., Fu, W., Egertson, J.D., Stanaway, I.B., Phelps, I.G., Carvill, G., Kumar, A., Lee, C., Ankenman, K., et al. (2012). Multiplex Targeted Sequencing Identifies Recurrently Mutated Genes in Autism Spectrum Disorders. Science *338*, 1619–1622.

Pause, A., Belsham, G.J., Gingras, A.-C., Donze, O., Lin, T.-A., Lawrence, J.C., Jr, and Sonenberg, N. (1994). Insulin-dependent stimulation of protein synthesis by phosphorylation of a regulator of 5'-cap function. Nature *371*, 762–767.

Phan, L., Zhang, X., Asano, K., Anderson, J., Vornlocher, H.-P., Greenberg, J.R., Qin, J., and Hinnebusch, A.G. (1998). Identification of a Translation Initiation Factor 3 (eIF3) Core Complex, Conserved in Yeast and Mammals, That Interacts with eIF5. Mol Cell Biol *18*, 4935–4946.

Piccirillo, C.A., Bjur, E., Topisirovic, I., Sonenberg, N., and Larsson, O. (2014). Translational control of immune responses: from transcripts to translatomes. Nat Immunol *15*, 503–511.

Pick, E., Hofmann, K., and Glickman, M.H. (2009). PCI Complexes: Beyond the Proteasome, CSN, and eIF3 Troika. Mol Cell *35*, 260–264.

Pino, E.C., Webster, C.M., Carr, C.E., and Soukas, A.A. (2013). Biochemical and High Throughput Microscopic Assessment of Fat Mass in *Caenorhabditis elegans*. J Vis Exp *30*, e50180.

Ray, A., Bandyopadhyay, A., Matsumoto, T., Deng, H., and Maitra, U. (2008). Fission yeast translation initiation factor 3 subunit eIF3h is not essential for global translation initiation, but deletion of eif3 h+affects spore formation. Yeast *25*, 809–823.

Ron, D. (2002). Translational control in the endoplasmic reticulum stress response. J Clin Invest *110*, 1383–1388.

Scheuner, D., Song, B., McEwen, E., Liu, C., Laybutt, R., Gillespie, P., Saunders, T., Bonner-Weir, S., and Kaufmann, R.J. (2001). Translational Control Is Required for the Unfolded Protein Response and In Vivo Glucose Homeostasis. Mol Cell *7*, 1165–1176.

Schwarz, J., Spies, J.-P., and Bringmann, H. (2012). Reduced muscle contraction and a relaxed posture during sleep-like lethargus. Worm *1*, 12–14.

Shah, M., Su, D., Scheliga, J.S., Pluskal, T., Boronat, S., Motamedchaboki, K., Campos, A.R., Qi, F., Hidalgo, E., Yanagida, M., et al. (2016). A Transcript-Specific eIF3 Complex Mediates Global Translational Control of Energy Metabolism. Cell Rep *16*, 1891–1902.

Siridechadilok, B., Fraser, C.S., Hall, R.J., Doudna, J.A., and Nogales, E. (2005). Structural Roles for Human Translation Factor eIF3 in Initiation of Protein Synthesis. Science *310*, 1513–1515.

Smith, M.D., Arake-Tacca, L., Nitido, A., Montabana, E., Park, A., and Cate, J.H. (2016). Assembly of eIF3 Mediated by Mutually Dependent Subunit Insertion. Structure *24*, 886–896.

Smith, M.D., Gu, Y., Querol-Audi, J., Vogan, J.M., Nitido, A., and Cate, J.H.D. (2013). Human-Like Eukaryotic Translation Initiation Factor 3 from Neurospora crassa. PLoS ONE *8*, e78715–10.

Smith, R.N., Aleksic, J., Butano, D., Carr, A., Contrino, S., Hu, F., Lyne, M., Lyne, R., Kalderimis, A., Rutherford, K., et al. (2012). InterMine: a flexible data warehouse system for the integration and analysis of heterogeneous biological data. Bioinformatics *28*, 3163–3165.

Sun, C., Todorovic, A., Querol-Audi, J., Bai, Y., Villa, N., Snyder, M., Ashchyan, J., Lewis, C.S., Hartland, A., Gradia, S., et al. (2011). Functional reconstitution of human eukaryotic translation initiation factor 3 (eIF3). Proc Natl Acad Sci USA *108*, 20473–20478.

Tursun, B., Cochella, L., Carrera, I., and Hobert, O. (2009). A Toolkit and Robust Pipeline for the Generation of Fosmid-Based Reporter Genes in C. elegans. PLoS ONE *4*, e4625–16.

Witham, E., Comunian, C., Ratanpal, H., Skora, S., Zimmer, M., and Srinivasan,

S. (2016). C. elegans Body Cavity Neurons Are Homeostatic Sensors that Integrate Fluctuations in Oxygen Availability and Internal Nutrient Reserves. Cell Rep *14*, 1641–1654.

Yahalom, A., Kim, T.H., Winter, E., Karniol, B., Arnim, von, A.G., and Chamovitz, D.A. (2000). Arabidopsis eIF3e (INT-6) Associates with Both eIF3c and the COP9 Signalosome Subunit CSN7. J Biol Chem *276*, 334–340.

Yen, H.-C.S., Gordon, C., and Chang, E.C. (2003). Schizosaccharomyces pombe Int6 and Ras HomologsRegulate Cell Division and Mitotic Fidelity via the Proteasome. Cell *112*, 207–217.

Yu, Z., Kleidfeld, O., Lande-Atir, A., Bsoul, M., Kleiman, M., Krutauz, D., Book, A., Vierstra, R.D., Hofmann, K., Reis, N., et al. (2011). Dual function of Rpn5 in two PCI complexes, the 26S proteasome and COP9 signalosome. Mol Cell *22*, 911–920.

Zhou, C., Arslan, F., Wee, S., Krishnan, S., Ivanov, A.R., Oliva, A., Leatherwood, J., and Wolf, D.A. (2005). PCI proteins eIF3e and eIF3m define distinct translation initiation factor 3 complexes. BMC Biol *3*, 14–16.

Zhou, M., Sandercock, A.M., Fraser, C.S., Ridlova, G., Stephens, E., Schenauer, M.R., Yokoi-Fong, T., Barksy, D., Leary, J.A., Hershey, J.W., et al. (2008). Mass spectrometry reveals modularity and a complete subunit interaction map of the eukaryotic translation factor eIF3. Proc Natl Acad Sci USA *105*, 18139–18144.

Zhu, P.J., Huang, W., Kalikulov, D., Yoo, J.W., Placzek, A.N., Stoica, L., Zhou, H., Bell, J.C., Friedlander, M.J., Krnjević, K., et al. (2011). Suppression of PKR Promotes Network Excitability and Enhanced Cognition by Interferon-γ-Mediated Disinhibition. Cell *147*, 1384–1396.

5

Using Induced mutants and natural variation to study nematode aggregation behaviour

Introduction

Dramatic behavioural differences are often seen between recently diverged species, while homologous adaptations can be observed in distantly related ones (Jovelin et al., 2003; Sturmbauer et al., 1996; Weber and Hoekstra, 2009). That behaviours can evolve quickly, and on multiple occasions, suggests that there is a rich pool of natural variation within wild populations. Indeed, behaviours are quantitative traits that are often continuously distributed among individuals of the same species (Mackay, 2001). Such variation is typically underpinned by a complex genetic architecture, with a polygenic basis and a prominent contribution from pleiotropic genes and epistatic interactions (Huang et al., 2012; SWARUP et al., 2012).

In humans, large-scale genome-wide association studies (GWAS) have been applied to complex traits with limited success (Visscher et al., 2012). Mapping behavioural quantitative trait loci (QTLs) in genetic model organisms offers significantly greater power for linking natural polymorphisms to behaviour because every locus can be tested many times in controlled genetic backgrounds (Bendesky and Bargmann, 2011). Moreover, QTL mapping can be complemented by the study of induced mutants, which remain the most powerful tool for studying the contribution of a gene to behaviour. Illustrating this point, a large cohort of loci associated with variation in aggression among wild *Drosophila* isolates have been validated by loss-of-function analysis (Shorter et al., 2015).

C. elegans has by now been isolated from all continents except Antarctica (Dolgin et al., 2008). In general, wild isolates exhibit very low levels of polymorphism - estimated to be 20-fold lower than among wild-caught *Drosophila melanogaster* (Barriere and Félix, 2005a), High levels of linkage-disequilibrium indicate that self-fertilization is the predominant mode of reproduction in the wild (Barriere and Félix, 2005b). Phenotypic variation, on the other hand, is widespread (Barriere and Félix, 2005a). Whether this points towards a greater contribution from individual loci than has been observed in other organisms is not

yet clear, although recent work that identified a QTL explaining ~40% of the variation in foraging strategy among wild strains suggests that this might be the case (Greene et al., 2016a; 2016b).

The sequenced genomes of nematodes both closely and distantly related to *C. elegans* have opened the door for cross-species comparative analyses to investigate mechanisms of behavioural evolution (Kumar et al., 2012; McGrath et al., 2012). To date, 23 *Caenorhabditis* species have been described (Kiontke and Sudhaus, 2006). Many of these are outcrossing species that exhibit greater levels of polymorphism that *C. elegans* (Jovelin et al., 2003). Importantly, they exhibit both divergence from and similarities to behaviours that are understood at a molecular and circuit level in *C. elegans* (Jovelin et al., 2003; Srinivasan et al., 2008). Therefore, nematodes may prove an informative model for studying behavioural evolution.

Here we combine the study of traditional genetic screens with analysis of wild *Caenorhabditis* isolates, with a view towards gaining a global picture of the molecular mechanisms that drive aggregation and contribute to natural variation. First, we summarize our study of forward genetic behavioural mutants. From these we establish a novel function for an uncharacterized but remarkably conserved gene, homologous to human suppressor of tumourigenicity 7 (ST7). We then describe intra- and inter- species diversity in avoidance of ambient O_2 and CO_2 among nematodes.

Results

Mutations in *egl-2*, *unc-22*, *unc-42* and *plc-1* disrupt aggregation

We localized the loci associated with loss of aggregation in five more EMS-induced mutants. Three mapped to well-characterized genes, *egl-2, unc-22*, and *unc-42* (Fig. 5.1A-C). These are known to be required in the nervous system (*egl-2* and *unc-42*) or in muscle (*unc-22*) for normal locomotion (Baran et al., 1999; Moerman et al., 1986; Weinshenker et al., 1999). Another localized to *plc-1*

(Fig. 5.1D), which encodes one of six *C. elegans* phospholipase C (PLC) enzymes that catalyze the break down of PIP_2 to IP_3 and diacyl glycerol (DAG). EGL-8 (PLCβ), an important producer of synaptic DAG (Lackner et al., 1999), is also required for aggregation (de Bono lab, unpublished). This suggests therefore that two PLCs, EGL-8 and PLC-1, function in parallel to promote avoidance of 21% O_2 – although the necessity of PLC-1 still requires confirmation.

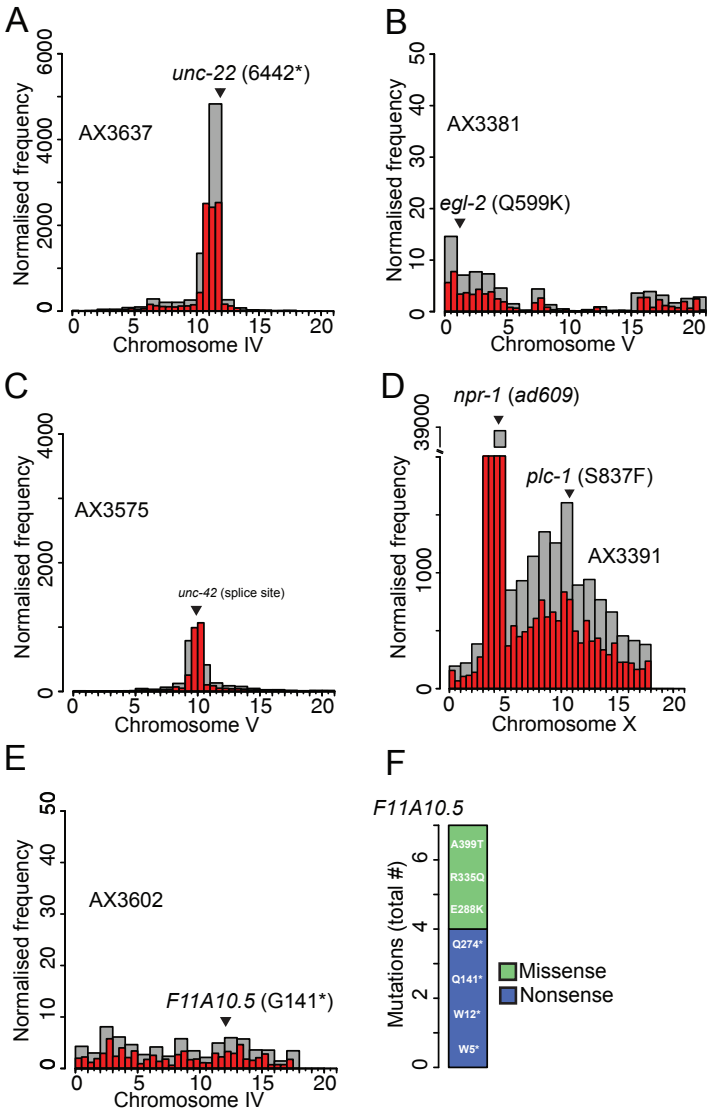

Figure 5.1 Mutations in *unc-22*, *egl-2*, *unc-42*, *plc-1* and *F11A10.5* are associated with loss of aggregation. (A-E) WGS-based CloudMap Hawaiian Variant Mapping of five EMS-induced mutants that fail to aggregate. Genomic regions surrounding mutations in *unc-22* (A), *egl-2* (B), *unc-42* (C), *plc-1* (D), and *F11A10.5* (E) are linked to the causative locus. The large peak on the on the left arm of Chr X in (D) corresponds to *npr-1*(*ad609*), which was present in both mutant and mapping strains. (F) Among the entire collection of non-aggregating mutants, 7 strains contain mutations in the protein-coding region of *F11A10.5*, four of which are predicted to encode premature termination codons (*).

C. elegans ST7 promotes aggregation

db692 was linked to chromosome IV, where we found a nonsense mutation in *F11A10.5* (Fig. 51E). Despite the fact that it is not an especially large gene, six additional mutations in *F11A10.5* were present within our collection, and several of these introduce premature termination codons (Fig. 5.1F). *F11A10.5* encodes a predicted membrane protein, with 2-3 transmembrane helices, that shows strong homology to mammalian ST7. ST7 was initially proposed to be a tumour suppressor, since it was deleted in several forms of human cancer (Zenklusen et al., 2001), although subsequent studies have suggested this is not the case (Fig. 5.1H and I) (Dong and Sidransky, 2002). Studies in cultured human cells provide experimental support for a membrane-localization of ST7 (Charong et al., 2010; Hooi et al., 2006). Nothing, however, is known about its function.

cDNA corresponding to WT *F11A10.5* rescued the defective 21% O_2 avoidance of *db640* mutants (Fig. 5.2A). Furthermore, an independent frameshift mutation in the *F11A10.5* locus induced hyper-avoidance of CO_2 and defective aerotaxis, consistent with reduced activity in the circuit that drives aggregation and escape of 21% O_2 (Fig. 5.2B). We expressed YC2.60 in URX and RMG to monitor Ca^{2+} response to 21% O_2, but did not detect any difference between *npr-1* and *npr-1;F11A10.5* animals (Fig. 5.2C and D). This suggests that F11A10.5 functions either downstream of RMG Ca^{2+} signaling, or elsewhere in the animal.

We generated several reporters to map the expression pattern of F11A10.5. In all cases we observed expression in a small number of neurons in the head, which have not been identified (Fig. 5.2E-G). Future work will address whether F11A10.5 functions in neurons to modulate behaviour.

Natural variation in O_2- and CO_2- avoidance

Unlike the laboratory strain N2, the Hawaiian wild isolate CB4856 aggregates and strongly avoids high ambient O_2 (de Bono and Bargmann, 1998; Persson et al., 2009). Interestingly, these differences are only partially explained by variation

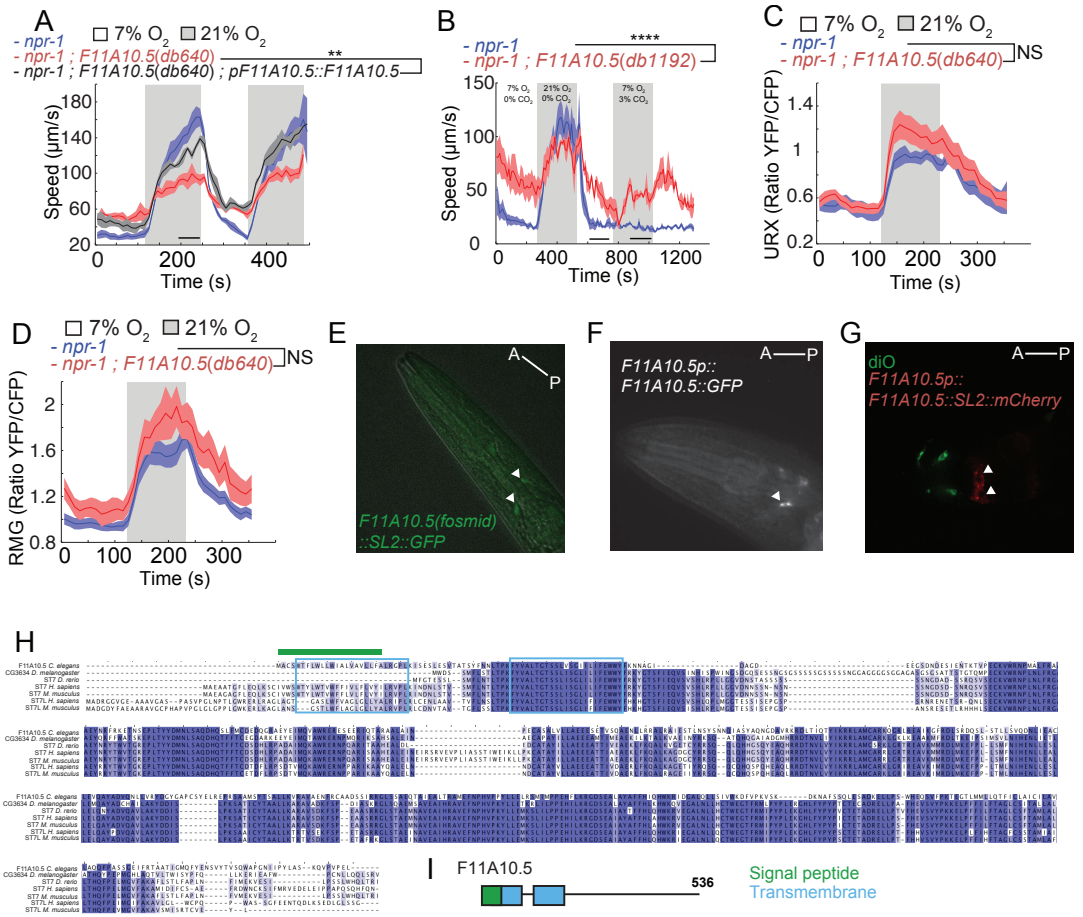

Figure 5.2 *C. elegans* ST7 promotes O_2-related behaviours. (A) The reduced speed of *db640* in 21% O_2 is rescued by *F11A10.5* cDNA expressed from its endogenous promoter (2.6 Kb), n ≥ 52 animals, N = 4 assays. (B) An 8bp deletion in the coding region of *F11A10.5*, generated by CRISPR/Cas9, shows reduced/delayed slowing in response to 7% O_2 and enhanced speed in 3% CO_2, n ≥ 77 animals, N = 7 assays. (C, D) Ca^{2+} transients, as reported by YC2.60, are comparable in URX (C, N≥6) and RMG (D, N≥13) in *npr-1* and *npr-1*;*F11A10.5* animals. (E) A fosmid-based reported expressing trans-spliced F11A10.5 and GFP is expressed in a small number of neurons in the head. (F) An *F11A10.5*(gDNA)::GFP fusion cloned downstream of *F11A10.5* upstream sequence (2.6 Kb) is also expressed in a limited number of neurons, and appears to be excluded from the nucleus. (G) The *F11A10.5p::F11A10.5::SL2mCherry* expression construct that restores behaviour to *db640* mutants (A) is expressed in a pair of cells posterior to diO-filled amphid sensory neurons (G). (H) Domain organization of F11A10.5. Transmembrane helices are predicted by the TMHMM 2.0, and the signal peptide by SignalP 4.1. (I) Sequence alignment of ST7 orthologs across species. Mammalian genomes encode two paralagous ST7 genes, ST7 and ST7-like (ST7L). Residue colouring indicates % identity. The first N-terminal transmembrane domain (cyan) is conserved between mammals and nematodes, but absent in fish and fly. The second (cyan) is almost universally conserved across all species. Only *C. elegans* is predicted to contain a signal peptide sequence (green). The C-terminal regions, which are predicted to be extracellular, are also highly conserved. Black bars indicate timepoints used for statistics. White arrows point to F11A10.5-expressing neurons. Average speed (line) and SEM (shaded regions) are plotted. ** = P < 0.01, **** = P < 0.0001, Mann-Whitney *U* test.

at the *npr-1* locus, indicating that other genetic factors contribute (Persson et al., 2009). As a resource with which to map these additional loci, ~1000 recombinant inbred advanced intercross lines (RIAILs) were previously generated by serial interbreeding between recombinant progeny of N2 and CB4856 (Weber et al., 2010). These strains should exhibit low levels of linkage disequilibrium, allowing small genomic intervals to segregate independently, which would confer high resolution to association studies.

I subjected a subset of RIAILs to a panel of environmental stimuli to obtain a picture of the behavioural diversity within the collection (Fig. 5.3A). This preliminary analysis showed that most RIAILS behaved either like N2 (small response to 21% O_2, large response to CO_2) or like CB4856 (large response to 21% O_2, small response to CO_2). A small number however, exhibited an intermediate phenotype that may be interesting to explore. Genome sequencing will be required to determine how well behaviour correlates with *npr-1* allele, and importantly to identify lines that do not behave as predicted based on the NPR-1 variant they encode.

Because the N2 genome has been sculpted by domestication, it is not a good model for exploring adaptation to conditions relevant in the wild. We found that a strain isolated in Madagascar, LKC34, exhibits reduced response to 21% O_2 and increased avoidance of CO_2 compared to CB4856 (Fig. 5.3B). As LKC34 has not been propagated in the laboratory, QTL mapping of loci linked to behavioural differences between LKC34 and CB4856 may identify more ecologically relevant behavioural polymorphisms.

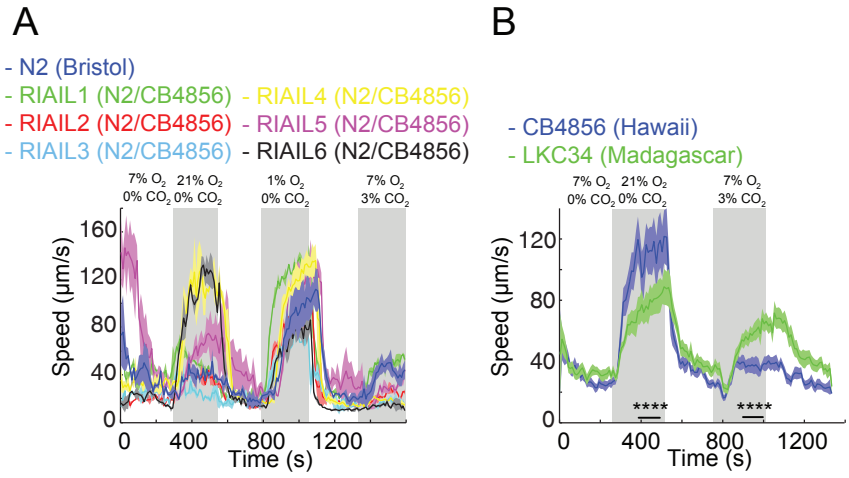

Figure 5.3 Natural variation in O_2- and CO_2- avoidance. (A) Most RIAILs generated from CB4856 (Hawaii) and the domesticated N2 (Bristol) strains exhibit behavioural fingerprints characteristic of one or the other of their parent strains (i.e. low speed in 21% O_2 coupled with high speed in 3% CO_2, or vice versa). Some, however, appear to show intermediate phenotypes (e.g. RIAIL 3 and RIAIL 5), N = 2 assays. (B) Wild-caught strains from Madagascar (LKC34) and Hawaii (CB4856) vary in their response to 21% O_2 and 3% CO_2, n ≥ 93 animals, N = 10 assays. Average speed (line) and SEM (shaded regions) are plotted. **** = P < 0.0001, Mann-Whitney *U* test.

Variation in aggregation within the *Caenorhabditis* genus

Although aggregation has been described in diverse nematodes, many species most closely related to *C. elegans* are solitary feeders - despite the fact that they encode the 215F version of NPR-1 associated with aggregation (Mario de Bono, unpublished). The genetic mechanisms that underlie inter-species differences in aggregation have not been explored. Additionally, it is not known whether aggregation has arisen multiple times in parallel, or once in an ancient ancestor before being widely lost.

I performed comparative behavioural analysis of species closely related to *C. elegans* (Fig. 5.4A-E). None of the species I assayed exhibited responses to 21% O_2 comparable to *C. elegans*. Interestingly, although *C. nigoni* showed dramatic avoidance of 3% CO_2 (Fig. 5.4C), most other species did not respond strongly to this cue. This suggests that different genetic changes underlie solitary behaviour in *C. nigoni* and other *Caenorhabditis* species. Additionally, as gain of NPR-1 function increases responsiveness to CO_2, this might mean that loci other than

npr-1 are responsible for absence/loss of aggregation in many species. The remarkable diversity among the six species we assayed indicates that O_2 and CO_2 avoidance behaviours are rapidly and continuously evolving in nematodes.

Discussion

One significant challenge faced by GWAS analyses in general is determining the functional relevance of loci linked to complex traits (Pickrell, 2014). A complete understanding of the molecular underpinnings of specific behaviours will be an important resource for dissecting natural variation. Building on previous knowledge, I describe induced mutations in five genes that are associated with loss of aggregation. *egl-2, unc-22*, *unc-44* and *plc-1* have all been previously implicated in neuronal processes or behavioural regulation, so that they are associated with aggregation is unsurprising (Baran et al., 1999; Kunitomo et al., 2013; Moerman et al., 1986; Weinshenker et al., 1999). The discovery that an ST7 ortholog promotes avoidance of 21% O_2, on the other hand, identifies an entirely novel role for a protein that is highly conserved across multicellular organisms.

My analysis of *F11A10.5* mutants represents the first *in vivo* KO of *ST7* in any species. In humans, ST7 is expressed in many tissues – including the brain (Zenklusen et al., 2001). Its function in the nervous system, or in any cell type, however, remains obscure. We show that worm ST7 is also expressed in neurons. Establishing the identities of these cells will help elucidate the function of F11A10.5, as it will allow targeted physiological analysis of loss-of-function mutants. It seems likely, based on domain annotation and a small number of studies from mammalian cell culture, that ST7 proteins function at the membrane, where they may interact with extracellular factors (Charong et al., 2010; Hooi et al., 2006). Future work should definitively address whether this is the case.

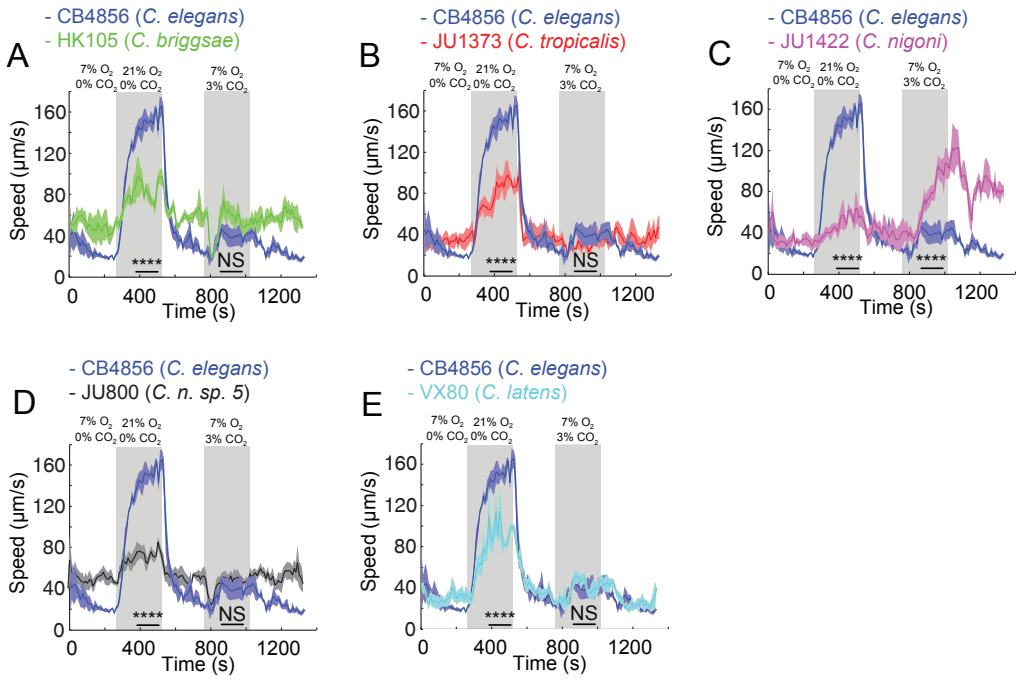

Figure 5.4 Interspecies variation in O_2- and CO_2- avoidance. The locomotory responses of six *Caenorhabditis* species to 21% O_2 and 3% CO_2 are shown. n ≥ 34 animals, N ≥ 3 assays. Average speed (line) and SEM (shaded regions) are plotted. **** = P < 0.0001, Mann-Whitney *U* test.

High-throughput screens that continue to extend the catalog of genes known to be required for avoidance of 21% O_2 will inform studies of natural variation. The LKC34 wild *C. elegans* isolate from Madagascar harbors a 3bp deletion in the *F11A10.5* locus. Whether this is linked to its slower speed in 21% O_2 is unknown, but there is no doubt that the more complete our molecular characterization of induced behavioural mutants, the more likely it is that we will be able to identify functional natural polymorphisms.

Similarly, several of the wild species analysed here have complete or draft genome assemblies (Kumar et al., 2012). To explore the genetic basis of their behavioural differences, genes known to regulate O_2 and CO_2 avoidance can be subject to comparative analyses, and tested for evidence of selection. Importantly, the recent development of genome-editing techniques such as CRISPR/Cas9 (Sugi, 2016) means that loss-of-function and transgenesis

experiments can now be used to test the functional relevance of natural polymorphisms.

Materials and methods

C. elegans maintenance, WGS-based Hawaiian Variant Mapping of EMS mutants, Ca^{2+} imaging, light microscopy and protein alignment were performed as described in Chapter 2.

Strains

The following strains were obtained from the CGC which is funded by NIH Office of Research Infrastructure Programs (P40 OD010440): LKC34 (*C. elegans*, Madagascar), HK105 (*C. Briggsae*, Japan), JU1373 (*C. tropicalis*, La Réunion), JU1422 (*C. nigoni*, India), JU800 (*C. n. sp. 5*, China) and VX80 (*C. latens*, China). Additional strains used in this study are listed in the Appendix.

Behavioural assays

In most cases (Fig. 5.2A, 3, and 4) 15-25 young adult hemaphrodites/females were picked onto low-peptone NGM plates seeded with 20 µl OP50 48h previously. [O_2] and [CO_2] were controlled using a Precision Pressure Regulator (Norgren, 11-818-999) and LabView software (National Instruments). Gas mixes were delivered to air-tight plastic chambers at 5ml/min using a Mass Flow Controller FMA5400/5500 (Omega Engineering). Video recordings were taken at 5fps with DinoCapture 2.0 software, using a Dino-Lite camera. In Fig. 5.2B aerotaxis was performed using the microfluidic system described in Chapter 2. Speed and reversals were measured using Zentracker (https://github.com/wormtracker/zentracker).

Molecular Biology

Gateway

Most expression constructs were generated using MultiSite Gateway Recombination (Invitrogen). To amplify the *F11A10.5* promoter from *C. elegans*

cDNA we used
ggggACAACTTTGTATAGAAAAGTTGTacaccatcttcggccaaaaaattcg and
ggggACTGCTTTTTTGTACAAACTTGgacccctaaaacactccaatattaggaaatataaaaac.
We cloned the *F11A10.5* protein-coding region (gDNA) using
ggggACAAGTTTGTACAAAAAAGCAGGCTtttcagaaaaatggcctgttcatggaccttcc
and ggggACCACTTTGTACAAGAAAGCTGGGTAgagctctggaacaggcacctg
To amplify cDNA corresponding to *F11A10.5* we used
ggggACAAGTTTGTACAAAAAAGCAGGCTtttcagaaaaatggcctgttcatggaccttcc
and
ggggACCACTTTGTACAAGAAAGCTGGGTAttagagctctggaacaggcacctgtttcg.

Fosmid recombineering
The SL2::GFP cassette from pBALU9 was amplified using
GAAATATCATTCCGTATTTAGCATCGAAACAGGTGCCTGTTCCAGAGCTCTA
Agctgtctcatcctactttcacctagttaac and
aagagtacaagattggaatgattggatagattgaaaaaaatatcacactatttgtatagttcatccatgccatg,
for *F11A10.5* fosmid recombineering (Tursun et al., 2009).

Gibson Assembly
To generate a lesion in the *F11A10.5* locus we co-expressed Cas9 and
atccataggagccacagga. The guide sequence was amplified for insertion into *E*co
RI-cut expression plasmids using
TTCTAGCTCTAAAACtcctgtggctcctatggatCacaacttgacgcgc and
gcgcgtcaagttgtGatccataggagccacaggaGTTTTAGAGCTAGAA.

Contributions
C Chen isolated EMS mutants and helped with mapping. G Nelson helped adapt the CloudMap procedure to our WGS data.

References
Baran, R., Aronhoff, R., and Garriga, G. (1999). The C. elegans homeodomain gene unc-42 regulates chemosensory and glutamate receptor expression.

Development *126*, 2241–2251.

Barriere, A., and Félix, M.-A. (2005a). Natural variation and population genetics of Caenorhabditis elegans. WormBook *1.43.1*.

Barriere, A., and Félix, M.-A. (2005b). High Local Genetic Diversity and Low Outcrossing Rate in Caenorhabditis elegans Natural Populations. Curr Biol *15*, 1176–1184.

Bendesky, A., and Bargmann, C.I. (2011). Genetic contributions to behavioural diversity at the gene–environment interface. Nat Rev Genet *12*, 809–820.

Charong, N., Patmasiriwat, P., and Zenklusen, J.C. (2010). Localization and characterization of ST7 in cancer. J Cancer Res Clin Oncol *137*, 89–97.

de Bono, M., and Bargmann, C.I. (1998). Natural Variation in a Neuropeptide Y Receptor Homolog Modifies Social Behavior and Food Response in. Cell *94*, 679–689.

Dolgin, E.S., Félix, M.-A., and Cutter, A.D. (2008). Hakuna Nematoda: genetic and phenotypic diversity in African isolates of Caenorhabditis elegans and C. briggsae. Heredity *100*, 304–315.

Dong, S.M., and Sidransky, D. (2002). Absence of ST7 gene alterations in human cancer. Clin Cancer Res *8*, 2939-2941.

Greene, J.S., Dobosiewicz, M., Butcher, R.A., McGrath, P.T., and Bargmann, C.I. (2016a). Regulatory changes in two chemoreceptor genes contribute to a Caenorhabditis elegans QTL for foraging behavior. eLife *5*, e21454.

Greene, J.S., Brown, M., Dobosiewicz, M., Ishida, I.G., Macosko, E.Z., Zhang, X., Butcher, R.A., Cline, D.J., McGrath, P.T., and Bargmann, C.I. (2016b). Balancing selection shapes density- dependent foraging behaviour. Nature *539*, 254–258.

Hooi, C.-F., Blancher, C., Qiu, W., Revet, I.M., Williams, L.H., Ciavarella, M.L., Anderson, R.L., Thompson, E.W., Connor, A., Phillips, W.A., et al. (2006). ST7-mediated suppression of tumorigenicity of prostate cancer cells is characterized by remodeling of the extracellular matrix. Oncogene *25*, 3924–3933.

Huang, W., Richards, S., Carbone, M.A., Zhu, D., Anholt, R.R.H., Ayroles, J.F., Duncan, L., Jordan, K.W., Lawrence, F., Magwire, M.M., et al. (2012). Epistasis dominates the genetic architecture of Drosophila quantitative traits. Proc Natl Acad Sci USA *109*, 15553–15559.

Jovelin, R., Ajie, B., and Phillips, P.C. (2003). Molecular evolution and quantitative variation for chemosensory behaviour in the nematode genus Caenorhabditis. Mol Ecol *12*, 1325–1337.

Kiontke, K., and Sudhaus, W. (2006). Ecology of Caenorhabditis species. WormBook *1.37.1*.

Kumar, S., Koutsovoulos, G., Kaur, G., and Blaxter, M. (2012). Toward 959 nematode genomes. Worm *1*, 42–50.

Kunitomo, H., Sato, H., Iwata, R., Satoh, Y., Ohno, H., Yamada, K., and Iino, Y. (2013). Concentration memory-dependent synaptic plasticity of a taste circuit regulates salt concentration chemotaxis in Caenorhabditis elegans. *Nat Commun 4*:2210.

Lackner, M.R., Nurrish, S.J., and Kaplan, J.M. (1999). Facilitation of Synaptic Transmission by EGL-30 Gqα and EGL-8 PLCβ: DAG Binding to UNC-13 Is Required to Stimulate Acetylcholine Release. Neuron *24*, 335–346.

Mackay, T.F.C. (2001). THE GENETIC ARCHITECTURE OF QUANTITATIVE TRAITS. Annu. Rev. Genet. *35*, 303–339.

McGrath, P.T., Xu, Y., Ailion, M., Garrison, J.L., Butcher, R.A., and Bargmann, C.I. (2012). Parallel evolution of domesticated Caenorhabditis species targets pheromone receptor genes. Nature *477*, 321–325.

Moerman, D.G., Benian, G.M., and Waterson, R.H. (1986). Molecular cloning of the muscle gene *unc-22* in Caenorhabditis elegans by Tc*1* transposon tagging. Proc Natl Acad Sci USA *83*, 2579–2583.

Persson, A., Gross, E., Laurent, P., Busch, K.E., Bretes, H., and de Bono, M. (2009). Natural variation in a neural globin tunes oxygen sensing in wild Caenorhabditis elegans. Nature *458*, 1030–1033.

Pickrell, J.K. (2014). Joint Analysis of Functional Genomic Data and Genome-wide Association Studies of 18 Human Traits. The American Journal of Human Genetics *94*, 559–573.

Shorter, J., Couch, C., Huang, W., Carbone, M.A., Peiffer, J., Anholt, R.R.H., and Mackay, T.F.C. (2015). Genetic architecture of natural variation in Drosophila melanogasteraggressive behavior. Proc Natl Acad Sci USA *112*, E3555–E3563.

Srinivasan, J., Durak, O., and Sternberg, P.W. (2008). Evolution of a polymodal sensory response network. BMC Biol *6*, 52–15.

Sturmbauer, C., Levinton, J.S., and Christy, J. (1996). Molecular phylogeny analysis of fiddler crabs: Test of the hypothesis of increasing behavioral complexity in evolution. Proc Natl Acad Sci USA *93*, 10855–10857.

Sugi, T. (2016). Genome Editing in C. elegans and Other Nematode Species. Int J Mol Sci *17*, 295–13.

Swarup, S., Harbison, S.T., Hahn, L.E., Morozova, T.V., Yamamoto, A., Mackay, T.F.C., and Anholt, R.R.H. (2012). Extensive epistasis for olfactory behaviour, sleep and waking activity in Drosophila melanogaster. Genet Res *94*, 9–20.

Tursun, B., Cochella, L., Carrera, I., and Hobert, O. (2009). A Toolkit and Robust Pipeline for the Generation of Fosmid-Based Reporter Genes in C. elegans. PLoS ONE *4*, e4625–16.

Visscher, P.M., Brown, M.A., McCarthy, M.I., and Yang, J. (2012). Five Years of GWAS Discovery. Am J Hum Genet *90*, 7–24.

Weber, J.N., and Hoekstra, H.E. (2009). The evolution of burrowing behaviour in deer mice (genus Peromyscus). Animal Behav *77*, 603–609.

Weber, K.P., De, S., Kozarewa, I., Turner, D.J., Babu, M.M., and de Bono, M. (2010). Whole Genome Sequencing Highlights Genetic Changes Associated with Laboratory Domestication of C. elegans. PLoS ONE *5*, e13922–10.

Weinshenker, D., Wein, A., Salkoff, L., and Thomas, J.H. (1999). Block of an ether-a-go-go-Like K^+ Channel by Imipramine Rescues *egl-2* Excitation Defects in *Caenorhabditis elegans*. J Neurosci *19*, 9831–9840.

Zenklusen, J.C., Conti, C.J., and Green, E.D. (2001). Mutational and functional analyses reveal that ST7 is a highly conserved tumor-suppressor gene on human chromosome 7q31. Nat Genet *27*, 392–398.

6

Conclusions and future directions

Mechanism and conservation of MALT1-mediated neuromodulation

The type 1 paracaspase MALT1 is a well-characterized signal transduction hub during B and T cell activation (Jaworski and Thome, 2015). In Chapter 2 we show that, in *C. elegans*, it is required for neuronal activation as well. In RMG hub neurons, MALT-1 functions together with other classical immune signaling molecules, ACTL-1, IRAK and IκBζ to mediate IL-17-driven neuromodulation. Our data suggest that, reminiscent of its role in immunity, MALT-1 functions as both a scaffolding site and a protease to activate downstream transcriptional effectors in neurons.

It is not surprising that MALT1 and IL-17 orthologs have related functions, as mammalian MALT1 is critical for the activation of T_H17 cells (a major source of IL-17) (Jeltsch et al., 2014). That MALT1 participates directly in IL-17 signaling, however, has not been described before. Our findings suggest a model in which MALT-1/ACTlL-1/IRAK complexes signal from IL-17 receptors to mediate activation of IκBζ in RMG and other neurons. Several questions arise from this discovery. Most importantly, are IL-17 signaling and/or neuromodulation conserved functions of paracaspases? All known mammalian immune receptors known to activate MALT1 contain phosphorylated immunoreceptor signaling motifs (ITAMs) (Jaworski and Thome, 2015). These drive phosphorylation of CARD-containing proteins, such as CARMA1 and CARMA3, which stimulate the assembly of CBM (CARD-Bcl10-MALT1) complexes. However, ITAM motifs and CARMA proteins appear to be unique to chordates (Finn et al., 2017; Staal et al., 2016). CARD-coiled-coil domains and Bcl10 homolgs have been found in some invetebrates, but other than MALT1, CBM orthologs are not present in *C. elegans* (Staal et al., 2016; Sullivan et al., 2009). Similarly the primary downstream target of CBM signaling, NF-κB, has not been found in nematodes (Sullivan et al., 2009). IL-17 cytokines, on the other hand, are present in many invertebrates; like MALT1 they have been identified in mollusks, annelids, arthropods and nematodes (Huang et al., 2015; Hulpiau et al., 2015). Therefore, it may be that type 1 paracaspases have an ancient role in IL-17 signaling. To explore this

possibility, IL-17 and MALT1 signal transduction pathways must be defined in more organisms, including invertebrates.

Additionally, it will be interesting to discover whether MALT1 mediates IL-17 signaling in any human cell types. A major hypothesis raised by our study is that mammalian MALT1 has a neuromodulatory role analogous to its *C. elegans* ortholog, perhaps explaining its expression in the brain (Gewies et al., 2014). To date however, no studies have assessed the impact of MALT1 disruption in mammalian neurons. Future work should aim to do so.

Several questions still remain regarding the role of MALT-1 in *C. elegans* neurons. First, how is MALT-1 activated by IL-17 receptor stimulation? It will be informative to test whether the association of MALT-1 with ACTL-1 and/or IRAK is dependent on IL-17 receptor activation. It is also possible that pre-formed complexes are post-translationally modified during IL-17 signaling. How MALT1 signals to IκBζ, and what role its protease activity plays in this pathway must also be addressed.

Finally, a major goal will be to identify the mechanisms by which MALT1/IκBζ activity promotes neuronal activity. Our transcriptomic analysis provides a global picture of how this pathway remodels animal physiology. Future efforts should be targeted to specific neurons to explore specifically how neuronal transcriptomes are affected.

How non-core eIF3 translation initiation factors regulate behavioural state

We show in Chapter 4 that EIF-3.K and EIF-3.L maintain the behavioural state associated with aggregation behaviour by enhancing the responsiveness of RMG neurons. The mechanism by which they do so is not clear, but the most obvious scenario, based on previous functional characterization of other eIF3 subunits, is that they regulate the translation of a specific subset of mRNAs (Choudhuri et al., 2013; Lee et al., 2015; Shah et al., 2016). Several recent technological advances

may help to test this possibility. Ribosome profiling, which isolates monosome-protected transcripts that are then reverse-transcribed and sequenced, can be used to purify and quantify mRNA that is in the process of being translated (Ingolia et al., 2009). PAR-CLIP (photoactivatable ribonucleoside-enhanced crosslinking and immunoprecipitation) is a method for directly identifying mRNAs that are physically bound to a protein of interest (Hafner et al., 2010), as illustrated by its elucidation of the mRNA-specificity of eIF3 in human 293T cells (Lee et al., 2015). Both techniques have been adapted to *C. elegans* (Aeschimann et al., 2015; Jungkamp et al., 2011), so provide feasible approaches to identify (i) transcripts whose translation is dependent on EIF.3-K/EIF-3.L, or (ii) EIF-3-mRNA interactions that are stabilized by these accessory subunits. To select for putative targets that regulate behaviour, these experiments should be specifically targeted to the nervous system, ideally to RMG interneurons.

The structure of eIF3 bound to the 43S pre-initiation complex suggests that eIF3e mediates the attachment of eIF3k and eIF3l to the assembly (des Georges et al., 2015). It would be informative to disrupt the conserved residues that lie at this interface to test whether the regulation of neuronal responsiveness by EIF-3.K and EIF-3.L depends on their insertion into the eIF3 complex. If their function turns out to be eIF3-independent, proteomic approaches might be helpful to identify other factors with which they interact.

Finally, we note that mutations in *eif-3.K* and *eif-3.L* induce a transcriptional state that partially overlaps with that induced by loss of IL-17 signaling. We do not know the significance of this relationship, so it will be important to determine whether the two phenotypes are additive. Additionally, once the downstream mechanisms of IL-17 signaling are established, it will be possible to ask whether eIF3 subunits modulate the expression of IL-17 targets.

The role of CAMTA transcription factors in activity homeostasis

Ca^{2+}-regulated transcription factors are an important link between neuronal activity and long-term change in the nervous system (West et al., 2002). In Chapter 3 we show that mutations in *C. elegans* CAMTA, a putative CaM-binding transcription factor, have complex effects on activity and adaptation in the URX-RMG circuit. Our analyses of multiple sensory neurons raise the hypothesis that one important function of CAMTAs is to limit the excitability of neurons. Given the link between deranged Ca^{2+} signaling and neurotoxicity (Berridge, 2010; Kasumu and Bezprozvanny, 2010), it may be that this function underlies the loss of cerebellar Purkinje cells in rodents lacking neuronal CAMTA1 (Long et al., 2014). Cell-specific loss-of-function experiments must be used to test directly whether CAMT-1 limits the excitability of neurons. It will also be important to extend this question to other cell types and other organisms to test whether preventing hyperactivity is a general function of CAMTAs.

We propose that CAMTA may be particularly important during homeostatic drives. Our data indicates that CAMT-1 limits the degree to which circuit activity is upregulated in response to sensory deprivation, suggesting that CAMTAs may be negative regulators of homeostatic plasticity. This model can be tested in mammalian systems, in which homeostatic phenomena have been well-characterized but are not completely understood at a molecular level (Turrigiano, 2011; Turrigiano and Nelson, 2004).

We observed large-scale disruption of the transcriptome when CAMT-1 levels were perturbed. It will be useful to complement this analysis with identification of CAMT-1 genomic binding sites using ChIP-seq, to establish which targets are likely to be direct. As our work suggests that CAMT-1 functions in an activity-dependent manner, it will be important to address whether the transcriptional activity of CAMT-1 is modulated by activity and by Ca^{2+} signaling. Like MALT-1 and EIF-3 subunits, CAMT-1 is broadly expressed in the nervous system. An

important goal for future studies of all three molecules will be to perform gene expression studies with single-neuron resolution.

Perspective

A theme throughout this thesis is that many, if not all, of the molecules that I find to be regulators of neural circuit activity, also play important roles in other physiological contexts. In light of this, it is interesting to consider the general surprise that greeted the assembly of the human genome - which revealed, in the words of Craig Venter, that *"there are far fewer genes than anyone imagined"* (The Observer, 11 Feb 2001). Current estimates suggest we have in the region of 20,000 protein-coding genes, not many more than nematodes, and substantially less than the water flea (Colbourne and et al, 2011; Consortium, 1998; Consortium et al., 2013; Ezkurdia et al., 2014). It may turn out to be the case that an important reason for this is that many, or most, genes perform more than one function. Probing the mechanism by which MALT1, CAMTAs and non-core eIF3 subunits control neural circuit activity will provide an interesting parallel for studies of their roles in other contexts, and inform attempts to manipulate their activity during disease.

References

Aeschimann, F., Xiong, J., Arnold, A., Dieterich, C., and Großhans, H. (2015). Transcriptome-wide measurement of ribosomal occupancy by ribosome profiling. Methods *85*, 75–89.

Berridge, M.J. (2010). Calcium Signalling and Alzheimer's Disease. Neurochem Res *36*, 1149–1156.

Choudhuri, A., Maitra, U., and Evans, T. (2013). Translation initiation factor eIF3h targets specific transcripts to polysomes during embryogenesis. Proc Natl Acad Sci USA *110*, 9818–9823.

Colbourne, J.K., and et al (2011). The Ecoresponsive Genome of Daphnia pulex. Science *331*, 555–561.

Consortium, T.C.E.S. (1998). Genome Sequence of the Nematode *C. elegans*: A Platform for Investigating Biology. Science *282*, 2012–2018.

Consortium, T.E.P., Consortium, T.E.P., data analysis coordination, O.C., data production, D.P.L., data analysis, L.A., group, W., scientific management, N.P.M., steering committee, P.I., Boise State University and University of North Carolina at Chapel Hill Proteomics groups (data production and analysis), Broad Institute Group (data production and analysis), et al. (2013). An integrated encyclopedia of DNA elements in the human genome. Nature *488*, 57–74.

des Georges, A., Dhote, V., Kuhn, L., Hellen, C.U.T., Pestova, T.V., Frank, J., and Hashem, Y. (2015). Structure of mammalian eIF3 in the context of the 43S preinitiation complex. Nature *525*, 491–495.

Ezkurdia, I., Juan, D., Rodriguez, J.M., Frankish, A., Diekhans, M., Harrow, J., Vazquez, J., Valencia, A., and Tress, M.L. (2014). Multiple evidence strands suggest that there may be as few as 19 000 human protein-coding genes. Hum Mol Genet *23*, 5866–5878.

Finn, R.D., Attwood, T.K., Babbitt, P.C., Bateman, A., Bork, P., Bridge, A.J., Chang, H.-Y., Dosztányi, Z., El-Gebali, S., Fraser, M., et al. (2017). InterPro in 2017—beyond protein family and domain annotations. Nucleic Acids Res *45*, D190–D199.

Gewies, A., Gorka, O., Bergmann, H., Pechloff, K., Petermann, F., Jeltsch, K.M., Rudelius, M., Kriegsmann, M., Weichert, W., Horsch, M., et al. (2014). Uncoupling Malt1 Threshold Function from Paracaspase Activity Results in Destructive Autoimmune Inflammation. Cell Rep *9*, 1292–1305.

Hafner, M., Landthaler, M., Burger, L., Khorshid, M., Hausser, J., Berninger, P., Rothballer, A., Ascano, M., Jr., Jungkamp, A.-C., Munschauer, M., et al. (2010). Transcriptome-wide Identification of RNA-Binding Protein and MicroRNA Target Sites by PAR-CLIP. Cell *141*, 129–141.

Huang, X.-D., Zhang, H., and He, M.-X. (2015). Comparative and Evolutionary Analysis of the Interleukin 17 Gene Family in Invertebrates. PLoS ONE *10*, e0132802–e0132815.

Hulpiau, P., Driege, Y., Staal, J., and Beyaert, R. (2015). MALT1 is not alone after all: identification of novel paracaspases. Cell Mol Life Sci *73*, 1103–1116.

Ingolia, N.T., Ghaemmaghami, S., Newman, J.R.S., and Weissman, J.S. (2009). Genome-Wide Analysis in Vivo of Translation with Nucleotide Resolution Using Ribosome Profiling. Science *324*, 218–223.

Jaworski, M., and Thome, M. (2015). The paracaspase MALT1: biological function and potential for therapeutic inhibition. Cell Mol Life Sci *73*, 459–473.

Jeltsch, K.M., Hu, D., Brenner, S., Zöller, J., Heinz, G.A., Nagel, D., Vogel, K.U., Rehage, N., Warth, S.C., Edelmann, S.L., et al. (2014). Cleavage of roquin and regnase-1 by the paracaspase MALT1 releases their cooperatively repressed

targets to promote TH17 differentiation. Nat Immunol *15*, 1079–1089.

Jungkamp, A.-C., Stoeckius, M., Mecenas, D., Grün, D., Mastrobuoni, G., Kempa, S., and Rajewsky, N. (2011). In Vivo and Transcriptome-wide Identification of RNA Binding Protein Target Sites. Mol Cell *44*, 828–840.

Kasumu, A., and Bezprozvanny, I. (2010). Deranged Calcium Signaling in Purkinje Cells and Pathogenesis in Spinocerebellar Ataxia 2 (SCA2) and Other Ataxias. Cerebellum *11*, 630–639.

Lee, A.S.Y., Kranzusch, P.J., and Cate, J.H.D. (2015). eIF3 targets cell-proliferation messenger RNAs for translational activation or repression. Nature *522*, 111–114.

Long, C., Grueter, C.E., Song, K., Qin, S., Qi, X., Kong, Y.M., Shelton, J.M., Richardson, J.A., Zhang, C.L., Bassel-Duby, R., et al. (2014). Ataxia and Purkinje cell degeneration in mice lacking the CAMTA1 transcription factor. Proc Natl Acad Sci USA *111*, 11521–11526.

Shah, M., Su, D., Scheliga, J.S., Pluskal, T., Boronat, S., Motamedchaboki, K., Campos, A.R., Qi, F., Hidalgo, E., Yanagida, M., et al. (2016). A Transcript-Specific eIF3 Complex Mediates Global Translational Control of Energy Metabolism. Cell Rep *16*, 1891–1902.

Staal, J., Driege, Y., Borghi, A., Hulpiau, P., Lievens, L., Gul, I., Sundararaman, S., Goncalves, A., Dhondt, I., Braeckman, B., et al. (2016). The CARD-CC/Bcl10/paracaspase signaling complex is functionally conserved since the last common ancestor of planulozoa. bioRxiv doi:10.1101–doi:10.046789.

Sullivan, J.C., Wolenski, F.S., Reitzel, A.M., French, C.E., Traylor-Knowles, N., Gilmore, T.D., and Finnerty, J.R. (2009). Two Alleles of NF-κB in the Sea Anemone Nematostella vectensis Are Widely Dispersed in Nature and Encode Proteins with Distinct Activities. PLoS ONE *4*, e7311–e7312.

Turrigiano, G. (2011). Too Many Cooks? Intrinsic and Synaptic Homeostatic Mechanisms in Cortical Circuit Refinement. Annu Rev Neurosci *34*, 89–103.

Turrigiano, G.G., and Nelson, S.B. (2004). Homeostatic plasticity in the developing nervous system. Nat Rev Neurosci *5*, 97–107.

West, A.E., Griffith, E.C., and Greenberg, M.E. (2002). Regulation of transcription factors by neuronal activity. Nat Rev Neurosci *3*, 921–931.

APPENDIX

Strain list

Strain	Genotype
Chapter II	
AX204	*npr-1(ad609)*
AX5876	*npr-1(ad609); malt-1(db1193)*
AX5877	*npr-1(ad609); malt-1(db1194)*
AX5978	*npr-1(ad609); malt-1(db1195*)
AX5989	*npr-1(ad609); malt-1(db1194)*; *dbEx614*[*gcy-37p::YC2.60:: unc-54 3'utr; ccRFP]*
Ax5797	*npr-1(ad609); ilc-17.1(tm5218)*; *dbEx614*[*gcy-37p::YC2.60:: unc-54 3'utr; ccRFP]*
AX5993	*npr-1(ad609); malt-1(db1195)*; *dbEx637*[*RMGp::YC2.60; ccRFP*]
AX5995	*npr-1(ad609); malt-1(db1194)*; *dbEx637*[*RMGp::YC2.60; ccRFP*]
AX6250	*npr-1(ad609); malt-1(db1194); dbIs*[*pnfki-1::nfki-1::GFP; ccRFP*]
AX6133	*npr-1(ad609); malt-1(db1194); pik-1(tm2167); [RMGp::YC2.60; ccRFP]*
AX6392	*npr-1(ad609); malt-1(db1194); dbEx925*[*rab-3p::malt-1::GFP; ccRFP*]
AX6745	*npr-1(ad609); edIs6[unc-119p::gfp; rol-6(su1006)]*
AX6415	*npr-1(ad609); malt-1(db1194); dbEx930*[*rab-3p::malt-1 (C374A) ::SL2mCherry; ccRFP*]
AX6742	*npr-1(ad609); malt-1(db1194); dbEx930*[*rab-3p::malt-1:: SL2mCherry ; ccRFP*]
AX6706	*npr-1(ad609); malt-1(db1194); dbEx888[plfp-5::malt-1::SL2mCherry ; ccGFP]*
AX6739	*npr-1(ad609); malt-1(db1194); dbEx982[gcy-32p::malt-1 ::SL2mCherry; ccGFP]*
AX6727	*npr-1(ad609); malt-1(db1194); dbEx978[hsp-16.41p::malt-1 ::SL2mCherry; ccRFP]*
AX6733	*npr-1(ad609); malt-1(db1194); dbEx979[malt-1p::malt-1::mCherry ; ccRFP]*

AX6762 *npr-1(ad609); rege-1(db1226)*

AX6793 *npr-1(ad609); rege-1(db1227)*

AX6836 *npr-1(ad609); malt-1(db1194)*; *dbEx637*[*RMGp::YC2.60; ccRFP*]; *dbEx996[npr-1p::malt-1::SL2mCherry; ccRFP]*

AX6859 *npr-1(ad609); malt-1(db1194)*; *dbEx996[npr-1p::malt-1::SL2mCherry; ccRFP]*

AX2073 *dbEx[flp-17p::YC3.60]*

AX6823 *malt-1(db1194)*; *dbEx[flp-17p::YC3.60]*

AX5689 *npr-1(ad609); ilc-17.1(tm5218)*

AX6010 *npr-1(ad609); nfki-1(db1197)*

AX6186 *npr-1(ad609); dbIs[pilc-17.1::ilc-17.1::mCherry]*

AX6130 *npr-1(ad609); dbIs[pnfki-1::nfki-1::GFP]*

Chapter III

AX6236 *npr-1(ad609); camt-1(ok515)*

AX3727 *npr-1(ky13); camt-1(db973)*

AX6592 *npr-1(ad609); camt-1(db1214)*

AX6314 *npr-1; camt-1(db973); dbEx614[gcy-37p::YC2.60::unc-54 3'utr; ccRFP]*

AX6340 *npr-1; camt-1(ok515); dbEx614[gcy-37p::YC2.60::unc-54 3'utr; ccRFP]*

AX6298 *npr-1; camt-1(db973); dbEx637[RMGp::YC2.60; ccRFP]*

AX6342 *npr-1; camt-1(db973); dbEx902[rab-3p::camt-1a::SL2mCherry; ccRPF]*

AX6344 *npr-1; camt-1(db973); dbEx908[npr-1p::camt-1a::SL2mCherry; ccRPF]*

AX6346 *npr-1; camt-1(db973); dbEx910[npr-1p::camt-1b::SL2mCherry; ccRPF]*

AX6348 *npr-1; camt-1(db973); dbEx911[flp-5p::camt-1a::SL2mCherry; ccRFP]*

AX6350 *npr-1; camt-1(db973); dbEx912[gcy-32p::camt-1a::SL2mCherry; ccRFP]*

AX6460 *npr-1; gcy-36(db66); dbEx614[gcy-37p::YC2.60::unc-54 3'utr; ccRFP]*

AX6386 *npr-1; camt-1(db973); gcy-36(db66); dbEx614[gcy-37p::YC2.60:: unc-54 3'utr; ccRFP]*

AX6460 *npr-1; gcy-36(db66); dbEx614[gcy-37p::YC2.60:: unc-54 3'utr; ccRFP]*

AX6461 *npr-1; unc-64(e246); dbEx614[gcy-37p::YC2.60:: unc-54 3'utr; ccRFP]*

AX6462 *npr-1; unc-64(e246); camt-1(db973); dbEx614[gcy-37p::YC2.60:: unc-54 3'utr; ccRFP]*

AX6387 *camt-1(db973); dbEx[flp-17p::YC3.60]*

AX6388 *camt-1(ok515); dbEx[flp-17p::YC3.60]*

AX6398 *camt-1(ok515); dbEx[flp-17p::YC3.60]; dbEx924[flp-17p::camt-1a:: SL2mCherry; ccRFP]*

AX6412 *npr-1; camt-1(db973); dbEx929[rab-3p::camt-1a(I962N):: SL2mCherry; ccRFP]*

AX6414 *npr-1; camt-1(db973); dbEx614[gcy-37p::YC2.60::unc-54 3'utr; ccRFP]; dbEx912[gcy-32p::camt-1a::SL2mCherry; ccRFP]*

AX1888 *npr-1; iaIs25[gcy-37p::GFP]*

AX6463 *npr-1; camt-1(db973); iaIs25[gcy-37p::GFP]*

AX6464 *npr-1; iaIs25[gcy-37p::GFP]; dbEx912[gcy-32p::camt-1:: SL2mCherry; ccRFP*

AX6509 *camt-1(db973); dbEX[gcy-8p::YC3.60; ccRFP]*

AX2047 *dbEX[gcy-8p::YC3.60; ccRFP]*

AX6597 *npr-1; dbIs14[camt-1(fosmid)::GFP; ccRFP]*

AX6631 *npr-1; camt-1(ok515); dbEx965[hsp-16.41p::camt-1::SL2mCherry; ccRFP]*

AX6697 *npr-1; dbEx971[rab-3p::NLS-camt-1a::GFP; ccRFP]*

AX6701 *npr-1; camt-1(db973); dbEx972[rab-3p::camt-1a(H190P)::*

SL2mCherry; ccRFP]

AX6804 *npr-1; nfki-1(db1197); dbIs14[camt-1(fosmid)::GFP; ccRFP]*

AX6815 *npr-1; camt-1(ok515); dbIs12[RMGp::YC2.60; ccRFP]*

AX6827 *otIs355[rab-3p::NLS::RFP]; dbIs14[camt-1(fosmid)::GFP; ccRFP]*

AX6830 *npr-1; T06D8.9(db1230)*

AX6831 *npr-1; T06D8.9(db1230)*

Chapter IV

AX3777 *npr-1(ky13); eif-3.L(db1015)*

AX6057 *npr-1(ad609); eif-3.L(485491)*

AX6071 *npr-1(ad609); eif-3.K(db1205)*

AX6072 *npr-1(ad609); eif-3.K(db1206)*

AX6195 *npr-1; eif-3.K(db817)*

AX6103 *npr-1; eif-3.L(db1015); eif-3.K(db1205)*

AX6293 *npr-1; eif-3.L(db1015); dbIs*[*pnfki-1::nfki-1::GFP; ccRFP*]

AX6234 *npr-1; ife-2(ok306)*

AX6294 *npr-1; eif-3.L(db1015); eif-3.K(db1205); gcn-2(ok871)*

AX6296 *npr-1; eif-3.L(db1015); eif-3.K(db1205); ife-4(ok320)*

AX6297 *npr-1; eif-3.L(db1015); eif-3.K(db1205); dbEx637[RMGp::*
YC2.60; ccRFP]

AX6569 *npr-1; eif-3.K(db1205); dbEx959[eif-3.K(fosmid)::GFP; ccRFP]*

AX6622 *npr-1; eif-3.L(db1205); dbEx959[eif-3.L(fosmid)::GFP; ccRFP]*

AX6297 *npr-1; eif-3.L(db1015); eif-3.K(db1205); dbEx637[RMGp::*
YC2.60; ccRFP]

Chapter V

AX3381 *npr-1(ky13); egl-2(db756)*

AX3391 *npr-1(ky13); plc-1(db766)*

AX3575 *npr-1(ky13); unc-42(db821)*

AX3637 *npr-1(ky13); unc-22(db883)*

AX3246 *npr-1(ad609); F11A10.5(db640)*

AX5859 *npr-1(ad609); F11A10.5(db1192)*

AX6061 *npr-1(ad609); F11A10.5(db640); dbEx614[gcy-37p::YC2.60::::unc-54 3'utr; ccRFP]*

AX6063 *npr-1(ad609); F11A10.5(db640)*; *dbEx637[RMGp::YC2.60; ccRFP] unc-54 3'utr; ccRFP]*

AX6212 *npr-1(ad609); F11A10.5(db640)*; *dbEx890[F11A10.5p::F11A10.5:: SL2mCherry; ccGFP]*

AX6465 *npr-1(ad609); F11A10.5(db640); dbEx940[F11A10.5(fosmid):: SL2GFP; ccRFP]*

cc = *unc-22p* (drives expression in coelomocytes)

RMGp = *ncs*-1::nCre *flp-21p*>Stop>GFP